SISSA **ISAS**

SCUOLA INTERNAZIONALE SUPERIORE DI STUDI AVANZATI
INTERNATIONAL SCHOOL FOR ADVANCED STUDIES

Gamma Ray Bursts: clues from the spectra and variability of the prompt phase

Thesis submitted for the degree of
Doctor Philosophiæ

CANDIDATE:
Željka Marija Bošnjak

SUPERVISORS:
Prof. Annalisa Celotti
Dr. Giancarlo Ghirlanda

October 2005

Table of Contents

Citations to Previously Published Works

Part of the work presented in this Thesis is the content of the following articles:

Published and submitted papers:

- *The peak luminosity - peak energy correlation in GRBs*
  Ghirlanda, G., Ghisellini, G., Firmani, C., Celotti, A. & **Bosnjak, Z.**, 2005, MNRAS, **360**, L45
- *Energetic - Spectral correlations vs. the BATSE Gamma-Ray Burst population*
  Bosnjak, Z., Celotti, A., Longo, F. & Barbiellini, G., submitted to MNRAS Letter, astro-ph/0502185
- *Gamma-Ray Bursts associated with Supernovae: A systematic analysis of BATSE GRB candidates*
  Bosnjak, Z., Celotti, A., Ghirlanda, G., Della Valle, M. & Pian, E., accepted for publication in Astronomy & Astrophysics, astro-ph/0510058
- *GRB 990413: Insight in the thermal phase evolution*
  Bosnjak, Z., Celotti, A. & Ghirlanda, G., submitted to *MNRAS Letter*

Conference Proceedings:

- *Low peak energies for dim GRBs: A clue for interpreting BATSE fluence distributions?*
  Bosnjak, Z., Celotti, A., Barbiellini, G. & Longo, F., Proceedings of XXII Texas Symposium on Relativistic Astrophysics at Stanford. December, 2004
- *Cosmological implications of Compton tails in long duration GRBs*
  Longo, F., Barbiellini, G., **Bosnjak, Z.** & Celotti, A., Proceedings of XXII Texas Symposium on Relativistic Astrophysics at Stanford. December, 2004
- *Cosmological implications of Compton tails in long duration GRBs*
  Longo, F., Barbiellini, G., **Bosnjak, Z.**, Celotti, A. & Ghirlanda, G., Proceedings of Gamma–Ray Bursts in the Afterglow Era, 4th Workshop, Roma. October, 2004
- *Firework Model: Time Dependent Spectral Evolution of GRB*
  Barbiellini, G., Longo, F., Ghirlanda, G., Celotti, A. & **Bosnjak, Z.**, Gamma-Ray Bursts: 30 Years of Discovery: Gamma-Ray Burst Symposium. September 2003, Santa Fe, New Mexico. AIP Conference Proceedings. Edited by E.E.Fenimore and M.Galassi. Melville, NY: American Institute of Physics, 2004, 727, 578

Acknowledgments

My deepest gratitude is given to Professor Annalisa Celotti who was my supervisor during these years. I thank her for encouraging me and trusting in me from the very beginning of my work at SISSA - even in the moments when I didn't have trust in myself. She has constantly challenged me to develop my ideas, and was open to share her energies and knowledge with me. I thank Giancarlo Ghirlanda who had the ability and endless patience to introduce me in the field that was completely new to me, and with whom I have done large part of the work. I acknowledge Professor Guido Barbiellini and Francesco Longo for useful discussions and conversations.

I particularly thank Professor Luigi Danese for his kind attention and support.

I thank Tom J. Maccarone with his persistent positive attitude, for the continuous encouragement and help that started when he was a postdoc at SISSA and continued on-line during his stay in Amsterdam and now in Southampton.

I thank my colleagues Francesco, Fabio, Sara and Francesca who helped me with my start at SISSA and with the start of my new life in Italy. I thank my best friend Ivana (and her little family) for always having her door open for me and being ready to listen and understand. Many thanks to Matteo, Nico, Andrea, Ugo, Elisa and my dance-class mate Marietta for their friendship during this last year in Trieste. I thank my friends from Zagreb, Domagoj, Mirej, Vanja and Damir for all the time we spent together, and who were with me in my highs and lows.

Finally, I thank my family who is always there for me, and without whom much of this would neither be possible nor worthwhile.

Chapter 1

Introduction

Gamma–ray bursts (GRBs) are bright ($\sim$ 3 photons cm^{-2} s^{-1} flux in the 50-300 keV band) flashes of gamma–rays that are detectable at Earth approximately once per day. They were discovered accidentally in the late 1960's by the *Vela* satellites that were primarily designed to monitor the potential gamma–rays from the nuclear tests outside the Earth's atmosphere. These first detections were soon proved to have a non 'terrestrial' origin and it became apparent that a new phenomenon was discovered. The searches for gamma–ray bursts from the early records of data were encouraged as gamma-ray emission during the initial stages of the development of supernovae was predicted (Colgate 1974). The first GRBs reported had characteristics consistent to what we know about them nowadays: they were described as short bursts of photons in the energy range 0.2–1.5 MeV with durations ranging from less than 0.1 s to $\sim$30 s (Klebesadel et al. 1973). The detection of bursts of gamma–rays was soon confirmed by other satellites (*IMP-6* and Russian *Konus*) and new space missions - dedicated to gamma–ray and X-ray observations - followed. For several years it was believed that GRBs originate from Galactic neutron stars on the basis of the low-energy absorption features, explained as cyclotron resonance lines (indicating strong magnetic fields), seen by the *Ginga* satellites and of high-energy emission features, interpreted as the 511 keV annihilation line originating near the surface of a solar-mass neutron star (Mazets et al. 1981, Murakami et al. 1988). The later demonstration that the majority of GRBs lie at cosmological distances (and the no-detection of these features by

other instruments than *Ginga*) made these explanations very unlikely.

The first major GRB catalog was obtained by the all-sky monitor *Compton Gamma–Ray Observatory* (CGRO) operating from April 1991 to May 2000, with the *Burst And Transient Source Experiment* (BATSE) on board. It detected over 2700 gamma–ray bursts in nine years and provided information on the nature of gamma–ray bursts that constitutes the basis of our knowledge of these phenomena. BATSE observations proved with high level of accuracy that gamma–ray bursts are isotropically distributed across the sky, implying their extra-galactic origin (Meegan et al. 1992). Furthermore, the number counts distribution of the BATSE bursts displayed a paucity of faint bursts relative to the number expected in an Euclidean space: this provided another piece of evidence for the cosmological origin of the sources (Fenimore et al. 1993). As a result, for the average flux of gamma–ray burst and a cosmological distance, the huge total luminosity of L $\sim 10^{51}$ ergs s^{-1} is inferred.

Due to the diversity in the observed properties, it is not possible to define a 'typical' event. Gamma–ray bursts exhibit an extremely large variety of time profiles: the durations range from several milliseconds to several thousands seconds and their time histories can have diverse morphologies, from single-peaked events to multiple peaked events with a complicated structure (Fishman & Meegan 1995). Several attempts have been made in order to categorize the bursts by their temporal morphologies; the only characteristic by which two distinct classes of bursts are identified is their duration. The distribution of burst durations appears bimodal and separates the bursts into short events (<2s) and long ones (>2s) (Kouveliotou et al. 1993). Gamma–ray burst spectra are non-thermal, with almost all of the luminosity emitted as high-energy photons, from ~100 keV to ~ 1 MeV (however this spectral range may suffer from selection effects due to instrumental sensitivity, Lloyd & Petrosian 1999). The peak energy of the spectra is around 250 keV, but can range from 50 to 1000 keV (Mallozzi et al. 1995). In recent years the evidence for GRBs with very low values of peak energy (E_{peak} <50 keV) has accumulated. Heise et al. (2001) discovered short transients in the *WFC* of *BeppoSAX*, which had little or no emission at energies above 40 keV, that is, much lower than the average for BATSE triggered GRBs; these events were

named X–Ray Flashes (XRFs). *HETE-2* has provided strong evidence that the properties of XRFs and GRBs form a continuum, and therefore these two types of bursts may be the same phenomena (Lamb et al. 2004, Sakamoto et al. 2004); clarifying the nature of XRFs and their connection to GRBs could provide a breakthrough in our understanding of the prompt emission of GRBs.

Already in the early studies of the GRB global properties (Kouveliotou et al. 1993) it was found that the temporal and spectral properties are linked: GRB durations are anticorrelated with their spectral hardness, that is, short gamma–ray bursts were found to be predominantly harder and long bursts softer.

The major obstacle in understanding the origin of gamma–ray bursts was the inability of determining their accurate positions and, consequently, of associating the phenomenon with some known population. The identification of GRB counterparts at longer wavelengths, i.e. the afterglow emission, provides the distance and clearly constrains the possible models for their origin. Actually theoretical scenarios for cosmological gamma–ray bursts involving radiation from relativistically outflowing plasma (Mèszàros & Rees 1993, Paczyǹski & Rhoads 1993) predicted the detection of emission in other wavebands (X–ray, O/UV and radio). Besides the localization problem, the afterglow observations are hampered by the transient nature of the event; for example, with the *Interplanetary Network* (IPN) GRBs are localized with a precision of several minutes of arc, however with long time delays with respect to the trigger.

The first X–ray afterglow detection (of GRB 970228) came in 1997 thanks to the Italian-Dutch *BeppoSAX* satellite that was equipped with an all-sky *Gamma–Ray Burst Monitor* (GRBM) for the gamma–ray energy range and a *Wide Field Camera* (WFC) for the X–ray energy range. It allowed fast and accurate positioning of the gamma–ray burst, facilitating also a quick start of ground based follow-up observations. The first measurement of a gamma–ray burst redshift from the optical absorption spectroscopy ($z \geq 0.835$, Metzger et al. 1997) was obtained for GRB 970508 confirming the cosmological distance of the

source. GRB 970508 was also the first GRB detected in radio: Frail et al. 1997 reported a variable radio source within the error box of GRB 970508 and coincident with the optical transient. The observed fluctuations in the radio emission were interpreted as a result of scintillation by the irregularities in the ionized Galactic interstellar gas and allowed the determination of the angular size of the source. These observations also led to the inference of super-luminal motion of GRB ejecta, supporting the view that relativistic motion is a fundamental property of gamma–ray bursts. Thus the observations of GRB counterparts have effectively ended the distance (and energetics) controversy on gamma–ray bursts.

The theoretical framework for the GRB origin followed the determination of their cosmological nature. According to what has become the 'standard' model the observed radiation arises as the outcome of a relativistically expanding 'fireball' - a large concentration of energy ($\sim 10^{51}$-10^{53} ergs) in a small region of space ($r \leq 10^8$cm, as implied by the short variability time scales $\sim$10 ms) in which there are relatively few baryons. The fireball is basically optically thick to its own radiation in the early phase; it expands adiabatically until high-energy photons can escape ($r \sim 10^{12}$cm). In the 'internal-shock' scenario a gamma–ray burst occurs at this stage from shocks forming within the irregular relativistic flow; the mechanism through which the internal energy dissipated in 'collisions' is converted into radiation is synchrotron (and inverse Compton). The afterglow would be produced at larger distances ($r > 10^{16}$cm) following 'external-shocks', when the fireball interacts with the circumburst medium and decelerates. As the Lorentz factor is decreasing, the radiation is shifted to lower energies, from soft gamma–rays through X–rays to optical and radio frequencies.

The plasma emitting the gamma–rays as well as the afterglow must be moving relativistically, thus the emitted radiation is expected to be strongly beamed and only a region with an opening angle $\sim 1/\Gamma$ off the line of sight can be observed. The first claims for narrow jets in GRBs came from Sari, Piran and Halpern (1999) who demonstrated that the temporal decay observed in the optical and X–ray afterglow of GRB 980519 is consistent with the evolution of a jet slowing down. Rhoads (1999) made the important point that

unless the jet is confined by some mechanism, it would expand laterally; he found that if the burst ejecta are beamed into an angle θ_0, the burst remnant evolution changes drastically once the bulk Lorentz factor $\Gamma \sim 1/\theta_0$. After this stage a further increase in the viewing angle results in a decrease of the radiation within the viewing cone and leads to a break in the afterglow light curve. Whether the relativistic flow is in the form of a jet or it is isotropic has strong repercussions on the total emitted energy, on the event rate and on the physical ejection mechanism.

As gamma–ray bursts are produced in the late, optically thin phase, observations can provide only indirect evidence on the nature of the 'inner engine' powering them. Thus, it is hard to discriminate observationally among the variety of models proposed. The feasible models for the progenitors of gamma–ray bursts come broadly in two classes: (i) mergers of compact objects, such as neutron star-neutron star mergers (e.g. Paczyński 1986, Eichler 1989) and neutron star-black hole mergers (e.g. Narayan et al. 1992, Mochkovitch et al. 1993); and (ii) the core collapse of very massive stars - collapsars, 'failed' supernovae or hypernovae (e.g. Woosley 1993, MacFadyen & Woosley 1999, Vietri & Stella 1998). The compact object merger models are a leading candidate model to account for short, hard GRBs; they are now disfavored for long bursts (although the possibility that a fraction of long gamma–ray bursts can originate in the merging process involving the final products of stellar evolution is not completely excluded). The favored scenario for long gamma–ray burst involves the core collapse of a massive star. The launch of a GRB jet is believed to develop from the black hole (BH)–accretion torus system resulting from the core collapse; either a one step collapse or a two step collapse is possible, depending on the mass and angular momentum of the progenitor core and the details of the collapse (thus the GRB is produced either simultaneously with a supernova event if the star collapses to a BH promptly, or a meta-stable object is formed during the collapse - a 'supramassive', rapidly rotating neutron star - and the GRB is delayed with respect to the supernova).

The first observational evidence of a GRB progenitor occurred in 1998 when SN 1998bw was identified in the *BeppoSAX Wide Field Camera* error box of GRB 980425

(Galama et al. 1998). This observation raised the issue of the association of gamma–ray bursts with supernova explosions, and even though this first direct evidence of coincidence of the two phenomena was taken with caution because of the peculiarity of both events, other compelling observations followed, strongly supporting the association of -at least some- long GRBs with SNe. The most convincing example is GRB 030329 (Hjorth et al. 2003, Matheson et al. 2003) with the spectral confirmation of a supernova component in its late-time afterglow. Spectroscopic evidence for SN light in a GRB afterglows was also reported for GRB 021211 (Della Valle et al. 2003), GRB 031203 (Malesani et al. 2004) and most recently for XRF 020903 (Soderberg et al. 2005). In contrast to the direct spectroscopic evidence, several cases of photometric indication of rebrightening in GRB afterglows have been reported, starting with the pioneering work on GRB 980326 (Bloom et al. 1999); Zeh et al. (2005) recently claimed that in fact all afterglows of long duration GRBs show the contribution of an associated supernova, as based on the systematic analysis of the sample of GRB afterglows with established redshifts. Extensive modeling of the supernovae associated with GRBs (that is, the 'hypernovae') predicts extremely large explosion energies ($>10^{52}$ergs) (Iwamoto et al. 1998). The observations of the GRB host galaxies properties may also provide clues to the progenitors; the magnitude and redshift distribution of host galaxies are typical of normal, faint field galaxies, as are their morphologies (e.g. Djorgovski et al. 2001). However there are asserts that the host galaxies are unusually blue and that they are strongly star forming (Fruchter et al. 1999, Le Floc'h et al. 2003), thus favoring the association with a young and massive stellar population.

All the present-day knowledge inferred from afterglow observations applies only to long duration GRBs because short GRBs have not been promptly enough localized by now to allow follow-up observations. If they indeed result from compact object mergers, they are expected to reside in low-density regions and therefore a very faint afterglow is predicted from short GRBs. The very recent observation of the first localized short GRB 050509b by *SWIFT* indeed confirmed these expectations: its afterglow was more than 100 times less luminous than that of typical long bursts (Gehrels et al. 2005). Moreover, its position on the sky is near a luminous, non-star forming elliptical galaxy and the interstellar density is

expected to be very low; this finding is very promising for the compact object merger model as such systems would be preferentially found in or near large ellipticals.

One of the great prospects for GRB research is that gamma–ray bursts could be used for cosmological studies at high redshifts, as they are not affected by the dust that obscures our view of the distant universe in optical light. If the long GRBs are indeed produced by the collapse of massive stars one expects GRBs to occur out to redshifts that are far larger ($z \sim 15$) than those expected for the most distant QSOs. The potential of gamma–ray bursts as standard candles has been raised greatly by the newly discovered relation (Ghirlanda et al. 2004a) between the geometry-corrected gamma–ray energies E_γ and the peak energy in the rest-frame prompt spectrum (E_{peak}). This correlation allows a reliable estimate of E_γ, making GRBs distance indicators and therefore probes for the determination of the cosmological parameters.

Even though the physics of gamma–ray bursts has been extensively investigated and nowadays we have a standard theoretical framework for the production of GRBs that is widely accepted and within which many observations are interpreted, we are still far from having fully understood the phenomenon. In particular there are issues which cannot be reconciled with the standard model. Here I focus on three aspects:

(1) GRB prompt emission. Some of the major problems concern the origin of the prompt gamma–ray emission itself. In the current fireball scenario internal shocks give a reasonable explanation for the observed temporal structure; however, it is not clear how the observed spectrum is produced. The recent findings on the importance of an initial thermal emission phase may be the key feature for understanding the prompt radiation of gamma–ray bursts: the prominent photospheric emission (predicted by the 'standard' fireball model) is determined by the initial fireball evolution parameters. The fireball content and the energy dissipation mechanism are the major uncertainties when interpreting the observed prompt spectra; thus understanding the contribution of thermal radiation to the

total emitted energy may give a clue to the mechanisms at work;

(2) Nature of the GRB progenitor. A fundamental open question regards the association of SNe/hypernovae events to GRBs. The firm, unambiguous association of GRB 030329 with the hypernova (HN) SN 2003dh, a highly energetic SN Ic, has confirmed that at least some long-duration GRBs are observationally connected with the explosion of massive stars. The rates of GRBs and HNe are comparable within the uncertainties and appear to be a small fraction of the global SN rate (Podsiadlowski et al. 2004). However, it seems that special circumstances are required to produce HNe/GRBs and there is no fully-consistent evolutionary model for the progenitors at this time;

(3) Cosmology with GRBs. Another puzzling issue concerns the positive correlations between energetics and spectral parameters of prompt GRB emission; the robustness of the claimed correlations is still a matter of debate and no unique interpretation for them has been found so far within the internal shock model. Clearly the possible use of GRBs as tools to investigate the high redshift Universe is conditioned by the reliability of these correlations.

Thesis outline

In this work I address the above open issues regarding the GRB physics, which are currently under debate and clearly inter-connected with each other. The structure of the thesis is the following: in Chapter 2 I review the observational findings and present the 'standard model' for the interpretation of the gamma–ray burst and of the afterglow emission. In Chapter 3 the BATSE instrument and data analysis procedure which is adopted in the present work are briefly described, together with the problems associated with the instrumental limitations. The connection between gamma–ray bursts and supernovae is investigated in Chapter 4; I present the systematic analysis of the prompt emission of the sample of BATSE GRBs that have an indication to be associated with SNe. The temporal and spectral analysis of this sample revealed that indeed statistically these GRBs have peculiar properties when compared to a large sample of BATSE GRBs. In Chapter 5 I discuss the contribution from a thermal phase to the prompt emission and focus in particular on the case of GRB 990413. This burst was studied in detail because the spectral analysis

unveiled thermal emission for the whole of the burst duration, and moreover, such thermal phase was interrupted intermittently during the initial period by short intervals dominated by non-thermal radiation. This behavior was consistent with the high variability in the temporal evolution of the burst, showing the alternating dominance of the two emission mechanisms. GRB 990413 was found independently of its spectral properties and this makes the finding of this bursts even more important, because it might indicate that the observed behavior may be more common than currently known. The energetics – spectral correlations are discussed in Chapter 6; in view of their putative applicability in constraining the cosmological parameters, it is of great importance to examine closely their validity on a large sample of GRBs. Our simulations indicate that such correlations can self-consistently account for the properties of BATSE GRBs. In the last Chapter I present a final discussion on these topics and indicate future perspectives.

Chapter 2

Observational facts and theoretical progress

2.1 Introduction

In this chapter I briefly discuss the state-of-the-art in the observations of gamma–ray bursts and the constraints they impose on the theoretical scenarios. Most of the results important for the understanding of GRBs are reviewed, and the influence of individual findings in the development of the model for the origin of gamma–ray bursts is emphasized. I consider with more attention the issues related to the work presented in this thesis, while more complete reviews can be found in e.g. Piran 1999, Zhang & Mèszàros 2004, Hurley et al. 2003.

In Sec. 2.2 I describe the experimental results and the important empirical laws inferred from the observations. I also outline the properties of the host galaxies of gamma–ray bursts and the indications they may provide on the GRB progenitor. Then I present the most important empirical correlations claimed among the observed GRB properties; these were derived mostly as a tool for determining intrinsic quantities because of the very limited number of direct redshift measurements. These findings make the basis for the 'standard model' that is presented in Sec. 2.3. In the last section I review the theoretical scenarios for the central engines of GRBs, stressing the association with supernovae as

strongly corroborated by observations.

2.2 Gamma–ray burst phenomenology

The wide variety of the observed gamma-ray burst properties makes it difficult to define a 'typical' event. I summarize the global characteristics of GRBs dividing them in the prompt emission and the afterglow emission. Prompt emission is what we usually identify as the gamma–ray burst itself, while the afterglow relates to the emission occurring on longer time scales at wavelengths from X–ray to radio.

Generally there is no apparent correlation found between the prompt and the delayed (afterglow) emission; this is in agreement with the standard GRB model where different mechanisms are at work for these two phenomena, i.e. internal vs. external shocks (see Section 2.3.2). The transition has been observed in several cases: the observations of the X–ray afterglow of GRB 970228 (Costa et al. 1997) suggested that its extrapolation back in time joins smoothly with the late prompt X–ray emission. Connaughton et al. (2002) examined the late-time components in burst emission ("postburst" emission, at energies traditionally associated with the prompt emission) and found that these tail components are independent and softer than the prompt burst emission. Therefore, the possibility is open that the components of late time emission are related to the afterglow, however the relation may not be simple because not all the bursts have lower energy afterglow emission, neither all the bursts have a detected late-time tail component.

2.2.1 Prompt emission

- Temporal properties

i. The gamma–ray burst light curves display rapid variability, down to the millisecond timescale (Bhat et al. 1992, Schaefer & Walker 1999). Historically the fast varying flux has provided the key justification for the compact size of the emitting region of gamma–ray bursts (see also Section 2.3.1). Cavallo & Rees 1978 examined the processes taking place in a fireball of high-energy (MeV) photons, pointing out that a source with the energy content and dimensions inferred for GRBs would be highly

opaque. This was formalized as the 'compactness problem' and invoking relativistic motion of the source to overcome it was decisive in understanding gamma–ray burst events.

ii. The light curves are very irregular (e.g. Fig. 2.1), consisting of single or multiple peaks that may be separated or overlap with each other. The time intervals between the peaks vary (during the burst itself) and sometimes the intervals of emission alternate with long quiescent periods. Bursts with a large number of pulses in the time history are found to have larger fluences and longer durations (Quilligan et al 2002).

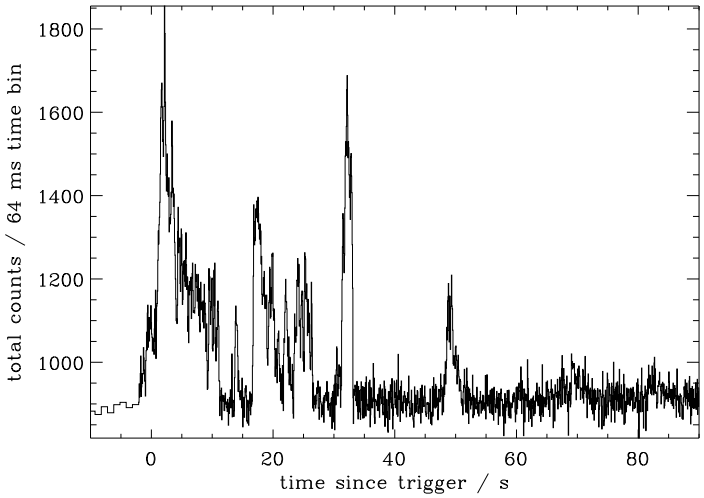

Figure 2.1: Light curve of GRB 000524 integrated over the four BATSE energy channels (approximately 30 - 1800 keV).

iii. The distribution of burst duration (in terms of T_{90}, i.e. the time interval in which the 90 per cent of the counts in the 50-300 keV is accumulated) is bimodal (Fig. 2.2); in the BATSE catalog the ratio of the number of observed long bursts (with T_{90} >2 s) to the observed short bursts (with T_{90} <2 s) is 3:1 (Piran 1999). This was first reported by Kouveliotou et al. 1993 who also found that short bursts are predominantly harder, while longer events are predominantly softer. Since the duration of the event reflects the demand on the inner engine to persist for (sufficiently) long time, it is suspected that the short- and long- duration events emerge from different types of progenitors.

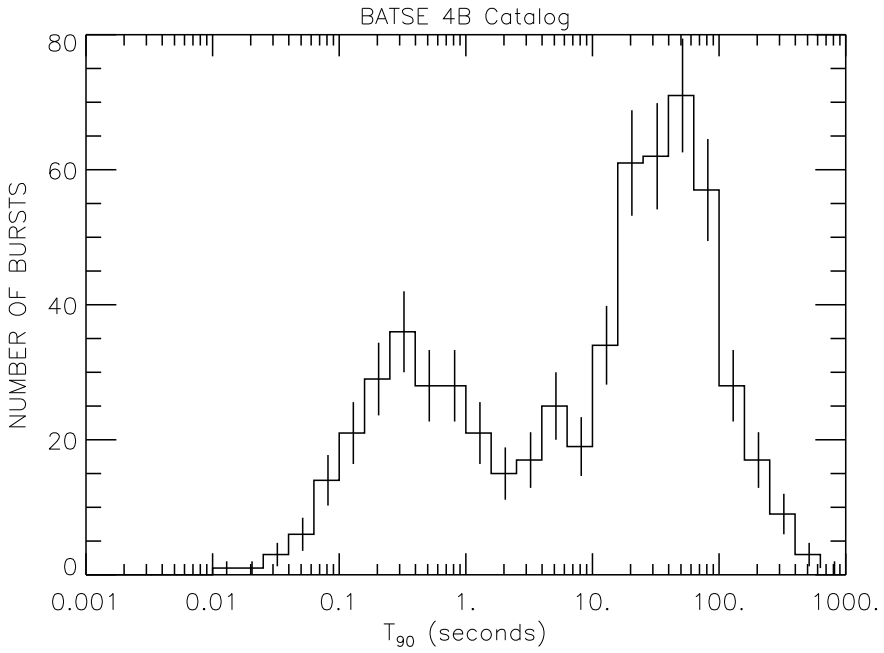

Figure 2.2: Distribution of T_{90} for BATSE bursts from Paciesas et al. 1999.

iv. The light curves consist of individual, highly variable pulses that are generally described by a FRED-like profile (Fast Rise Exponential Decay)(Norris et al. 1996). Time histories are different in different energy bands and at higher energies the overall burst duration as well as the rise and decay time scales are shorter than those at lower energies (Link et al. 1993).

- Spectral properties

i. The gamma–ray burst continuum spectrum appears to be non-thermal in the gamma–ray band, i.e. ∼0.1 -1 MeV. The GRB spectra (observed by BATSE) were investigated by Band et al. 1993 who characterized them by two smoothly connected components: at low energies a power-law continuum with an exponential cutoff, $N_E(E) \propto E^{\alpha} exp(-E/E_0)$, and a steeper power law, $N_E(E) \propto E^{\beta}$ with $\alpha > \beta$, at high energies. A larger sample of BATSE bursts was analyzed by Preece et al. 2000 who considered several spectral shapes including the Band function; they reported the

distributions of the observed sets of parameters. The peak energy of the νF_ν GRB spectrum ranges from below 100 keV to more than 400 keV, and peaks around 250 keV with only a small fraction of the spectra peaking at higher energies. Also for the spectral parameters α and β there is no universal value, but their distributions peak at $\sim$ –1 and $\sim$ –2.5, respectively.

The observed spectral parameter diversity must be addressed by any physical model of the emission processes. In the standard model (see sec. 2.3) the radiation we observe in a gamma ray burst is produced when shock-heated plasma loses its internal energy through synchrotron and inverse Compton emission (e.g. Mèszàros & Rees 1993, Katz 1994). The peak energy and the high-energy photon index β are associated to the characteristics of the particle energy distribution, while the low-energy photon index α, and in particular its harder limit, depends significantly on the radiation process at work and thus gives the possibility of distinguishing between the different scenarios for the GRB emission (Lloyd & Petrosian 2000) (see Chapter 5).

ii. Ford et al. 1995 examined the spectral evolution of the energy of the peak in νF_ν for long and bright gamma–ray bursts and found that the peak energy decreases with time (the 'hard-to-soft' evolution was found also within individual pulses in GRBs). This might indicate that the physical conditions evolve with time, or that various emission processes dominate at different times, and/or that the spectral evolution is directly related to the central engine physics. The study of the spectral evolution of the low energy photon spectra in GRBs (Crider et al. 1997) revealed that in the flux rise phase the spectrum can be harder than $E^{-2/3}$ which is the limiting photon spectral slope predicted by the optically thin synchrotron model (e.g. Tavani et al. 1996); this finding invoked alternative models that could account for hard low energy spectra (for a detailed discussion see Chapter 5).

iii. There is the possibility that there exists a population of harder gamma–ray bursts that emit most of the energy in the MeV range. It is in fact not clear whether there is an upper cutoff in the GRB hardness because of the bias by the BATSE sensitivity range ($\sim$ 50-300 keV) or GRB emission is effectively rare at MeV energies. For example,

combining the BATSE and *EGRET* (The Energetic Gamma Ray Experiment) data for GRB 941017 it was discovered a high energy tail that extended to ∼200 MeV (Gonzalez et al. 2003); the flux of the high-energy component decayed more slowly and its fluence was greater than the lower-energy component (at late time, 150 s after the trigger, the very high energy 10 - 200 MeV tail contained 50 times more energy than the main γ-ray energy band, i.e. 30 keV - 2 MeV). However, these high energy components are found in only few cases and this issue will be probably settled by the forthcoming high energy missions *AGILE* and *GLAST*.

iv. Recently X-ray rich gamma–ray bursts (XRRs) and X-ray flashes (XRFs) have been discussed in the context of being a natural extension of gamma–ray burst events toward softer energy regimes. XRFs is the term used for events whose energy fluence in the X–ray energy band (2-30 keV) is larger than that in the gamma–energy band (30-400 keV), while XRRs are the events intermediate between XRFs and 'classical' GRBs. Sakamoto et al. 2004 studied 45 GRBs observed by *HETE-2*, focusing on the properties of XRFs and XRRs; he found that the spectral properties of the XRFs and XRRs are similar to those of gamma–ray bursts, except for the fact that the values of the peak energy and the energy fluence of X–ray flashes are much smaller. This finding was interpreted as the strong evidence that all three kinds of bursts arise from the same phenomena (Fig. 2.3).

2.2.2 Afterglow emission

The afterglow emission is the X–ray, optical/infrared and radio emission following the gamma–ray burst on longer time scales. It was predicted (Katz 1994, Mèszàros & Rees 1997) before its discovery as a consequence of the evolution of the physical conditions responsible for the GRB event. In the standard fireball model the afterglow is produced when the relativistic ejecta interact with the surrounding medium and decelerate. Therefore, the emission is expected to shift progressively to the softer energy bands as the burst remnant evolves. Early searches for GRB counterparts at in the X–ray/optical band were not successful due to the transient nature of the event and the lack of accurate localizations

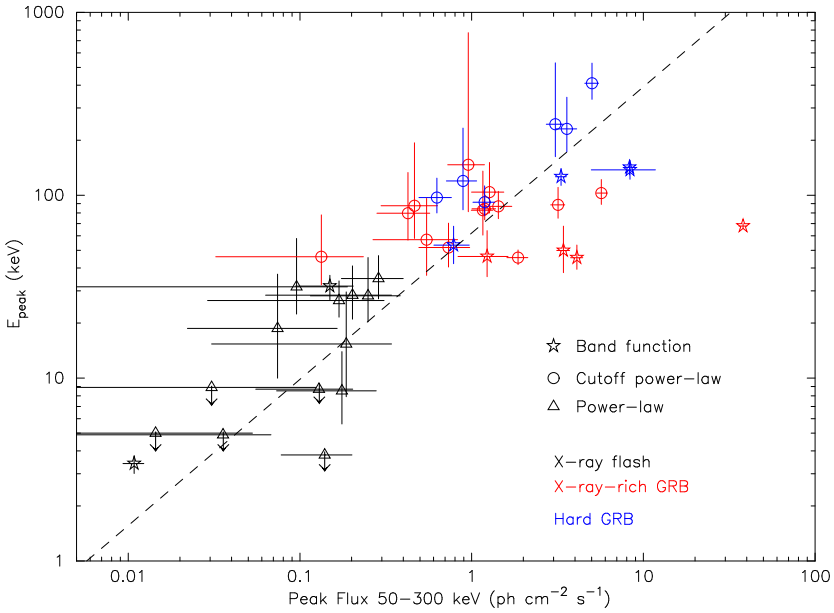

Figure 2.3: Distribution of bursts in the E^{obs}_{peak}-F(50-300 keV) plane. The dashed line corresponds to the best linear fit to the burst distribution. Different symbols correspond to the different spectral fit models. From Sakamoto et al. 2004.

of gamma–ray bursts. The breakthrough in the afterglow observations came in 1997 when the Italian–Dutch *BeppoSAX* satellite provided (within a matter of hours) the *Wide Field Camera* (WFC) arc-minute size error box for GRB 970228 that facilitated rapid follow-up observations (Fig. 2.4). The X-ray afterglow source was detected with the X-ray telescopes aboard the same satellite (Costa et al. 1997). GRB 970228 was also the first burst for which the optical afterglow was discovered (van Paradijs et al. 1997) and the close proximity to the center of a faint galaxy suggested its cosmological distance (see Sect. 2.2.5).

The first radio afterglow was detected for GRB 970508 (Frail et al. 1997); the multiwavelength observations (including millimeter, optical, infrared and X–ray counterparts) of this burst allowed the reconstruction of the afterglow spectrum (Fig. 2.5, Galama et al. 1998a). Sari, Piran & Narayan 1998 calculated the broadband spectrum and corresponding light curves within the framework of a spherical relativistic shell propagating into a uniform medium: both the spectrum and the light curves consist (in first approximation) of several power-law segments with related indices. Generally the observed afterglow light curves display a continuum power-law decay in each band. The initial rise phase has been detected

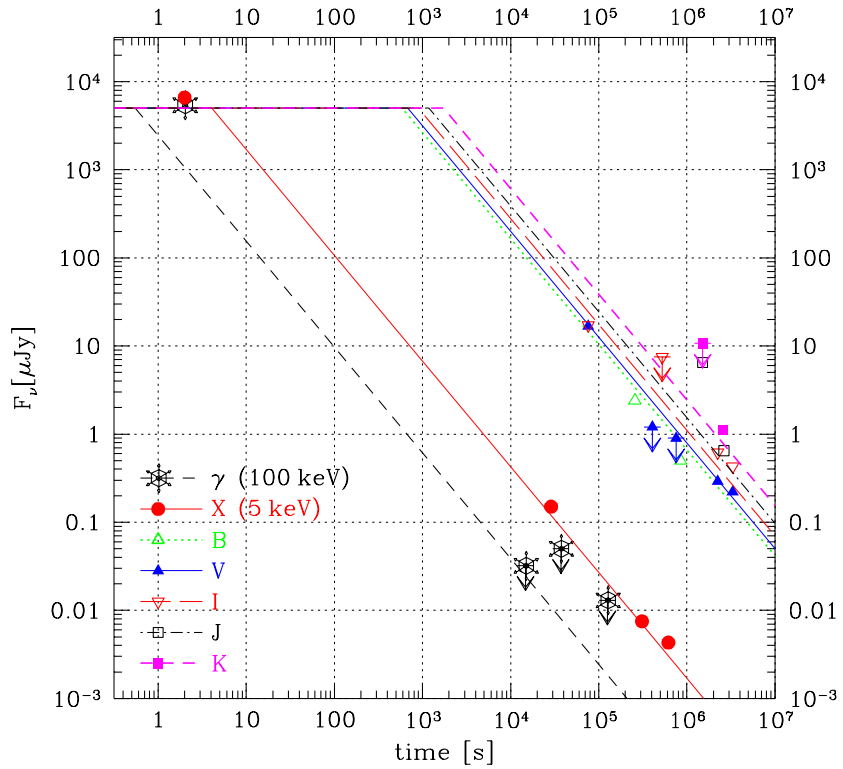

Figure 2.4: The light curves of GRB 970228 from gamma–rays to near–infrared. The lines indicate the predictions for a relativistic blast–wave; from Wijers et al. 1997.

in a few bursts in the optical band, and in many GRBs in the radio, while X–ray afterglows have been detected only in the decay phase. In some GRBs a significant steepening of the optical afterglow light curve was seen after a time t_{break} of the order of days; Rhoads (1999) explored the effects of beaming on the burst remnant dynamics and observed emission and attributed this break to the presence of a jet. Panaitescu & Kumar 2001 from modeling the observed afterglows of a handful of GRBs inferred the physical parameters of the ejecta such as the initial jet energy (10^{50}-10^{51} ergs), opening angle (1^o - 4^o) and external medium density (ranging over three orders of magnitude, from 10^{-3} to 1 cm^{-3}).

The deviations of the observed afterglow properties from the general theoretical predictions may provide a good diagnostic for the burst environment. For example, the strong fluctuations in the radio afterglows light curves at early times are interpreted as interstellar scintillation effects and permit the indirect measurements of the afterglow angular size (Goodman 1997); the existence of the class of 'dark GRBs', that is, GRBs that did not

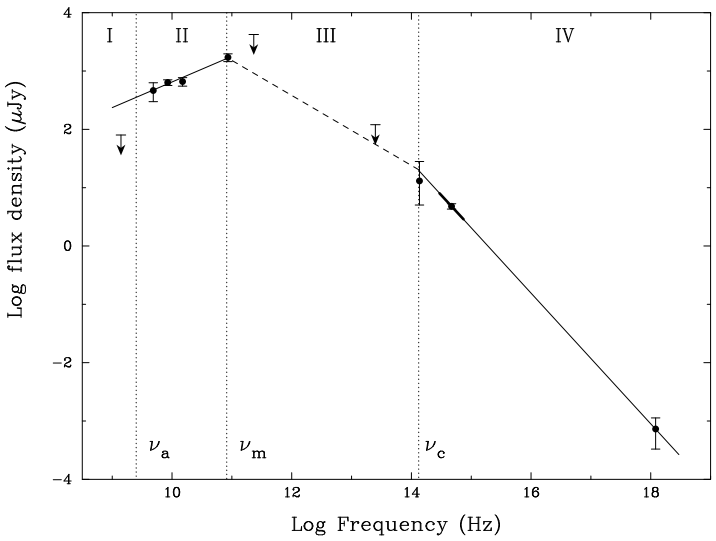

Figure 2.5: X–ray to radio spectrum of GRB 970508 12.1 days after the event. Indicated are the rough estimates of the break frequencies. From Galama et al. 1998a.

have optical afterglow bright enough to be detectable ($\sim$ 40% of GRBs that had the X–ray afterglow detected) probably indicates that they occurred in molecular clouds, where dust might extinguish the optical afterglow (Reichart & Price 2002).

Another important characteristic of the afterglow emission is the polarization; a degree of polarization at the level of a few percent has been detected in several GRBs (e.g. Wijers et al. 1999 reported the detection of significant linear polarization of 1.6% in R band of GRB 990510, 0.86 days after the trigger). High polarization would be the natural signature of synchrotron radiation, but moreover it can be used as a tool for further constraining the jet models. In the case when the ejecta is 'funneled' into a jet, and the line of sight to the observer does not coincide with the jet axis, the spherical symmetry will be broken and the polarization produced by synchrotron radiation in different parts of the shock surface is not annulled (e.g. Ghisellini & Lazzati 1999).

The first detection (at 99.3% significance level) of redshifted iron emission lines in the X–ray afterglow of GRB 970508 observed by *BeppoSAX* has been reported by Piro et al. 1999 (higher statistical significance was found for GRB 991216, Piro et al. 2000). A very large density ($\sim 10^9$ cm^{-3}, Piro et al. 1999) was inferred to be necessary to account for the observed spectral feature, having as a tentative consequence for the burst progenitor

scenarios that the burst site might be embedded in a large mass of material, consistent with the pre–explosion ejecta of a very massive star.

2.2.3 Host galaxies

The majority of the up-to-date GRB redshifts were measured from the spectroscopy of the absorption/emission lines of their host galaxies. Ground–based observations of the first well–localized gamma–ray burst, GRB 970228, revealed a close proximity with the optical light of a faint galaxy (van Paradijs et al. 1997). Subsequent *HST* imaging showed that the afterglow was embedded in a faint galaxy (Sahu et al.1997), and given the low probability of a coincidence with a random field galaxy, it was identified as the likely host of GRB 970228 (van Paradijs et al. 1997). The redshift determination (z=0.695) of the host was first reported by Djorgovski et al. 1999 as based on the [OII] 3727 emission line, and later confirmed by Bloom et al. 2001. The prompt localization of GRB 970508 and the spectroscopic observations of its optical counterpart revealed the absorption lines in an otherwise featureless continuum spectrum, that were attributed to the presence of an absorption system along the line of sight at redshift z=0.835 (Metzger et al. 1997). The continuum source (GRB 970508) thus would be either more distant and absorbed by a gas cloud at this redshift, or perhaps located physically within the cloud; the absorption placed a lower limit to the redshift of GRB 970508, $z \geq$0.835. Later spectroscopy and imaging revealed a very faint dwarf galaxy with z=0.835 nearly coincident on the sky with the transient source (Bloom et al. 1998).

Observations of the gamma–ray burst host galaxies and their immediate environment may provide important clues on the nature of the progenitors; I outline here some of the main results:

- Galama et al. 2001 studied the sample of bursts with detected optical and X–ray afterglows. They found evidence for high column densities (10^{22}-10^{23} cm^{-3}) of gas around the burst site, indicating the possibility that GRBs were located inside large molecular clouds. Moreover, they found that optical extinctions are 10 -100 times

smaller than expected from the high column densities. This favors the theoretical models in which the hard radiation from GRBs might destroy the dust in the burst environment, 'opening the path' for the optical afterglow to escape from the cloud.

- The K-band photometry of a sample of GRB host galaxies (for which an optical and/or radio afterglow was identified) at redshifts $0.5 \leq z \leq 1.5$ revealed (Le Floc'h et al. 2003) that they exhibit very blue colors, comparable to those of faint blue star-forming sources at high redshift. They are also sub-luminous in the K-band, suggesting a low stellar mass content. The absolute B magnitudes for the whole sample of GRB host galaxies with known redshifts indicate that those are statistically less luminous than the faint blue sources which mostly contributed to the B-band light. This points to the formation of GRBs being favored in systems with very low luminosities and, therefore, low metallicities (Le Floc'h et al. 2003).

- Lyα emission lines detected in several hosts have rest frame equivalent widths larger than 20 $\AA$; this is found in only $\sim$25% of the Lyman-Break selected galaxies at similar redshifts (Fynbo et al. 2003). Lyα emission with EW larger than 20 $\AA$ is locally found only in starburst galaxies with low metallicity. Also Sokolov et al. 2001 showed that broad-band optical spectra of GRB host galaxies are best fitted by the spectral properties of template spectral energy distributions of starburst galaxies. This evidence seems to suggest a preference of GRB progenitors to be metal-poor.

- Bloom et al. 2002 found from the *HST* observations of a sample of GRB host galaxies the consistent offset of gamma–ray bursts from their apparent host galaxy centers (the median projected angular offset is $0.''17$). This suggests a strong connection of GRBs with regions of detectable rest-frame ultra-violet light of their hosts. Since UV light is predominantly produced by young and massive stars, it provides strong evidence for the connection of GRBs to star formation regions.

- Christensen et al. 2004 by analyzing the spectral energy distributions of GRB host galaxies found them to be similar to young starburst galaxies with low extinction; a comparison of UV star-formation rates with those of high-redshift galaxies in the

Hubble Deep Fields shows that GRB hosts are similar to the field galaxies with the largest specific star formation rates.

2.2.4 Spatial distribution

The afterglow observations provide the most direct proof of the gamma–ray burst cosmological origin; however even before the first redshifts measurements established the cosmological nature of GRB sources, *BATSE* observations of a large sample of GRBs provided strong evidence of their cosmological nature.

The information on the cosmological distribution of the sources can be obtained from their apparent flux (or count) distribution. For a spatially extended homogeneous distribution of sources, in an Euclidean space, the cumulative count distribution follows the -3/2 law, that is $N(>C) \propto C^{-3/2}$, where $N(>C)$ is the number of bursts with more than C counts. The observations indicate a much flatter distribution (Fig. 2.6) that is characterized by a paucity of weak bursts compared with what would be expected for a homogeneous distribution (Meegan et al. 1992); the data are compatible with the distribution expected for a cosmological population. The statistical test for the hypothesis that the observed GRB distribution is drawn from a spatially homogeneous sample yields $< V/V_{max} > \sim 0.3$, while the average value characteristic of a homogeneous distribution is 1/2 (Meegan et al. 1992). The distribution in Galactic coordinates of the locations of 1637 GRBs from the fourth revised *BATSE* catalog is shown in Fig. 2.7 and it appears highly isotropic. The dipole and quadrupole moments (e.g. Hartmann & Epstein 1989) characterizing this distribution are $< \cos\theta >$=–0.025± 0.014 and $< \sin^2 b - 1/3 >$=–0.001± 0.007, and these deviate from the values expected for an isotropic distribution (after correction for the anisotropic sky exposure) by -1.1, and $+0.4\sigma$ respectively (Paciesas et al. 1999), and are thus consistent with isotropy. Both of these results, the isotropy and non-homogeneity of gamma–ray bursts sources, were the first strong pieces of evidence for their cosmological origin and the huge energetics involved in these events.

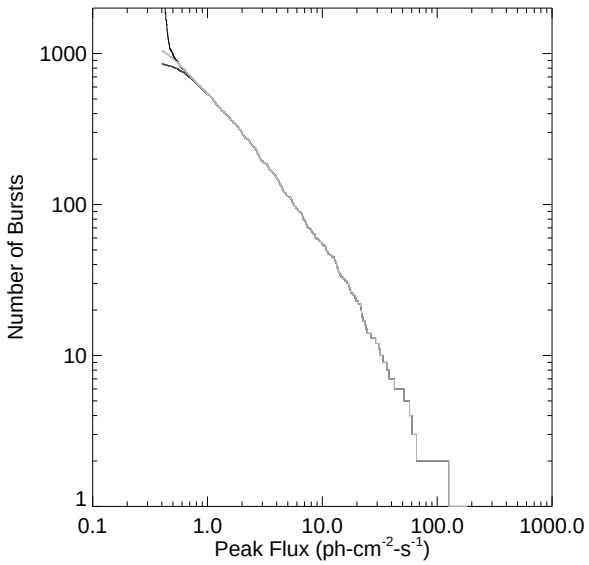

Figure 2.6: Cumulative log N - log P distributions for the events above the trigger threshold on 256 ms timescale. Near the trigger threshold, the distribution diverges into three distinct branches which illustrates how the instrument trigger threshold influences the measurement of the GRB population intensity distribution near threshold. That is, the BATSE sensitivity is strongly dependent on the burst spectrum, and the three different peak flux distributions were calculated using different peak energies E_p in the Band spectral representation. From Paciesas et al. 1999.

2.2.5 GRBs and cosmology

The discovery of GRBs at high redshifts (GRB 971214 at z=3.4, Kulkarni et al. 1998; GRB 000131 at z=4.5, Andersen et al. 2000) and the theoretical considerations on the properties (mass and metallicity) of possible GRB progenitors (see Heger et al. 2003) open the possibility to use gamma–ray bursts as a tool for studying the early universe, particularly the very first population of stars, the intergalactic medium and the star formation rates in regions where the optical estimates are affected by dust. However the number of gamma–ray bursts with measured redshifts is only a small fraction of the total number of bursts detected by the present space missions and therefore a larger sample of GRBs with measured redshifts would be required to test/calibrate the relevant correlation used to make GRBs standard candles.

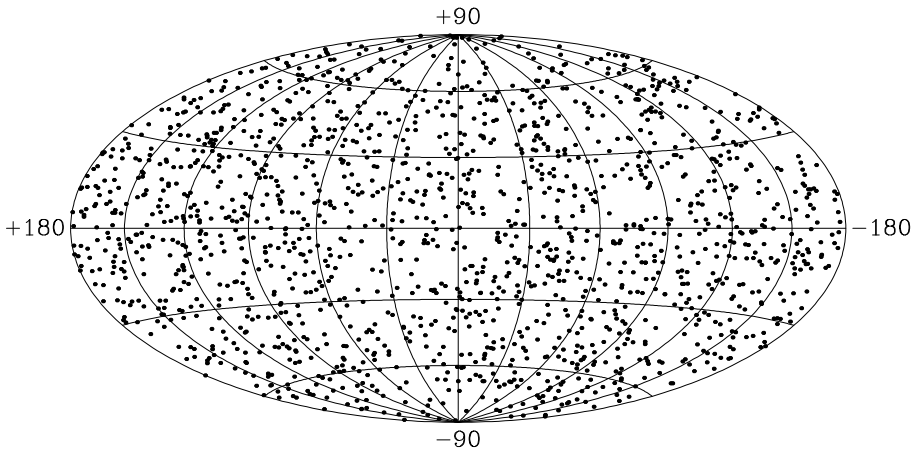

Figure 2.7: Sky distribution of 1637 GRBs from the BATSE 4B revised catalog in Galactic coordinates. From Paciesas et al. 1999.

The first claims of a possible way of estimating the GRB energetics regarded the standard energy release in gamma–ray bursts: Frail et al. 2001 derived the GRB jet opening angles based on the observed broadband achromatic breaks in their afterglow light curves. By accounting for the fact that the true energy released, E_γ, is smaller than the isotropic energy E_{iso} by the beaming fraction (Rhoads 1999, Sari et al. 1999) $f_b = (1-\cos\theta_j) \cong \theta_j^2/2$, they found that, correcting the isotropic energies for the derived distribution of jet opening angles (that span from 1^o to more than 25^o, with a strong concentration near 4^o), the prompt gamma–ray burst energy clustered around 5×10^{50}ergs. Examining a larger sample of GRBs and incorporating more realistic measurements of the ambient density, Bloom et al. 2003 considered the possibility of constructing a GRB Hubble diagram; however, they concluded that the observed scatter was simply too large to make any meaningful impact on present cosmographic measurements.

The analysis of gamma–ray burst temporal evolution yielded correlations between empirical and intrinsic properties that may be used as redshift indicators for the bursts without afterglow observations. For a sample of six bursts with known redshifts Norris et al. 2000 found evidence that the spectral evolution time scale (spectral time lag τ) is anticorrelated with the intrinsic peak luminosity, $L/10^{53}$ erg s$^{-1} \propto (\tau/0.01s)^{-1.14}$. Fenimore & Ramirez-Ruiz (2000) (see also Reichart et al. 2001) derived a Cepheid-like relationship between the time variability of the burst light curves and the absolute luminosity of the

burst. They discovered that intrinsically less luminous bursts have smoother, less-spiky emission ($L/10^{56}$ erg s$^{-1} \propto V^{3.3}$; V is the measure of variability defined as the difference between the GRB light curve and its smoothed version). This correlation was then used to derive the redshifts of 220 GRBs from the *BATSE* catalog and explore the possible cosmological consequences, e.g. the event rate and the evolution of the GRB luminosity function. However, the large scatter and the very limited sample of the GRBs used for calibration of both relations has prevented their wider application to bursts without determined redshifts.

By studying the spectral and energetic properties of twelve gamma–ray bursts with redshift estimates detected by *BeppoSAX*, Amati et al. 2002 found a positive correlation between the total isotropic energies E_{rad} and the peak energy E_{peak} (in νF_ν spectral representation): $E_{peak} \propto E_{rad}^{0.52}$ (see also Lloyd et al. 2000a). Yonetoku et al. 2004 combined the data for E_{peak} and the peak luminosities of GRBs detected by *BeppoSAX* and *BATSE* and discovered a relation between the spectral peak energies and the peak luminosities, $L/10^{47}$ erg s$^{-1} \sim (E_{peak}(1+z)/1$ keV$)^{2.0}$. They then estimated the redshifts of a large sample of long duration GRBs from the *BATSE* catalog without known distances. Based on this new sample, the GRB event rate was inferred and turned out to well correlate with the star formation rate for $0 \leq z \leq 2$, but for higher redshifts remained constant. Finally Ghirlanda et al. 2004a derived the bolometric isotropic equivalent energies for the largest possible sample of 24 GRBs with determined redshift and estimated jet opening angle, and corrected the energy for the collimation angle. They discovered a very tight correlation between the rest frame peak energy and the collimation corrected energy E_γ, namely $E_{peak}/$ keV $\sim (E_\gamma/10^{50}\text{erg})^{0.7}$ (Fig. 2.8); the small spread of this correlation allowed, for the first time, the use of GRBs as cosmological tools for constraining cosmological parameters and provide a probe for the intermediate-redshift universe evolution (z$<$ 10)(Ghirlanda et al. 2004b). These correlations are going to be discussed further in Chapter 6, in connection to their validity for the whole sample of detected gamma–ray bursts and to the plausible consequences on the GRB formation rate and the evolution of their luminosity function.

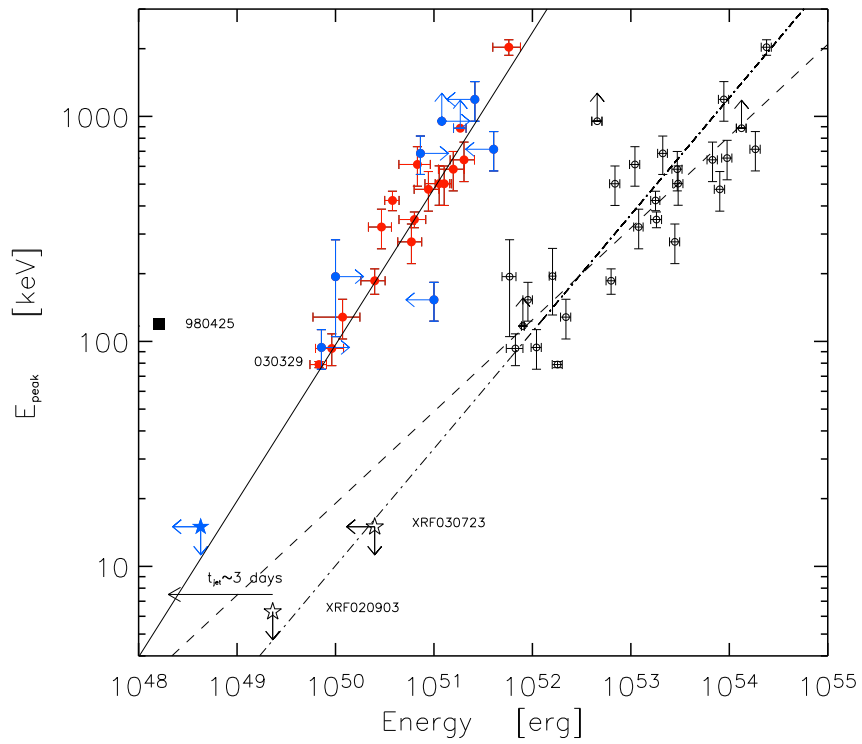

Figure 2.8: Rest frame spectral peak energies vs. bolometric energies for the sample of GRBs with measured redshift. The lines represent the correlation reported by Amati et al. 2002 (dot-dashed line), the Ghirlanda et al. 2004 fit for the extended set of data (dashed line) and the best fit to the correlation of E_{peak} with the isotropic energies, i.e. corrected for the collimation angle (solid line). Black symbols present the quantities obtained for the isotropic energy release, while the colored symbols present those obtained after the correction of the emitted energy for the collimation. From Ghirlanda et al. 2004.

2.3 The standard model

2.3.1 The compactness problem

Phenomenological considerations have led to the general agreement that, independently of the mechanism responsible for the primary energy production in gamma–ray bursts, the emitting material producing the prompt and afterglow emission must be moving relativistically. This argument stems from the solution of the 'compactness problem' for GRBs (Cavallo & Rees 1978, Goodman 1986); that is, given a typical GRB fluence $F \sim 10^{-7}$ erg cm^{-2}, and distance $D \sim 3$ Gpc, the total (isotropic) energy at the source is huge,

E=$4\pi D^2 F$ $\sim 10^{50}$ ergs. This has to be released within the short variability time scales $\sim$ 10 ms, i.e. in a volume of linear dimensions $R \sim c\delta t$=3 $\times$ 10^8 cm (δt/10 ms); assuming that a fraction f_p of photons is above the energy threshold for the electron–positron pair production $\sim 2m_e c^2$, the optical depth for this process is:

$$\tau_{\gamma\gamma} = \frac{f_p \sigma_T F D^2}{(c\delta t)^2 m_e c^2} \sim 10^{13} f_p (F/10^{-7}\text{erg cm}^{-2})(D/3\text{Gpc})^2(\delta t/10\text{ms})^{-2} \qquad (2.1)$$

where σ_T is Thomson cross section. Such a copious pair production would generate an optically thick fireball, leading to thermalization of the photons and leptons. This is inconsistent with the observed non-thermal spectrum of gamma–ray bursts. The relativistic motion of the emitting plasma (characterized by a Lorentz factor Γ) would reduce the optical depth in two ways (see the detailed discussion in Lithwick & Sari 2001): first, photons in the source comoving frame would be softer by a factor $1/\Gamma$; therefore a smaller fraction f_p of photons is above the pair production threshold. f_p is modified by a factor $\Gamma^{-2\alpha}$, where α is the photon number spectral index ($N(E)dE \propto E^{-\alpha}dE$). Second, the real physical scale of the emission site moving toward the observer with Lorentz factor Γ is $\Gamma^2 c\delta t$; this effect modifies the optical depth by a factor of Γ^{-4}. The combination of these two effects reduces the optical depth to

$$\tau_{\gamma\gamma} = \frac{f_p \sigma_T F D^2}{\Gamma^{2\alpha+4}(c\delta t)^2 m_e c^2} \sim \frac{10^{13}}{\Gamma^{2\alpha+4}} f_p (F/10^{-7}\text{erg cm}^{-2})(D/3\text{Gpc})^2(\delta t/10\text{ms})^{-2} \qquad (2.2)$$

and for a typically observed spectral index $\alpha \sim 2$, the lower limit to the Lorentz factor Γ required to satisfy the demand of an optically thin source is $\Gamma > 10^{13/2\alpha+4} \approx 100$.

A pure photon fireball fails to account for the duration and time structure observed in gamma–ray bursts, that is, it would result in a very short burst, with a quasi thermal spectrum emitted after the expanding fireball becomes optically thin (Goodman 1986, Paczyński 1986). If the initial energy deposition is accompanied by a baryon polluted flow (Shemi & Piran 1990, Mèszàros & Rees 1992), during the expansion of the fireball the radiative energy is converted into the kinetic energy of the entrained baryons. In this case baryons carry essentially all of the energy of the initial fireball, and the main emission of the

observed gamma–ray radiation occurs when the bulk of the kinetic energy of the baryons is re-randomized and radiated away.

Assuming that gamma–ray bursts result from the slowing down of ultra-relativistic matter, the total amount of the allowed baryonic mass (in order to obtain high Lorentz factors) is $M_0 = E_0/\Gamma c^2 \leq 10^{-5} M_\odot$. The value of the initial baryon loading $\eta = E_0/M_0 c^2$ thus determines the dynamics of the fireball, in particular the relative amount of energy in the bulk kinetic form and in $e^{\pm}$ /radiation form. From the dynamical point of view, initially the fireball bulk Lorentz factor Γ increases linearly with distance/radius r, and as the expansion occurs at the expense of the comoving thermal energy, the temperature T drops as r^{-1}. After the maximum bulk Lorentz factor $\eta = E_0/M_0 c^2$ is reached, the fireball coasts with constant velocity. As the fireball expands the photon density and the typical photon energy drop; at a radius $r_{ph} \sim 10^{12} - 10^{13}$ cm the fireball becomes optically thin and (although most of the energy is converted to the kinetic energy of the baryons) some energy will be radiated away with a thermal, approximately black body, spectrum. This is the first signal expected from the fireball.

2.3.2 Internal/External shocks

The production of the observed gamma–rays is usually associated to the formation of shocks within the relativistic flow itself (Rees & Mèszàros 1994). Internal shocks are expected to arise in the flow if e.g. the initial distribution of Lorentz factors (i.e. the time dependence of the ejection velocity of the outflow) is highly variable. The flow is usually modeled by a succession of relativistic shells of different Lorentz factors, mimicking the time dependence of the properties of a wind, and the shocks take place when faster-moving shells catch up with slower ones. A collision of two shells is the elementary process that produces a single pulse in gamma–rays. Thus in the internal shock scenario the temporal structure (e.g. pulse durations) directly reflects the temporal behavior of the inner engine (Ramirez-Ruiz & Fenimore 2000).

In the standard scenario one considers an 'inner engine' with a variability time scale δt (that can be down to the order of ms) and a typical distance between adjacent shells $c\delta t$. If we suppose that a rear shell moves faster than a leading one, i.e. $\Gamma_2 \gg \Gamma_1 \sim \Gamma$,

the internal shock takes place at a typical radius

$$r_{IS} \simeq 2c\delta t\Gamma^2 \simeq 6 \times 10^{13}\mathrm{cm}\ (\Gamma/100)^2\ (\delta t/0.1\ s) \tag{2.3}$$

where Γ is the typical Lorentz factor and δt is roughly equal to the observed fluctuations in the light curve of the burst. In internal shocks the relative kinetic energy of the shells is converted into random/internal energy. The observed prompt gamma–ray burst spectrum is generally considered to be due to the synchrotron/inverse Compton emission from leptons accelerated in such shocks.

The main difficulties of this model are: 1) a rather low efficiency for the conversion of the kinetic energy of the flow into internal energy as only the relative energy of the shells can be randomized, and 2) the synchrotron emission process cannot simply account for the hardness of the low energy part of the spectrum observed in some GRBs.

The afterglow would be produced when the relativistic flow -after most shells have merged- interacts with the ambient medium and decelerates. Approximately (for a short enough fireball duration) the deceleration radius corresponds to the distance where the ISM mass collected by the fireball is equal to $(1/\Gamma)$ of its rest mass, i.e. $M_{ISM} \simeq \Delta M/\Gamma$, where ΔM is the total baryon loading of the fireball. For a constant density medium n, this radius is

$$r_{ES} \simeq (5.4 \times 10^{16}\mathrm{cm})(E_{iso,52}/n)^{1/3}(\Gamma/100)^{-2/3}. \tag{2.4}$$

Sari et al. (1998) calculated the broadband spectrum and corresponding light curve of synchrotron radiation from electrons accelerated by the shock into a power-law distribution ($N(\gamma_e) \propto \gamma_e^{-p}$). Both the spectrum and the light curve consist of several power-law segments with related indices, $F(\nu, t) \propto \nu^{-\beta}t^{-\delta}$; the breaks correspond to the critical frequencies of transitions between different regimes of emission (see e.g. van Paradijs et al. 2000).

The simplest model is derived under the assumptions of: i) isotropic fireball; ii) uniform ambient density; iii) synchrotron emission of the electrons; iv) constraints on the

microphysical parameters (e.g. no evolution, $p > 2$). It predicts that the evolution of the fireball with radius r and with the observer's time t follows

$$\Gamma \propto r^{-3/2} \propto t^{-3/8}, \quad r \propto t^{1/4} \tag{2.5}$$

$$\Gamma \propto r^{-3} \propto t^{-3/7}, \quad r \propto t^{1/7} \tag{2.6}$$

The first scaling is valid for an adiabatic evolution of the fireball, i.e. in which the energy $E \propto nr^3\Gamma^2$ remains constant. This is generally valid at late epochs (later than hours) in all afterglows and at early epochs for many afterglows. The second scaling is valid for the evolution of a 'radiative' fireball in which the total fireball energy decreases prominently due to radiative losses, while the momentum $\propto nr^3\Gamma$ is conserved. According to the current afterglow observations this behavior does not seem to occur and usually a quasi-adiabatic treatment is adopted with small radiative corrections.

2.4 Progenitor scenarios

Despite of the rather general agreement on the model for the prompt gamma–ray burst emission and for the afterglow of long GRBs, the issue of the nature of the 'inner engine' powering the energy release has remained unclear. I discuss various models and the observations that helped to discriminate among the proposed scenarios.

The observational clues for constraining the plausible progenitors refer to:

- GRB energetics: the 'inner engine' must be able to generate the total energy involved $\sim 10^{51}$ ergs, including the acceleration of a baryonic load $\sim 10^{-5} M_\odot$ to relativistic velocities.

- GRB variability time scale: the source needs to be variable on the observed timescales $\delta t \sim 10$ ms, but also to last for $t \sim 10 - 100$ s in the case of long bursts (for short bursts $\delta t/t \ll 1$ still holds). This excludes progenitor models leading to simple single explosions as the engine needs to persist for longer times.

- GRB occurrence rate: the rate of gamma–ray bursts is estimated to be $\sim 3 \times 10^{-5}$ yr^{-1} per galaxy (Podsiadlowski et al. 2004) taking into account an effective (but

uncertain) beaming angle[1] of 5^0. This rate is however uncertain as it was derived from the sample of GRBs with afterglow observations, i.e. long GRBs, and there is no robust evidence that the selection effects are the same for long and short events.

The models for gamma–ray bursts that can account for the observed properties come in two classes: i) double neutron star mergers, and black hole/neutron star mergers that are capable of producing short gamma–ray bursts, and ii) core collapses of very massive stars ('collapsar' and 'supranova' models) that are expected to give rise to long gamma–ray bursts. In both classes of models the gamma–ray burst follows the formation of a black hole with a debris torus around it; the energy extraction in such systems comes either from the spin energy of the black hole or from the gravitational energy of the orbiting debris, requiring however complex mechanisms of transformation of energy into outflowing relativistic plasma.

The gravitational energy available in the debris torus is generally postulated to be extracted in two modes:

1. Woosley (1993) considered gamma–ray bursts from stellar mass accretion disks around black holes; he suggested that the thermal energy of the torus produced by viscous dissipation may be deposited effectively by neutrino annihilation along the rotation axis and give rise to a relativistic pair-dominated wind. Neutrino emission is capable of extracting approximately 10^{50} ergs s^{-1} inside the accretion column. The prediction is that collapsars will always make supernovae similar to SN 1998bw (see sect.2.4.1); hard, energetic bursts shorter than a few seconds are difficult to produce in this model.

2. The mechanism proposed by Narayan et al. (1992) (see also Paczyński 1991) is based on magnetic fields threading the torus. Mèszàros & Rees (1997) estimated that even for very low efficiencies of the conversion of rest mass into magnetic energy a burst of isotropic energy 10^{53} ergs could be easily produced.

[1]The result by Podsiadlowski et al. 2004 is based on the jet opening angle estimate by Frail et al. 2001 (correction factor for beaming ~ 500) and on the estimate that a fraction of about 5% of observed SNe Ib/c are hypernovae (see Section 2.4.1); it implies that the rates of GRBs and hypernovae are quite comparable. However Della Valle et al. 2004 argue that the ratio GRBs/hypernovae spans the range $\sim 0.2 \div 0.03$, taking into account the result by Guetta, Piran & Waxman 2005 for the GRB beaming correction (correction factor ~ 75), and inferring for the fraction of hypernovae in the sample of SNe Ib/c $\sim 8\%$.

However, a black hole formed either from a coalescing binary or from the core-collapse of a massive star could contain a reservoir of spin energy larger than the torus. This energy is in principle available via the Blandford-Znajek mechanism, which can extract $\leq$10% of a near-maximally rotating Kerr black hole rest mass, leading to isotropic energies $>10^{53}$ ergs (Mèszàros & Rees 1997a).

2.4.1 The Collapsar/Supranova models

The progenitor models involving a black hole-torus system resulting from the core collapse of a massive star predict the launch of a fireball either simultaneously with a supernova (SN) or with a significant time delay (days to years), generally depending on the mass and angular momentum of the progenitor core and the details of the collapse.

The collapsar model was initially addressed by Woosley (1993) who considered the outcome from the collapse of a single Wolf-Rayet star endowed with rotation (the so called 'failed' supernova). The main ingredients of this model are a sufficiently massive core to form a black hole and a sufficient rotation rate at the time of the collapse to form a disk (Heger & Woosley 2002). MacFadyen & Woosley (1999) performed the detailed numerical calculations of the relativistic outflow propagation through the stellar envelope of a collapsing star.

According to their model ('collapsar' or 'hypernova' model) the candidates for the production of gamma–ray bursts are massive stars of M$\sim$25-35$M_{\odot}$ (helium core mass $\sim$9-14$M_{\odot}$) in which the iron-core collapse does not produce an outgoing shock but instead forms a black hole of a few solar masses. For angular momentum in the range (3×10^{16}cm^{2}s^{-1} < j <2×10^{17}cm^{2}s^{-1}) an accretion disk forms at a distance at which the gravitational binding energy can be efficiently radiated. Initially the infall of the matter along the rotational axis is uninhibited and the depletion funnel forms in the polar regions. The accretion of the disk occurs at the rate $\sim$0.1 M$_{\odot}$s^{-1}. The process by which the energy is deposited is neutrino annihilation, which can deposit up to $\sim10^{50}$ergs s^{-1} in the polar regions. The GRB production stage starts several seconds after the initial collapse and continues for another

$\sim$15 s, after which the accretion rate starts to decline. The energy deposited near the black hole and along the rotation axis gives rise to a jet that blows aside what remains of the star within 10^o-20^o from the poles; a relativistic Lorentz factor $\Gamma \sim 100$ is reached after the jet erupts from the surface of the star. (Zhang et al. 2003 speculate that the breakout of the relativistic jet and its collision with the stellar wind produce a brief transient with properties similar to the class of short/hard GRBs).

Because of the sensitivity of neutrino efficiency on the accretion rate, the jet produced by neutrino energy deposition can change in response to the accretion rate (e.g. varying the accretion rate from 0.05 to 0.1 $M_\odot s^{-1}$ will change the energy deposition by a factor of 20). Thus a highly variable energy source for the jet is expected.

The 'supranova' model (Vietri & Stella 1998) was initially introduced to solve the baryon-contamination problem, as hypernova explosions are suspected to arise in the massive star environment whose winds carry out large amounts of mass. The model involves a two step collapse: first, the supernova explosion leaves behind a rotationally supported supramassive neutron star; the gamma–ray burst is assumed to arise in the second phase, when the neutron star implodes to a black hole by gradual angular momentum loss via a pulsar wind. The baryon-clean environment is obtained during the phase in which the neutron star-driven wind effectively sweeps up the baryonic matter remained in the vicinity of the central object. The time delay between the supernova event and the gamma–ray burst could be large, ranging from months to years (Inoue et al. 2003). This model however cannot account for the short time delays between the supernova and gamma–ray burst, as suggested by some observations (SN–GRB time lag is found to range from +1.5 to -8 days, see Della Valle et al. 2004 for a review; a negative time lag indicates that the supernova explosion precedes the gamma–ray burst); also, lacking the star envelope the collapse cannot produce a long gamma–ray burst (the time scale of the burst is determined by the accretion time of the disk; Narayan et al. 2001 argue that long lived $\sim$ 50 s accretion disks must be large and hence extremely inefficient) and the collimation mechanism is not clear.

Observational evidences

Present observations provide strong support to these types of scenarios; the pieces of evidence for the association of gamma–ray burst with supernovae (SNe) are based on the direct temporal and directional coincidence of the two events, and/or on the signatures of the accompanying SN event in the late-time afterglow. The very first direct observation of the GRB/SN association came in 1998 with the discovery of the optical transient in the *BeppoSAX WFC* error box of GRB 980425 (Galama et al. 1998). The optical light curve and the spectrum revealed that the transient is a very luminous Type Ic supernova, SN 1998bw. Both events were however peculiar with respect to their classes: the gamma–ray burst was 'underenergetic' by 4 orders of magnitude with respect to 'typical' GRBs (its total energy budget being $\sim 10^{47}$erg), and its light curve consisted of a very smooth single peak. SN 1998bw had a peak luminosity unusually high ($\sim 10^{43}$ erg s^{-1}) compared with typical Type Ic SNe, implying the production of large quantities ($\sim 0.7 M_{\odot}$) of ^{56}Ni (Galama et al. 1998). The extensive modeling (Iwamoto et al. 1998) showed that the SN 1998bw spectrum can be reproduced by an extremely energetic explosion of a massive carbon+oxygen star that has lost its outer envelope, with kinetic energies more then ten times what previously known for SNe Type Ic (Fig. 2.9).

As a natural consequence of a physical relation between the explosion of massive stars and gamma–ray bursts, supernova light should become prominent in the afterglow flux, and probably even dominate under favorable conditions. The most convincing example was GRB 030329 (Hjorth et al. 2003) at z=0.1685 with spectral confirmation of the presence of SN emission in its afterglow (see sect. 4.2) (Matheson et al. 2003); spectroscopic evidence for SN light was later also reported for GRB 021211 (Della Valle et al. 2003), GRB 031203 (Malesani et al. 2003) and most recently for XRF 020903 (Soderberg et al. 2005).

More indirect indications are based on the photometric detection of 'excess' light (or 're-brightening') in gamma–ray burst afterglows with respect to the decaying light curve (see e.g. Zeh et al. 2004, Bloom et al. 1999, Garnavich et al. 2003), suggesting the presence of an underlying source coincident with the GRB. The pioneering work was done by Bloom et al. 1999, who reported the GRB 980326 optical transient rebrightening approximately 3 weeks after the burst (Fig. 2.10). They found a bump in the flux light curve ~60

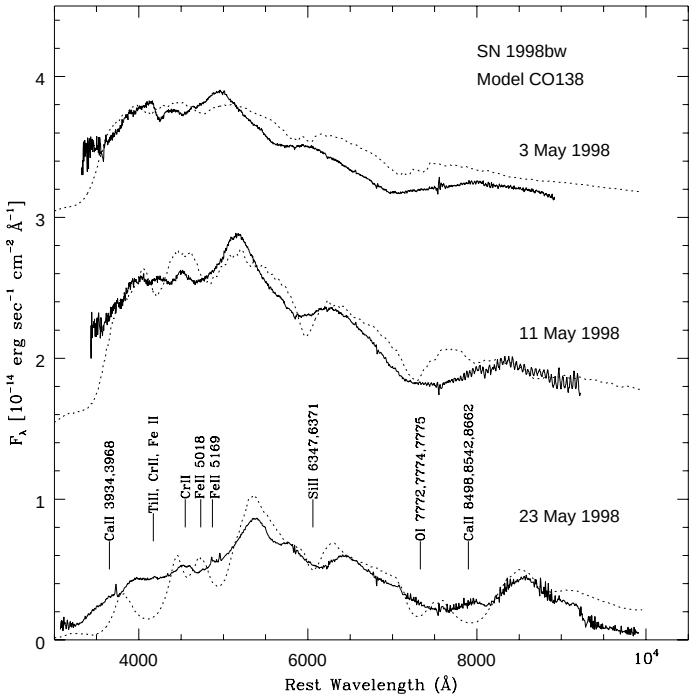

Figure 2.9: SN 1998bw: three observed spectra where the galaxy background has been subtracted. They are compared with the synthetic spectra computed with a Monte Carlo code using model CO138 to predict the outcome of a collapse-induced explosion of a massive carbon + oxygen (C+O) star of $M_{CO} = 13.8 M_\odot$. From Iwamoto et al. 1998.

times larger than the extrapolation from the rapid decay seen at earlier times. Possible explanations for this emission were investigated. Panaitescu et al. 1998 suggested that the rebrightening seen in GRB 970508 may be due to a shock refreshment/delayed energy injection by the extremely long-lived central engine that produced the GRB. In GRB 980326 the very red spectrum on 23 April 1998 ($F_\nu \sim \nu^{-2.8}$) rules out a synchrotron origin for the rebrightening phase (for the typical synchrotron spectrum the expected flux would be $F_\nu \propto \nu^{-1}$). Alternatively, GRB could have occurred in a dusty region and the afterglow would rebrighten as the dust is sublimated by the afterglow. The observed spectral evolution of the afterglow of GRB 980326 from a relatively blue spectrum (29 March 1998) to red (23 April 1998) moves in a direction opposite to that expected in this model (Bloom et al. 1999). Thus Bloom et al. 1999 advanced the hypothesis that the observed source is due to

an underlying supernova revealed only after the afterglow emission has sufficiently faded. As the GRB redshift was $z \sim 1$, it was also the first evidence for a GRB/SN connection at cosmological distances. Zeh et al. 2004 recently reported the 'a posteriori' discovery of weak supernova excess in the afterglow light curves of a large sample of gamma–ray bursts; they also explained the general lack of a detection of a SN component from the GRBs coming from redshifts larger than ~ 0.7 by selection effects, suggesting that in fact all afterglows of long duration gamma–ray bursts contain light from an accompanying supernova.

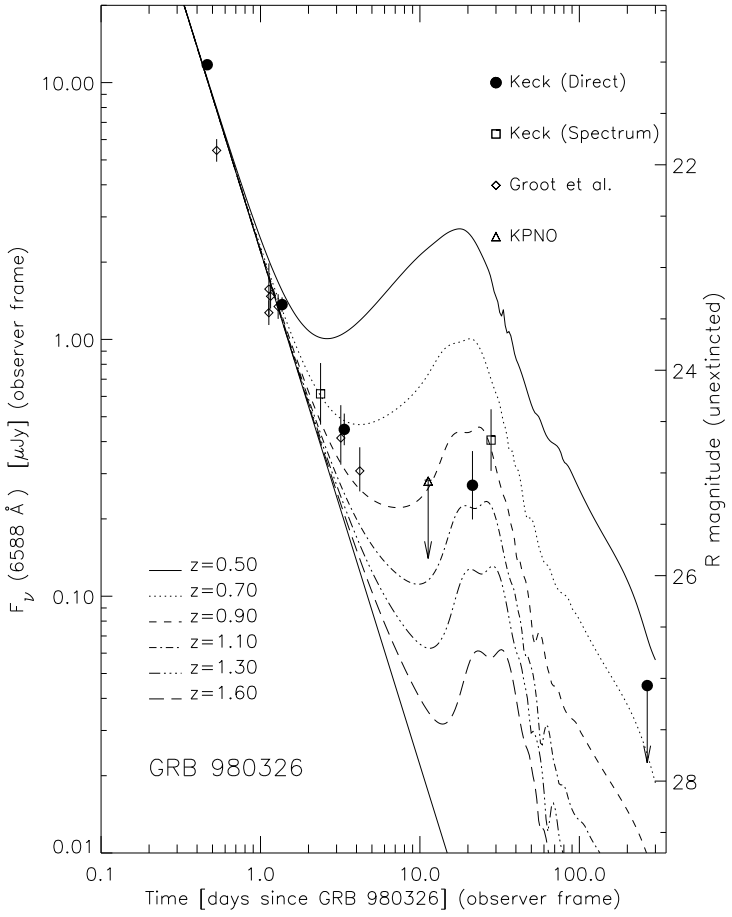

Figure 2.10: The R-band light curve of the afterglow of GRB 980326. Overlaid is a power-law afterglow decline summed with a bright supernova light curve at different redshifts. The template multi-band light curve of SN 1998bw has been used. From Bloom et al. 1999.

The further evidence pointing toward the association of gamma-ray bursts with

the death of massive stars regards the circumburst environment. As discussed in Section 2.2.3, from the observation of the host galaxies it was found that the locations of the long-duration bursts are predominantly UV regions and thus they are presumably associated with young and massive stellar populations. Furthermore, the X–ray line features reported in several afterglows by now (Piro et al. 1999) suggest the presence of pre-ejected material surrounding the burst site. The star forming region and the massive pre-explosion winds together would imply a mass–rich environment in the close burst vicinity ($\sim 10^{15}$cm).

Chapter 3

The BATSE data analysis

3.1 Introduction

Since its beginnings the evolution of the gamma–ray burst field has been closely related to the constraints imposed by the detection instruments. With the progress done in understanding gamma–ray bursts, the urge to address the details of the GRB phenomena has been growing and over the years a number of different space missions dedicated to gamma–ray surveys were launched. I focus here on the presentation of the BATSE instrument only, because a major part of the work for this thesis consisted in the analysis of the spectral and temporal properties of GRBs from the BATSE, which is presently still the most complete basis for the study of large samples of GRBs.

In this Chapter the characteristics of the BATSE instrument are described together with the main issues regarding the burst detection and the types of data it provided; the main properties of gamma–ray bursts based on the analysis of the various samples of GRBs observed by BATSE are then presented.

3.2 The BATSE instrument

The *Burst and Transient Source Experiment* (BATSE) was one of the four experiments on board the *Compton Gamma Ray Observatory* (CGRO). This satellite operated from April 1991 till June 2000 and its primary objective was to perform broad-band gamma–

ray observations (15 keV to 30 GeV) with a better angular resolution (<2 deg) and better sensitivity (10^{-7}erg cm^{-2}s) than previous missions. The BATSE instrument detected and localized more than 2000 gamma-ray bursts, providing the data for accurate spectral and temporal studies. Secondary objectives of the BATSE experiment included the study of transient sources, X–ray pulsars and solar flares.

The summaries of the first results can be found in e.g. Fishman et al. 1993, Gehrels et al. 1994. Among the major discoveries of BATSE are[1] :

- the isotropic and radially non-uniform distribution of gamma–ray bursts
- the statistical diversity of GRB time profiles and GRB spectra
- the bursting pulsar GRO J1744-28
- the discovery of several new X-ray pulsars
- the long term frequency histories of X-ray pulsars
- the terrestrial gamma–ray flashes

BATSE consisted of eight uncollimated detector modules placed on the corners of the *Compton Gamma Ray Observatory*, providing a nearly complete sky coverage. Each detector module contained two scintillation detectors, a Large Area Detector (LAD) (that was optimized for detecting transient sources and recording their time histories) and a Spectroscopy Detector (SD) (that was optimized for spectral studies of transient sources) and associated electronics[2]. An illustration of a BATSE module is shown in Fig. 3.1.

The data examined here are derived only from the Large Area Detectors. Those are 50.8 cm diameter by 1.27 cm thick sodium iodide scintillators, covered by a 0.63 cm thick plastic scintillator for charged particle rejection. Counts in the detector are produced by the conversion of the energy of gamma–rays in the NaI(Tl) crystal to visible light,

[1] http://heasarc.gsfc.nasa.gov
[2] NASA - CGRO Guest Investigator Program

which is collected in the three photo-multiplier tubes coupled to the detector and converted in a voltage pulse by a preamplifier. The pulses are amplified and shaped before being sent onto two different paths for analysis by the on-board electronics. On one branch, a (slower) pulse height analyzer (PHA) system produces a high resolution spectrum (out of 2752 linear channels) and compresses the data into 128 quasi-logarithmic energy channels. The PHA output can be further rebinned into 16 channels resulting in the medium energy resolution data types. On the other branch the pulse passes through the high-speed, 4-channel discriminator electronics and is accumulated into four integral data channels. The nominal energies of the upper three discriminators for the LADs are 60, 110 and 325 keV; the lower-level discriminator is set near 20 keV. That is, the 4 data channels have the boundaries ($\sim$ 20 - 60 keV), (60 - 110 keV), (110 - 325 keV) and ($>$ 325 keV)[3]

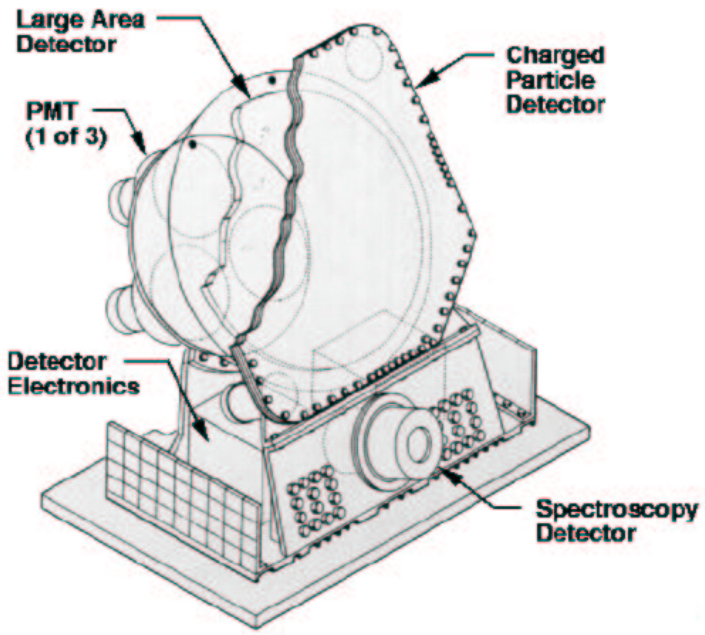

Figure 3.1: One of the eight identically configured BATSE detector modules. From NASA - CGRO Guest Investigator Program.

[3]The thresholds were however slightly changed during the mission and these are the most typical energy boundaries.

Data Types

Data from the detectors were recorded in several formats, of which the six recorded by the LADs are of primary interest for this work:

- **DISCLA.** LAD discriminator background data consisting of 1.024 s accumulation of the four discriminator channels, the total counts and the charged particle detector counts for the eight LADs. This data type is collected continuously (independently of a burst occurrence).

- **PREB.** The pre-burst data consisting of discriminator counts (with 64 ms resolution) form the eight LADs immediately before the burst trigger for the interval of 2.048 s.

- **DISCSC.** The output of Discriminator Science Data begins immediately after a burst trigger and continues for an interval of ~4 min (early in the CGRO mission), or ~10-11 min. It consists of 64 ms resolution discriminator data summed from each of the LADs that were triggered by the burst.

- **TTE.** Time-Tagged Event data providing the time of occurrence, discriminator channel, and detector number of 32 768 individual LAD events. When the burst trigger occurs, data are entered only from the LADs that triggered the burst. Accumulation data stops after 3/4 of the memory fills. The other 1/4 of the memory contains data from all eight LADs immediately prior to the trigger.

- **HERB.** The High Energy Resolution Burst data consist of 128 separate spectra stored during a burst. The selection of detectors and storage times is under software control. Nominally, the accumulation time is rate dependent. Spectra from four LADs are stored, with the more brightly illuminated detectors stored more often, e.g. the second "brightest" detector records one spectrum for every two the brightest detector records, while the third and the fourth brightest detectors record one spectrum for every two recorded in the second brightest.

- **MER.** Medium Energy Resolution data consist of 4096 spectra with 16-energy channel resolution summed from triggered detectors. The nominal accumulation time is 16 ms

for 2048 spectra, followed by 64 ms for the remaining 2048 spectra for a total duration of about 164 s.

A burst that triggered the on-board data system was processed and its data were stored in the Individual Burst Data Base (IBDB).

Detector Response Matrix

The response characteristics of the BATSE detectors are contained in the Detector Response Matrices (DRMs); they were constructed to convert the source count spectra to source photon spectra (see Pendleton et al. 1995). The detector response relates the incident photon input energy with the measured detector output energy, and depends on the angle between the detector normal and the source direction.

Fig. 3.2 shows the total detector response in units of effective area as a function of the incident photon energy for a source along the detector axis (Pendleton et al. 1999). The effective area is smaller than the total geometric area at low energies because the charged particle detector in front of the LAD absorbs the low energy photons before they get into the detector crystal. At higher energies instead the thinness of the crystal reduces the photon conversion frequency. The detector response peaks in the nominal BATSE trigger energy range of 50-300 keV. The detector angular response is cosine-like at lower energies and flatter (as a function of the incidence angle) at higher energies (Fig 3.3).

The contribution of the off-diagonal elements in the detector response matrix is shown in Fig.3.4 (Preece et al. 2000). That is, besides the photopeak coming from the photoelectric absorption of photons that interact with the detector crystal, there is a large contribution of photons generated by the iodine K-shell photon cross section edge at $\sim$33 keV. Below the K-shell ionization energy, the lower cross section results in the loss of the low energy photons from the detector. If the escaping photon was the X-ray fluorescence product of the photoelectric absorption of a high energy photon, a lower total energy will be recorded for the original photon. This effect is seen in Fig. 3.4 as the broad second peak in the response diverging from the photopeak at lower energies. Photons that scatter in the detector from the various sources (detector housing, the spacecraft, Earth's atmosphere),

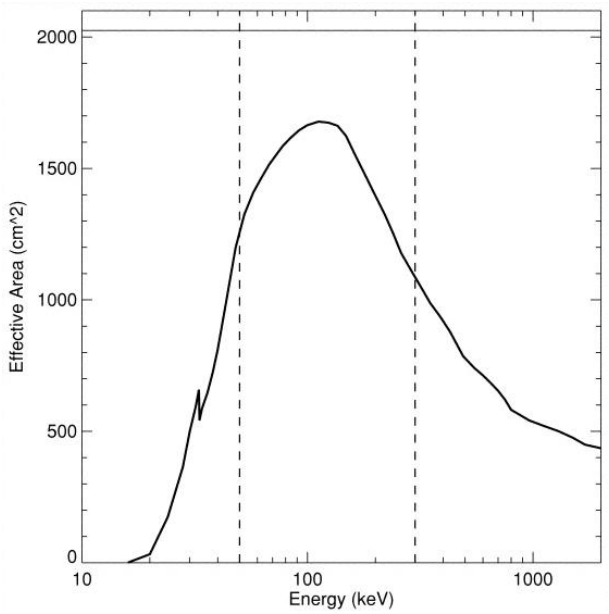

Figure 3.2: LAD response as a function of incident photon energy along the detector normal. The vertical dashed lines indicate the nominal burst trigger energy range. The solid line shows the LAD geometric area. From Pendleton et al. 1999.

including those that Compton scatter out of the detector, make a broad lower diagonal contribution from the higher energy photons (Preece et al. 2000). Thus the correct modeling of the nonlinear contributions is necessary to perform spectral analysis accurately.

These effects can be seen in the counts predicted for photons of a single energy interacting with the detector, as shown in Fig. 3.5 for the background spectral line features at 68, $\sim$ 200, and 511 keV. It presents the typical High Energy Resolution background spectrum with five underlying components: a low energy portion, a $\sim$ –1 spectral index high energy power law and background lines at 511, $\sim$200 and 68 keV. The data were fitted using these photon models propagated through the detector response matrix as shown in Fig. 3.4. All the effects described above are properly accounted for in reconstructing the BATSE DRMs as provided for the final guest investigator analysis.

3.2.1 Physical background

The physical origin of the gamma–ray background is a time-varying combination of several components (Rubin et al. 1996): (i) the diffuse cosmic gamma–ray background;

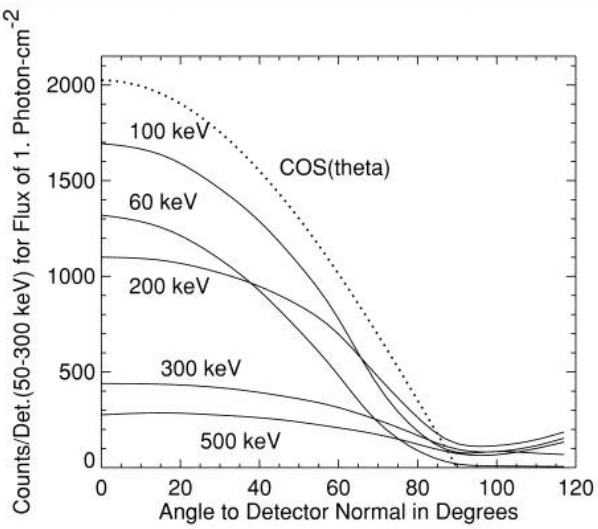

Figure 3.3: LAD angular response as a function of the source viewing angle for several incident photon energies. From Pendleton et al. 1999.

(ii) atmospheric gamma–rays; (iii) background due to gamma–rays and neutrons produced by local cosmic rays; (iv) decays of radionuclides activated by cosmic-ray bombardment; and (v) transient events, such as solar flares. The diffuse cosmic gamma–ray background, which is the strongest background component below 300 keV, is effectively isotropic. The atmospheric gamma–ray background depends on the local position of the spacecraft and on the rigidity of the terrestrial magnetic field. The local background is produced primarily in the form of gamma–rays by the interactions of cosmic ray protons with the detector materials; it becomes more important with increasing energy, especially above 200 keV. The bombardment by cosmic rays and by trapped protons in the South Atlantic Anomaly (SAA) also produces radionuclides that decay with various lifetimes, creating a delayed background.

3.2.2 Trigger criteria

A burst trigger is generated by BATSE by examining if two or more detectors register a significant increase of the count rate above the background on each of three time scales: 64 ms, 256 ms and 1024 ms. The discriminator rates in channels 2 and 3 (approximately 60 to 325 keV) are used. The required increase is specified in terms of

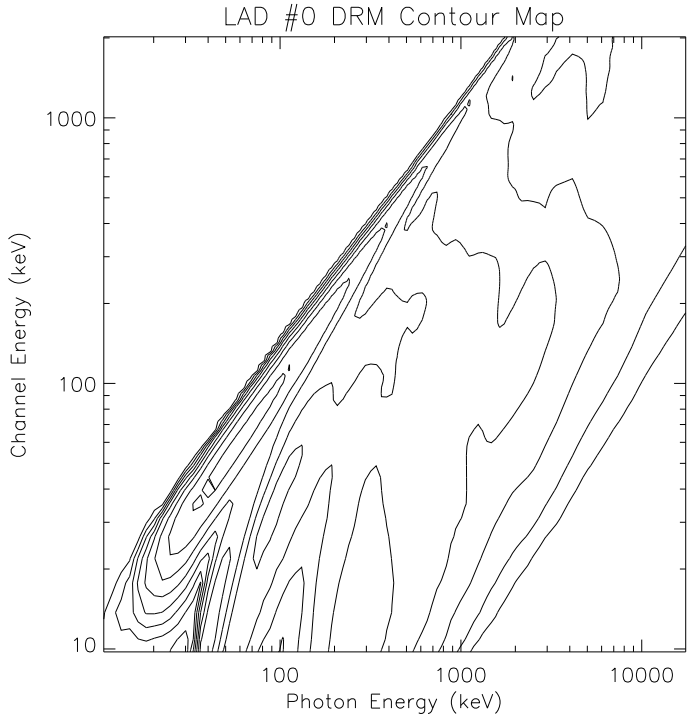

Figure 3.4: BATSE LAD response matrix with equal levels of effective area indicated by eight logarithmically spaced contour lines, between 0 and the maximum of 63 cm^2keV^{-1}. The response to a photon energy incident upon the detector can be traced by a vertical slice through the contour map at that energy. The photopeak is visible along the diagonal, while the iodine K-escape feature shows up along the bottom at 33 keV. From Preece et al. 2000.

standard deviation above the background; this threshold was set at 5.5σ on each of the three time scales. The average background rate was determined for each detector over a time interval of 17.4 s. When a burst trigger occurred, data were stored at high sampling rate into the memory for 240 s. An additional condition for burst triggering was required because of the possibility of detecting charged particles: the detector with the greatest increase of the count rate had to have an increase of the charged particle rate that was less than a specified fraction of the increase in the neutral rate, which is instead due to the particle contribution.

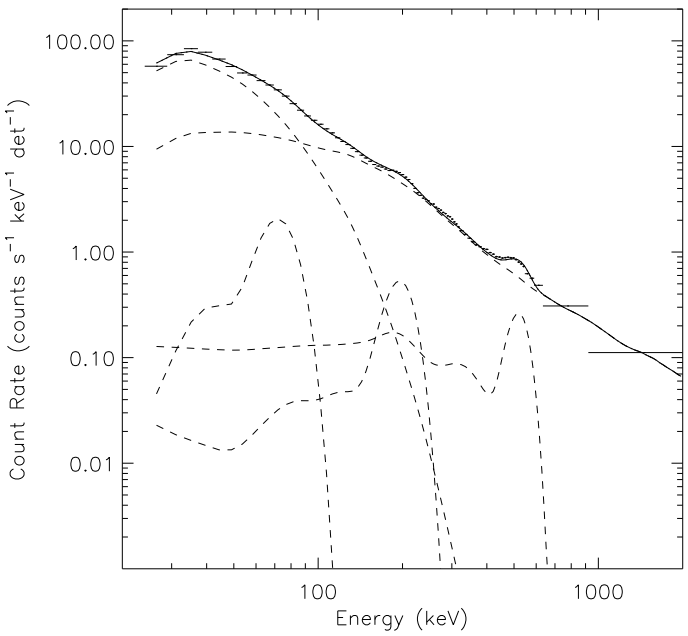

Figure 3.5: Typical HER background showing various contributions (see the text for details). Some of the background continuum counts are due to particles, not due to gamma–ray photons. From Preece et al. 2000.

3.2.3 Burst Locations

Directions to burst sources were determined by comparing the count rates among the illuminated detectors. Since the eight planes of the detectors were mounted parallel to the eight faces of a regular octahedron (whose orthogonal axes were aligned with the coordinate axes of the CGRO spacecraft), any burst would trigger four detectors. The count rate on each LAD changed approximately as the cosine function of the angle between the detector normal and the direction to the source; the location algorithm used the detector response as a function of energy and angle of incidence as determined by calibrations and corrected for scattering from the Earth's atmosphere (Fishman et al. 1994). Thus, in the first BATSE catalog the statistical errors depend on the burst intensity (that is, the signal-to-noise ratio) and the systematic errors were found to be about 4 degrees and around 13 degrees near the trigger threshold (systematic errors include e.g. inaccuracies in the assignment of energies to channel boundaries, in the dead-time correction of high count rates and in the detectors response model, deviations of the actual GRB spectra from the

power law assumed in most cases). In the following releases of the BATSE catalog a number of improvements have been made; the most significant was including six detectors (rather than four) in the χ^2 minimization, that is including the two LADs from the opposite face of the spacecraft (Meegan et al. 1996). Thus the systematic error was reduced to $\sim$1.6 deg. In the lower intensity bursts the statistical error however dominates.

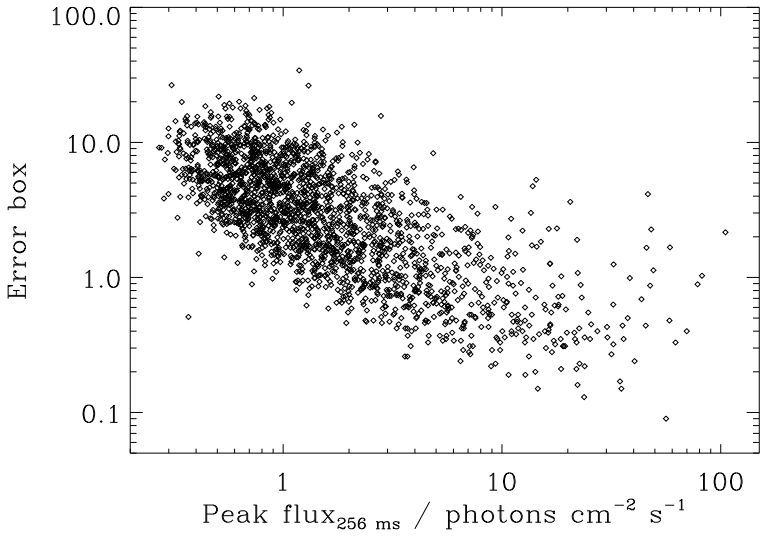

Figure 3.6: BATSE (statistical) error boxes vs. peak photon fluxes for 2135 gamma–ray bursts.

The error distribution of the BATSE GRB locations was also characterized in several works by modeling the distribution of separations between the BATSE locations and the locations obtained with the Interplanetary Network (IPN) (see e.g. Briggs et al. 1999); it was found that the location error distribution is Gaussian modified with an exponential tail (the simplest model having a systematic error of 1.9 degree with probability 73%).

3.3 Temporal analysis

The temporal profiles of gamma–ray bursts are highly irregular and complex and differ enormously from one burst to another. A number of statistical studies were performed in the attempt to characterize any structure of the gamma–ray burst light curves

(as a function of the spectral energy band) and thus identify the physical properties of the underlying emission mechanism. The most important results include (see also sect. 2.2.1):

i. the pulses in the GRB time histories are asymmetric (Nemiroff et al. 1994); Norris et al. 1996 in their extensive analysis of burst time profiles found that the burst asymmetry on short time scales results from the tendency for most (∼90%) pulses to rise more quickly than they decay, the majority having rise-to-decay ratios of ∼0.3–0.5, independently of energy;

ii. the pulse width distribution for long bursts has been found to be consistent with a lognormal distribution (Li & Fenimore 1996, Quilligan et al. 2002). In some gamma–ray bursts (that is, in 15% of bursts of the analyzed sample) "quiescent intervals" in the gamma–ray emission have been observed and the durations of these intervals are found to be positively correlated with the duration of the emission episode following the quiescence (Ramirez-Ruiz & Merloni 2001);

iii. the average peak width is a function of energy. By using the average autocorrelation function of a sample of bright GRBs in four BATSE energy channels, Fenimore et al. 1995 showed that the pulse width narrows with energy following a power law (with slope ∼–0.4);

iv. the time variability of gamma–ray burst time histories appeared to be correlated with the absolute luminosity of the burst: smooth bursts were found to be intrinsically less luminous (Fenimore & Ramirez-Ruiz 2000). As mentioned in Section 2.2.5 this Cepheid-like relationship can be used to determine the redshift of a GRB from parameters measured only in the gamma-ray energy range.

Data Types

Several BATSE data types were used in this work to study the temporal properties of gamma–ray bursts, in order to obtain the GRB light curves at 64 ms and 2 ms time resolution. All data types are derived from the on-board data stream of BATSE LADs

and come in four energy channels with approximate channel boundaries: 25-55 keV, 55-110 keV, 110-320 keV and >320 keV (see Fig. 3.7). Higher spectral resolution (16 channels) is available at finer temporal resolution (16 ms) starting at trigger and for the time intervals of 32 s. However the advantage of a high temporal/spectral resolution has the drawback that only a few bursts have sufficient intensity to derive statistically sound results.

The 64-ms light curves of gamma–ray bursts available in the BATSE current catalog[4] are obtained as the concatenation of three standard data types, DISCLA, PREB and DISCSC (see sect. 3.2). PREB and DISCSC data have 64 ms time resolution, therefore the counts in each 1.024 s DISCLA sample were divided equally into 16 64-ms samples with the last one (which can overlap with the PREB data) being truncated. The truncation was accomplished by subtracting the counts in that portion of the PREB data which overlaps with the last DISCLA sample, and then equally dividing the remaining DISCLA counts into 16 or fewer. DISCS data are summed only over those detectors which triggered on a burst, whereas DISCLA and PREB data exist for all eight LADs. Thus the concatenation was accomplished using only counts from triggered detectors for the DISCLA and PREB data types.

The high temporal resolution data (TTE) are convenient to capture temporal fluctuations in short duration (T_{90} <2 s) gamma–ray bursts only because of the limited data buffer. This data type contains the information on: 1) the photon arrival time at 2-microsecond resolution, and 2) the discriminator energy channel into which the photon was pulse-hight analyzed (the channel boundaries are the same as those for the DISCLA, DISCSC and PREB data types). There is approximately 30 ms offset between the trigger time and the TTE data load time. In order to get a reasonable S/N we have binned these data into 2-ms time bins.

The background contribution is determined by inspection of the time history in the non-burst emission regions. Commonly two intervals were selected, one starting at the beginning of the concatenated data stream and ending ∼10 seconds before the trigger, and the second one starting ∼10 seconds after the end of the burst and lasting until the end of the available data. A 2nd or 3rd order polynomial is fitted to the selected non-burst

[4]http://cossc.gsfc.nasa.gov/batse/batseburst/

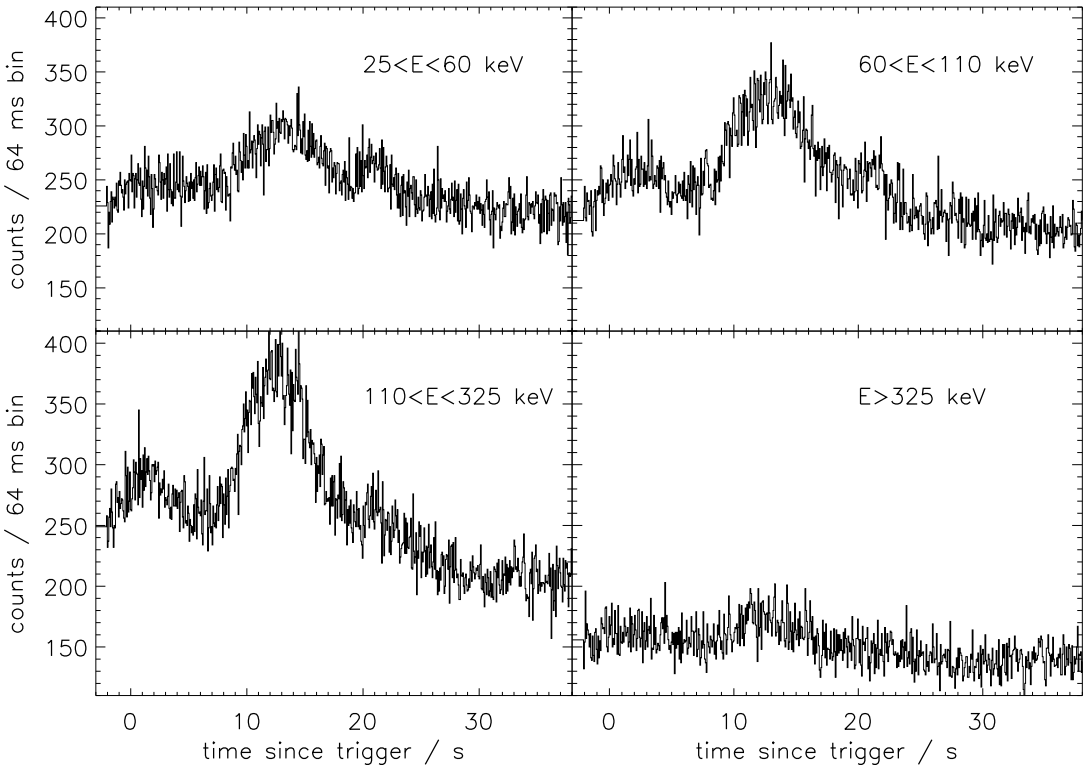

Figure 3.7: An example of the 64-ms resolution light curve for GRB 980703 obtained in four BATSE energy channels.

portions of the light curve, extrapolated to the GRB time interval and subtracted from the GRB data.

GRB Time Profiles

As noted by Norris et al. 1996, a self-similar shape for all pulses within a burst does not adequately represent the variations observed from pulse to pulse. A phenomenological model that permits a wide variation of pulse shapes has been proposed for the light curve analysis (Norris et al. 1996):

$$I(t) = \begin{cases} A \exp[-(|t - t_{max}|/\sigma_r)^\nu] & t < t_{max} \\ A \exp[-(|t - t_{max}|/\sigma_d)^\nu] & t > t_{max} \end{cases}$$

where t_{max} is the time of the pulse's maximum intensity A; σ_r and σ_d are the rise ($t<t_{max}$) and decay ($t>t_{max}$) time constants respectively; ν is a measure of the peak sharpness (or

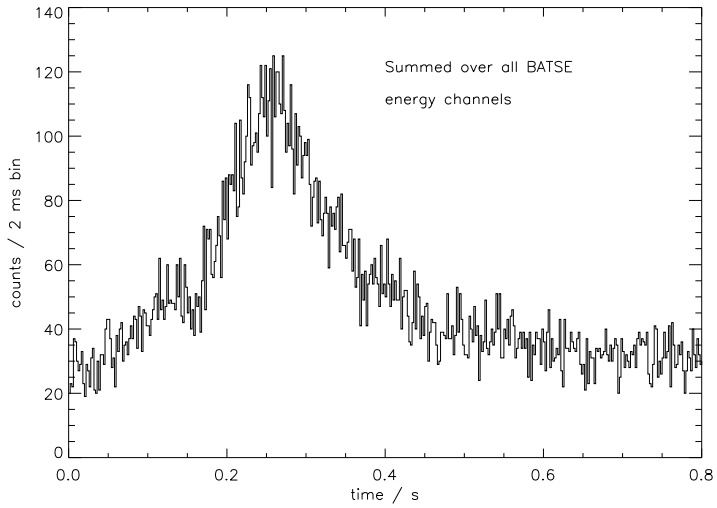

Figure 3.8: An example of the 2-ms resolution light curve for GRB 991002 (T_{90}=1.92 s) obtained by summing the counts from all four BATSE energy channels into a single channel.

"peakedness"). This model clearly allows the investigation of the range of rise and decay time constants (σ_r and σ_d), with the peakedness parameter characterizing the transition across the pulse peak (e.g. ν=1 or 3 describes a two-sided exponential or a Gaussian, respectively), and thus is well suited to describe a FRED–like (Fast Rise Exponential Decay) shape, which probably characterizes the majority of burst pulses.

The distributions of pulse widths are energy dependent, with the maximum shifting from ∼600 ms at low energies to ∼200 ms at high energies. The distribution of intervals between pulses exhibits a broad maximum near 1 s, presumably a characteristic time scale in the long GRB emission. In approximately 90% of pulses in the examined sample of long gamma–ray bursts the σ_r/σ_d ratio is less than unity, that is, the pulses with reversed-FRED shape - exponential rise, fast decay - are rare or do not exist (Norris et al. 1996). In general the distributions of the parameters characterizing the burst emission in time (FWHM, fall and rise constants, pulse amplitudes, pulse 'areas' and time intervals between the pulses) are found to be very similar, i.e. very broad, covering about three orders of magnitude and all compatible with a lognormal distribution (Quillligan et al. 2002).

The characteristics of the GRB time profiles have been investigated in some detail for what concerns two aspects (Norris et al. 1996): the pulse shapes and placements

(including width, peakedness and interval distributions), and the energy dependence of the pulse shapes (including any dependence of rise and decay times and peakedness).

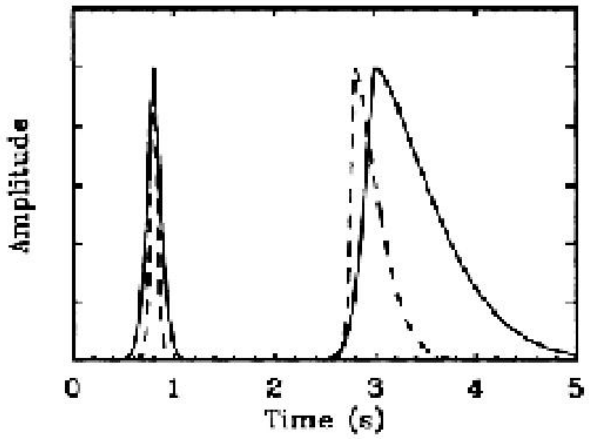

Figure 3.9: Pulse asymmetry/energy-shift paradigm proposed by Norris et al. 1996. The solid curve is the low-energy emission ($\propto$ few $\times$ 10 keV) and the dashed curve represents the high energy emission ($\propto$ few $\times$ 100 keV).

The pulse widths were found to decrease at higher energies and, by examining the rise-to decay ratios for individual pulses as a function of energy, it was also found that pulse shapes remain similar across different energy bands. The rise-to-decay time ratio scales approximately as σ_r=$0.33\sigma_d^{0.83}$, essentially independently of energy; that is, there is an apparent trend for wider pulses to be more asymmetric. Considering the time lags between the peak centroids in two energy channels, in most cases the lower energy pulse lags the higher energy one, and this effect is more evident for the more asymmetric pulses (with rise-to-decay ratio much less then unity). This is the famous asymmetry/width/softening paradigm for the GRB pulses (see Fig. 3.9).

3.4 Spectral analysis

Characterizing the spectrum of gamma–ray burst is clearly crucial for understanding the nature of the events; it can provide information on the burst energetics, particle distributions and acceleration mechanism, and the overall evolution of the expanding fireball.

Data Types

BATSE provides several data types for the spectral analysis. In view of the objectives of our work, we used the HERB data type accumulated by the LADs. The HERB data have the high time resolution (with a minimum accumulation time of 128 ms, being however rate-dependent) and a high energy resolution (128 energy channels distributed between 30 keV and 1.8 MeV). These are sufficient to determine spectral model fit parameters with good precision for the range of fluences of the sample of GRBs we considered (that is, bursts that are not in the brightest tail of the BATSE fluence distribution). In the cases when the burst event is not intense enough to provide the minimal number of counts required for the fitting procedure (χ^2 minimization), the MER data (with 16-energy channels distributed approximately in the same energy range) may be a valid alternative.

The spectral data are accumulated only for the four detectors that have the highest count rates at the time of trigger. The typical response efficiency (in terms of the effective detector area) as a function of the incident photon energy for the LAD is reported in Fig. 3.10. The spectral analysis procedure begins by selecting the detector that was most aligned with the source, i.e. that recorded the highest photon flux after the burst trigger and may provide the best S/N for the source spectrum.

Time-Integrated Spectral Analysis

The time-integrated spectrum of a burst is obtained by integrating the count spectra from the most illuminated detector over the burst duration; the integration time typically starts after the trigger and lasts for the duration of T_{90} (see Fig. 3.11).

This time integrated count spectrum (Fig. 3.12) is a superposition of the source spectrum and the background (convolved with the detector response matrix). The background contribution (to be subtracted from the time integrated spectrum) is estimated as the average over the count spectra in two time intervals not affected by the burst emission (i.e. before and after the burst).

The lowest seven channels of the 128 LAD energy channels are at or below the lower level discriminator ($\sim$ 25 keV) and are unusable; the highest few channels suffer from saturation in the pulse amplifier and thus are also excluded. The remaining channels are

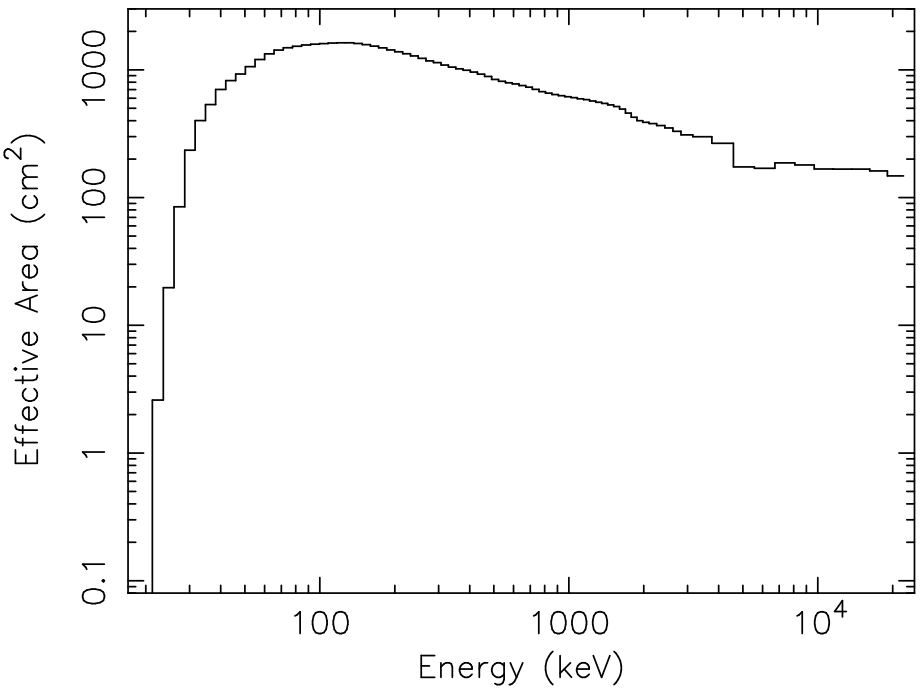

Figure 3.10: Response of the most illuminated detector (LAD #3 for GRB 980703) expressed as the effective detector area for the incident photons energies.

spaced quasi-logarithmically in energy, falling between approximately 28 keV and 2 MeV. In order to have a sufficient count rate per bin so that the χ^2 statistics can be applied and the spectral model parameters determined with meaningful accuracy, the bins were rebinned in energy according to a S/N criterion.

Spectral Parameters

The photon spectrum of most gamma–ray bursts in the BATSE energy range (~25 - 2000 keV) can be parametrized by a phenomenological model consisting of two smoothly connected low- and high- energy power laws with spectral indices α and β and a 'break' energy E_{break} (Band et al. 1993):

$$N(E) = \begin{cases} A\Big(\frac{E}{100\mathrm{keV}}\Big)^{\alpha}\exp\Big(-\frac{E(2+\alpha)}{E_{peak}}\Big), & E < (\alpha-\beta)E_{peak}/(2+\alpha) \equiv E_{break} \\ A\Big[\frac{(\alpha-\beta)E_{peak}}{(2+\alpha)100\mathrm{keV}}\Big]^{\alpha-\beta}\exp(\beta-\alpha)\Big(\frac{E}{100\mathrm{keV}}\Big)^{\beta}, & E \geq (\alpha-\beta)E_{peak}/(2+\alpha) \end{cases}$$

The parameter E_{peak} corresponds to the peak of the spectrum in a νF_ν representation; E_{break} marks the lower boundary in energy of the high-energy power law component.

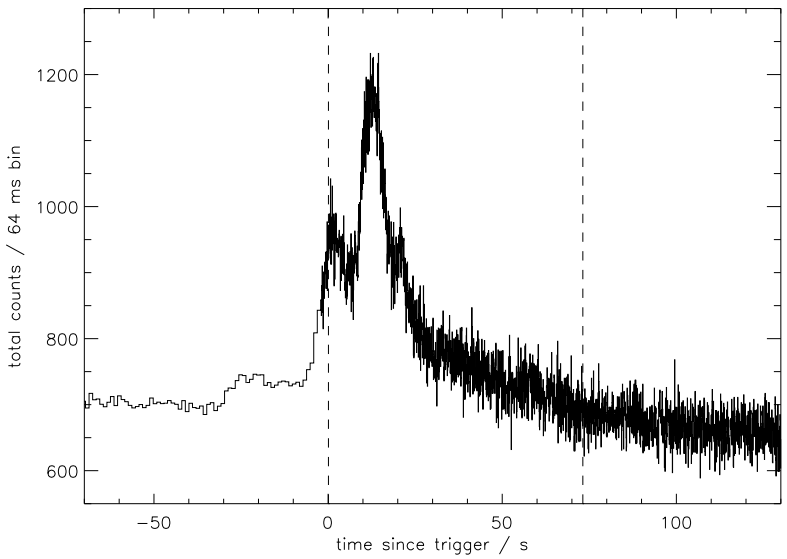

Figure 3.11: Light curve of GRB 980703 at 64 ms resolution and integrated over the four BATSE energy channels (approximately 30 - 1800 keV). The time interval for the spectra integration is indicated.

It is worth noting that this functional form for the GRB spectrum does not have direct implications on the underlaying physical processes; in addition, many 'standard', simpler spectral shapes can be represented by this model, e.g. single power law or power law with a high energy exponential cutoff. An example of the model fit to the BATSE GRB spectrum is reported in Fig. 3.13.

It was suggested (Katz 1994) that a likely source of radiation in GRBs is synchrotron emission from electrons accelerated in the internal shocks within the ultrarelativistic flow; an optically thin synchrotron spectrum from a power law distribution of relativistic electrons with a sharp minimum energy cutoff ($N(\gamma) \propto \gamma^{-p}$, $\gamma > \gamma_{min}$, where γ is the electron Lorentz factor) and with an isotropic pitch angle distribution provides a good fit to some bursts. This model, however, predicts that the asymptotic value of the low energy power law photon index α should not exceed $-\frac{2}{3}$ (see further discussion in sect. 5.2 and 5.3).

Figure 3.14. shows the α distribution from Preece et al. 2000. They reported the results of the spectral analysis for 156 bursts selected for either their high peak flux or high fluence (the Preece et al. 2000 distributions of spectral parameters contain the results of

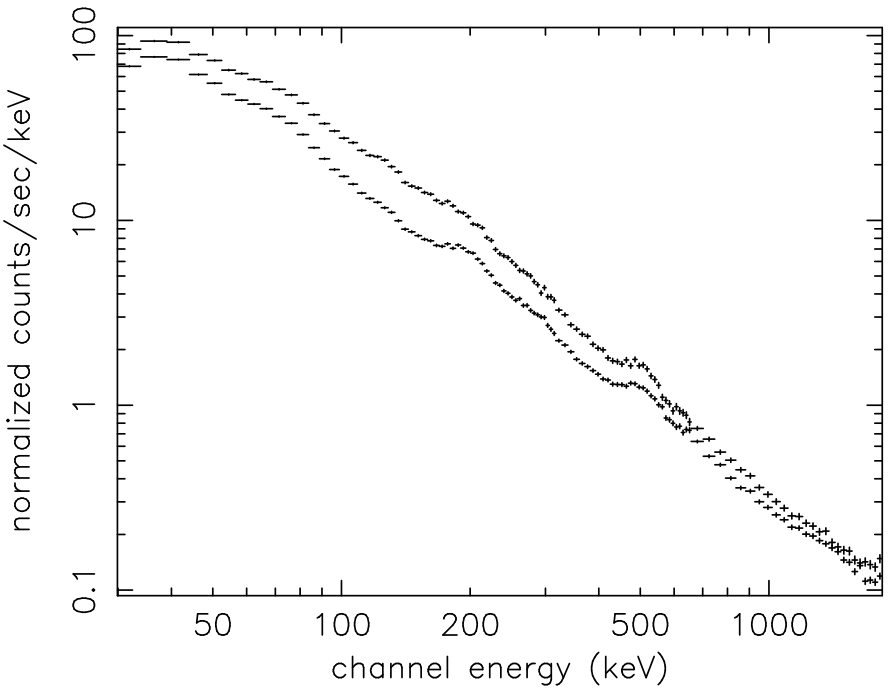

Figure 3.12: Background spectrum and the superposition of the source and the background spectrum (the integration time is indicated in Fig.3.11).

the time resolved spectral analysis, that is, the spectral fit parameters obtained by fitting the spectra accumulated for a sequence of time intervals covering the burst duration). The distribution of α shows as the most likely value for the low energy power law index of –1. As this value should arise naturally out of the physics of the emission mechanism, clearly the simple synchrotron model is not the only option for the burst emission.

The high energy photon index β (Fig. 3.15) usually reflects the steepness of the particle energy distribution in models for synchrotron emission; the observed values of $\beta \sim$ –2.1 indicate value of $p \sim 2.2$ for the simple cooling model (the high energy photon index for a simple cooling spectrum is -(p+2)/2) (detailed discussion of emission processes is given in sect. 5.2). This value for the power law index p is consistent with the values expected from the studies of particle acceleration in relativistic shocks (e.g. Gallant et al. 2000). However, we note that β is usually not very well constrained by the data due to the low S/N ratio in the high energy channels of the analyzed spectra.

In Fig. 3.16 the distribution of the break energies is reported; E_{peak} (or E_{break})

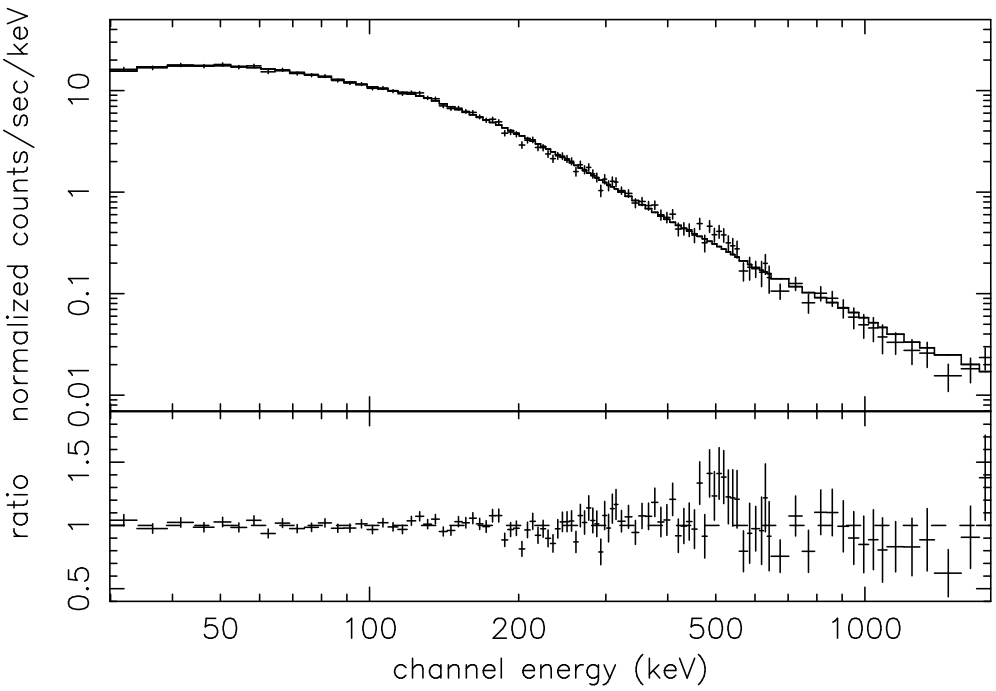

Figure 3.13: Top panel: Fit to the time-integrated spectrum of GRB 980703 with the model proposed by Band et al. 1993 (after background subtraction and convolution with the detector response matrix). Bottom panel: data to model ratio.

reflects the characteristic electron energy in most models of GRB emission. The break energies do not seem to spread over the pass band of the detector, but they are rather confined within a single decade in energy (centered around ∼225 keV). When considering the observed distributions of the spectral parameters it is important however to keep in mind the possible biases involved e.g. in the sample selection or caused by the finite bandwidth of the BATSE instruments. For example, (as discussed in sect. 2.2.1) X-ray rich GRBs and XRFs observed by *HETE-2/FREGATE* (in the energy range 7-400 keV) have low-energy and high-energy photon indices –1 and ∼–2.5, respectively, which are similar to those of gamma–ray bursts, but they have spectral peak energies E_{peak} that were much lower than those of GRBs. Thus it has been suggested (Sakamoto et al. 2004, Lamb et al. 2004a) that XRFs nad XRR might represent an extension of the GRB population to bursts with low peak energies.

The observed values and variability of all three spectral parameters are decisive in evaluating the wide variety of proposed models for gamma–ray burst emission. Liang &

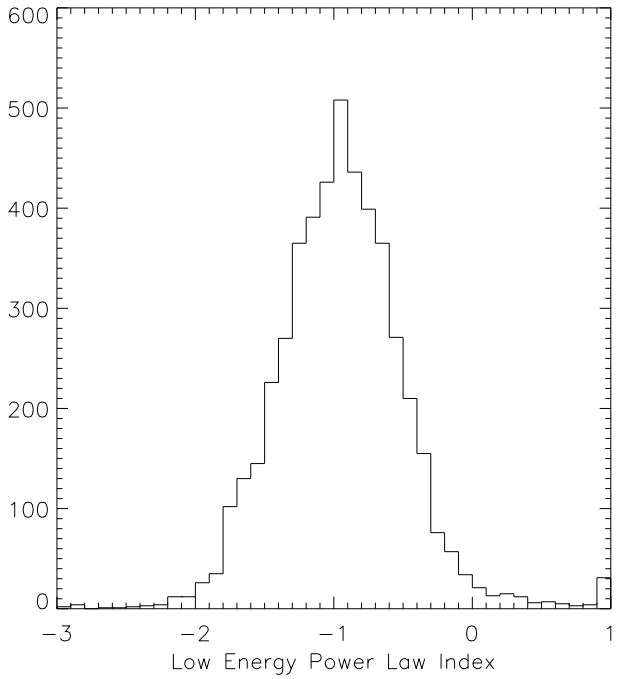

Figure 3.14: Low energy power law index distribution for the sample analyzed by Preece et al. 2000.

Kargatis 1996 showed that E_{peak} often decays exponentially in bright, long, smooth GRB pulses as a function of the photon fluence. It has also been found (Crider et al. 1997) that the asymptotic low energy power law slope (far from the break or peak photon energy) evolves with time rather than remaining constant and that its evolution is correlated with that of the spectral break energy. These issues are further discussed in Chapter 5, where the alternative models that can account for the variety of observed spectral parameters are investigated.

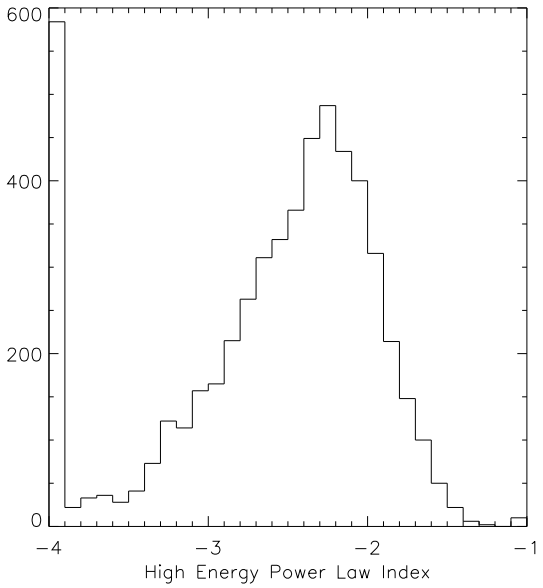

Figure 3.15: High energy power law index distribution for the sample analyzed by Preece et al. 2000; all spectra that either do not have determined β values or that have values < -4 have been included in the lowest bin.

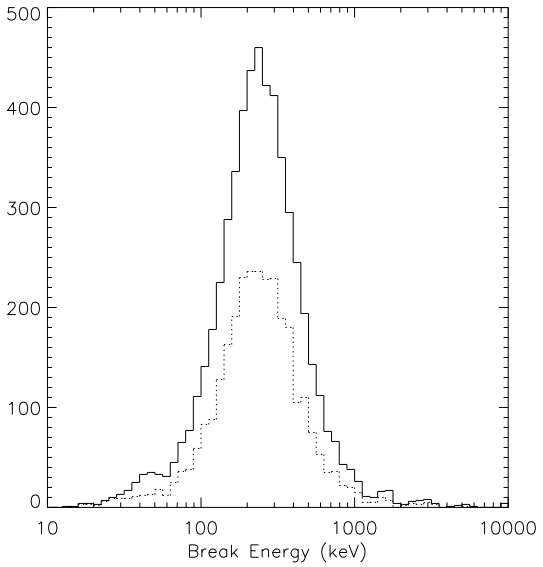

Figure 3.16: Break energy distribution for the sample analyzed by Preece et al. 2000. The subset of burst not fit by the Band model (Band et al. 1993) is also shown (dotted line); spectra of these bursts were best fitted by alternative models, i.e. broken power law or COMP model (consisting of a power law and high energy exponential cutoff). These spectra are also characterized by power law indices and a characteristic break energy.

Chapter 4

The GRB/Supernova Connection

4.1 Introduction

The gamma–ray burst physics has been overall interpreted within the framework of the fireball scenario (see Section 2.3); however, as there are no direct observations of the inner engine, the understanding of the mechanism that powers gamma–ray bursts has remained elusive (see Section 2.4). Moreover, while there are clues on what is the origin of long gamma–ray bursts, there is no evidence on the progenitors of short bursts.

The increasing number of recent observations supports the association of (at least) some long GRBs with supernova (SN) events, stimulating both the theoretical understanding/modeling of GRB progenitors and intensive observational campaigns aimed at finding further and more detailed evidence of associations. In this chapter the properties of a sample of BATSE gamma–ray bursts with indication of being associated with a SN event are examined. I first review (Sect. 4.2.) the observational (direct and indirect) pieces of evidence for GRB/SN associations; in Section 4.3 I describe on what basis the sample of GRBs associated with SNe was selected from the BATSE catalog. The global properties of this sample are presented in 4.4, while in the following sections its temporal (Sect. 4.5 and 4.6.) and spectral (Sect. 4.7) properties are examined in detail. The estimate of the GRB distance scale - as feasible test on the reality of the associations - is described in Section 4.8. The results are reconsidered and discussed in the last Section.

4.2 Observations of GRBs associated with supernovae

Coincident events: GRB 980425/SN 1998bw

GRB 980425 was the first burst with tantalizing evidence for a physical association with a SN (Galama et al. 1998). The optical transient that occurred in the *BeppoSAX Wide Field Camera* error box (of radius 8') of GRB 980425 within about a day of the gamma–ray burst was consistent in terms of its light curve and spectrum with a very luminous Type Ic supernova (SN 1998bw). The 'a posteriori' probability of chance coincidence (considering the size of the error box, the peak magnitude of the supernova and the causal time window) is $\sim 10^{-4}$. The achieved luminosities were unprecedented at the time for a core-collapse supernova and implied substantial amounts of ^{56}Ni ($\sim$0.7 $M_\odot$) synthesized in the explosion (typical values of ^{56}Ni mass are $\sim$0.1 $M_\odot$). The radio observations of the supernova (Kulkarni et al. 1998) revealed that the radio emitting shell in SN 1998bw must be expanding at relativistic velocities ($\Gamma > 2$) and the associated relativistic shock could have produced the GRB at early times. The GRB/SN was located at z=0.0085, and the total inferred energy budget of the gamma–ray burst was 8.5×10^{47} erg.

The association of the two events has been discussed in the frame of models involving the core collapse of massive stars (e.g. Woosley et al. 1999; MacFadyen & Woosley 1999; Vietri & Stella 1998). However, the unusual properties of both events within their classes – i.e. the extraordinary high luminosity of the SN, the unusually low luminosity and variability of the GRB γ–ray emission and the lack of detected X–ray afterglow – as well as the uniqueness of this association, have not allowed to draw firm conclusions about the possible progenitor for a few years.

Spectroscopic associations:
GRB 030329/SN 2003dh and GRB 031203/SN 2003lw

More recently two further GRB/SN associations based on the spectroscopic detection of a SN spectrum in the GRB afterglow added robust evidence to the association of the two phenomena. GRB 030329 (Hjorth et al. 2003; Vanderspek et al. 2004) has been associated to SN 2003dh from the appearance of typical SN Ic spectral features in its

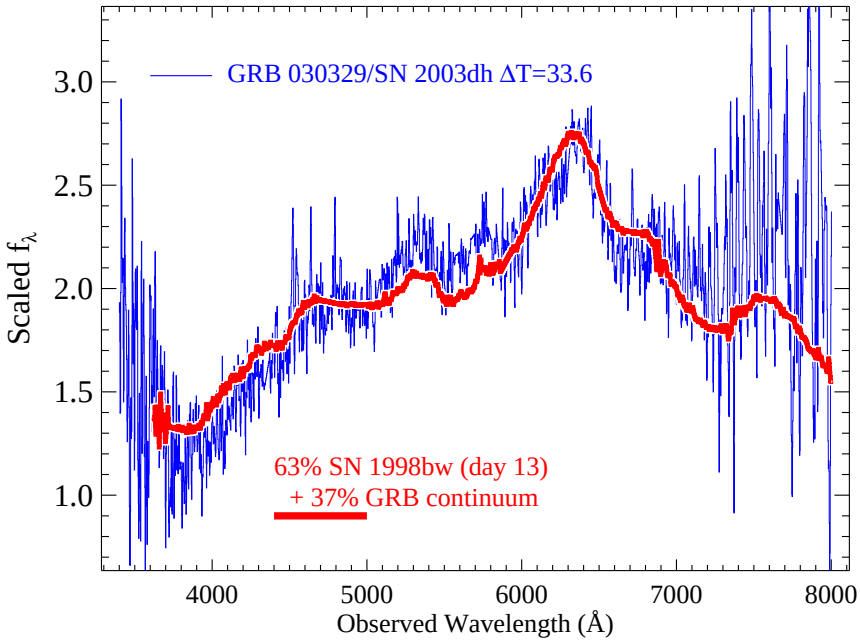

Figure 4.1: Thin line: observed spectrum of the GRB 030329/SN 2003dh afterglow at ΔT=33.6 days after the GRB. Thick line: model spectrum consisting of 37% continuum and 63% of the SN 1998bw flux at 13 days after maximum. From Matheson et al. 2003

optical spectrum (Fig. 4.1). The early photometry showed a complicated light curve that could not be simply fitted as a typical optical afterglows; at late times it was dominated by the supernova component, following the light curve of SN 1998bw fairly well. GRB 030329, unlike the GRB 980425, was a "typical" gamma–ray burst. Its total isotropic energy release was 9 $\times 10^{51}$erg at the redshift of z=0.1685. A very bright afterglow was detected at all wavelengths, from X–rays to radio.

GRB 031203 was the following case of an under-energetic gamma–ray burst associated with a supernova. A few days after the GRB a rebrightening was apparent in all optical/NIR bands consistent with the contribution of an underlying type Ic SN (SN 2003lw; Malesani et al. 2004). Also the spectra of SN 2003lw were remarkably similar to those of SN 1998bw at comparable epochs. Despite of these promising findings, the paucity of cases of GRB directly associated with SN Ib/c, some peculiar properties of both the GRB and SN events in these few robust associations and the uncertainties on the event rates in both

classes (however Podsiadlowski et al. 2004 estimated that a fraction of about 5% of observed SNe Ic are 'hypernovae' (HN) and able to produce a gamma–ray burst; thus the rates of HNe and GRBs result quite comparable, with a rate of 10^{-6}–10^{-5} yr-1 per galaxy) do not allow a clear insight and different possibilities are still open: selection effects might play a role in detecting SN features, there might be an (inverse) relation between the energetics of the two events (underluminous GRB vs Hypernova event), or bursts associated with core collapse SN could represent a subset of the whole population, which might be even characterized by properties (e.g. energetics, duration, temporal variability) intermediate between the two classes of events (e.g. Della Valle 2004 for an overview; Soderberg 2004).

Evidence for SN light in the gamma–ray burst afterglow

Given the limited number of 'direct' associations (i.e. with evidence of SN spectral features in the GRB afterglow), in order to test for the nature of any physical connection and thus investigate the progenitor(s) of GRB, other more indirect indications could be considered to select candidates GRB/SN associations. These include the re–brightening in the optical afterglow light curve decay, possible signature of SN emission emerging at times when the GRB has sufficiently faded (Bloom et al. 1999; Germany et al. 2000). Indeed about ten associations have been claimed on such a basis (Zeh et al. 2004). Interestingly Zeh et al. (2004) found indication of such re-brightening in all GRB with known redshift $z < 0.7$. They re-analyzed all observed GRB afterglows in an attempt to detect the predicted SN light component; the photometric light curves were fitted as the sum of an afterglow, an underlying host galaxy and a SN component, using SN 1998bw as a template (Fig. 4.2).

Similar findings (i.e. a bump in the late time light curve) have been confirmed also in the case of a few XRFs (Fynbo et al. 2004, Soderberg et al. 2005). This results point toward the association of XRFs with the death of massive stars for the first time (one possible scenario for XRFs is that they are classical gamma–ray bursts seen off-axis).

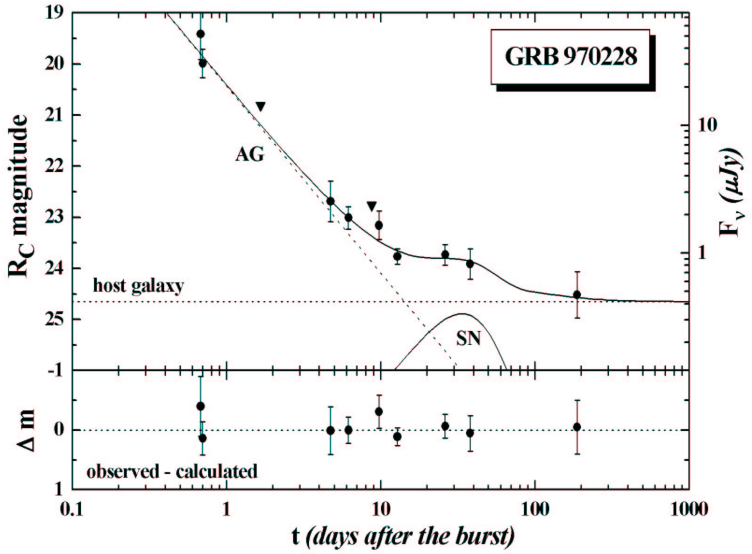

Figure 4.2: The late-time bump in the optical afterglow of GRB 970228 interpreted as a signature from a SN explosion. From Zeh et al. 2005

GRB/SN catalogs cross-correlation

An even more indirect and uncertain, but possibly more efficient approach, consists of systematic searches for directional and temporal coincidences of GRB and SN from the cross correlation of GRB and SN catalogs (Wang & Wheeler 1998, Hudec et al. 1999). The GRB/SN associations found by catalog cross-correlation refer to the associations occurring in the 'local' Universe as most SNe listed in supernova catalogs have been discovered within $z < 0.1$. These searches are clearly affected by i) the large uncertainties in the GRB position (typically of a few degrees) (e.g. Kippen et al. 1998) leading to possible serious overestimates of the number of real associations, but also ii) the completeness and flux limit of the SN/GRB catalogs used. Nevertheless, if the indications by Zeh et al. (2004) prove to hold, catalog cross-correlations should indeed find evidence for a significant number of real associations.

In principle a more powerful method for selecting candidate associations from the catalog cross correlation could be envisaged if GRB associated to SN were characterized

by particular temporal and/or spectral properties with respect to the whole of the GRB population. Indeed Norris et al. (1999) explored the hypothesis that there exists a subclass of GRB related to SN whose γ–ray prompt light curve presents a single smooth peak, similar to that of GRB 980425 (as suggested by Bloom et al. 1998a), but with negative results.

In summary, the most up-to-date sample of GRB/SN candidates includes the three robust cases of association (GRB 980425, GRB 030329, GRB 031203); 11 cases where the afterglow light curve re–brightening gives evidence for a coincident SN explosion, namely GRB 021211 (Della Valle et al. 2003), GRB 011121 (Garnavich et al. 2003), GRB 020410 (Levan et al. 2004), GRB 041006 (Stanek et al. 2005) and 7 GRBs examined by Zeh et al. (2004) (GRB 970228, GRB 980703, GRB 990712, GRB 991208, GRB 000911, GRB 010921, GRB 020405). Here we re-consider the possibility that the prompt emission of GRB associated with SN might have characteristic properties.

4.3 GRB/SN sample selection

To this aim here we focus on examining the possible peculiarities of the candidate events by investigating the temporal and spectral properties of GRBs for which there is an indication of being associated with a SN as a "class". More specifically we considered direct and indirect (tentative) associations, the latter ones based either on the light curve re–brightening or on the positional-temporal coincidence from catalogs cross correlations. To this aim we also extended the number of candidates by cross correlating more recent GRB and SN catalogs.

Clearly, if GRB in this sample turned out to be statistically (although not individually) characterized by any peculiar property – with respect to a random GRB sample – this would have interesting implications: i) it would indicate the existence of a SN-related sub–class of GRB; ii) it would provide an empirical tool for efficiently identifying such events; iii) most importantly, it would offer clues on the physical understanding of their origin (indicating a mechanism different from that underlying GRB without SN signatures).

Let us describe the (heterogeneous) sample considered here, which basically includes the BATSE GRBs with indications of association with SN and for which temporal

and spectral information could be retrieved, for a total of 36 GRB/SN. The whole sample with its basic properties is listed in Table 4.1 and 4.2 and for simplicity hereafter referred to as the GRB/SN sample. The three robust associations based on the spectroscopic identification of a SN, namely GRB 980425, GRB 031203 and GRB 030329 will be considered as reference cases throughout this work.

More precisely the GRB/SN sample comprises:

i) 7 GRB/SN suggested by a bump in the late-time optical afterglow (Bloom et al. 1999, Zeh et al. 2004), robust spatial and temporal association (GRB 980425) or an indication of a line feature in X-rays (Piro et al. 1999), or exceptional SN properties (high luminosity, peculiar spectrum; e.g. Germany et al. 2000). Of all the claimed cases we included those with available BATSE data;

ii) 15 GRB/SN from the previous searches of temporal and spatial coincidence based on the cross–correlation of BATSE and SN catalogs: 11 pairs by Wang & Wheeler (1998) and 4 pairs by Hudec et al. (1999);

iii) 14 GRB/SN identified in this work from an update of the catalog cross–correlation (including approximately the dates previously not covered, after Nov. 20, 1997 up to May 26, 2000). In this period the BATSE GRB catalog[1] contains 721 GRB and the SN catalog of IAUC[2] reports 495 SN.

The catalog cross correlation method that we adopted is based on the following criteria. For the positional coincidence we required a SN to be within the BATSE GRB error box to which the constant 1.6 degrees of r.m.s. systematic error has been added. The exact SN phase at detection is not known (typically the optical maximum is reached after $\sim$20 days) and furthermore no robust guess is possible for the delay between the SN and GRB explosions, as any estimate is strongly model dependent (see Section 2.4.1): $\sim$ a few months up to few yrs are allowed in the supranova model (Vietri & Stella 1998) while the explosions occur almost simultaneously in the collapsar model (e.g. MacFadyen & Woosley 1998). Although the latter case is theoretically and observationally favored (e.g. Della Valle 2004 for a review), a large temporal window has been allowed for the possible correlation

[1] http://cossc.gsfc.nasa.gov/batse/BATSE_Ctlg/index.html
[2] http://cfa-www.harvard.edu/iau/lists/SN.html

of the two events, requiring the SN date to be between -10 to +30 days with respect to the GRB trigger. No further constraints were imposed in the selection of either events (we believe that the bias toward Type Ic supernovae reinforced by the three robust cases of GRB/SN coincidence would not justify the selection of Type Ic SN only in our search) and thus the results are biased by the SN sky distribution and the detection incompleteness at faint magnitudes; we considered both long and short GRB and no limit was imposed on the GRB count rate.

Note that in the previous catalogs cross correlations analysis different search conditions were imposed. Wang & Wheeler (1998) searched for SN with coordinates within 2σ BATSE error boxes and supposed different time delays (according to the SN type) between SN and GRB. They also limited their search to SN at $z < 0.1$. As this latter limit, however, would exclude 2 (GRB 030329 and GRB 031203) out of the 3 more robust associations we did not impose any redshift cut. Hudec et al. (1999) reported the correlations for SN detected within the GRB error box up to 30 days after the GRB. Thus the compiled sample is non-homogeneous as different criteria were applied; still the re-selection of the GRB/SN associations by applying the same conditions would not increase the completeness of the sample or remove the biases. The sensitivity of the BATSE instrument changed during its lifetime and the re-selected sample would suffer from this further bias and incompleteness.

The updated cross-correlation yields 16 new GRB/SN coincident events. However, coordinates from the IPN[3] for two GRB revealed that the associations were spurious (and thus excluded from the sample). In Fig. 4.3 error boxes and time delays are displayed for 31 GRB/SN (2 GRB had multiple associations and 3 GRBs had an indication of an underlying SN from the afterglow observations).

The significance of such blind (catalog based) searches was studied by Kippen et al. (1998), who assigned a significance to the observed correlation statistics by generating a set of random GRB catalogs. They find no evidence for association for GRB having precise BATSE/Ulysses localizations, although they could not exclude it for a subset of weak bursts. While these results point toward a very low chance to select real coincidences with such a procedure, the peculiarity of some properties of the GRB/SN sample is instead

[3]http://www.ssl.berkeley.edu/ipn3/interpla.html

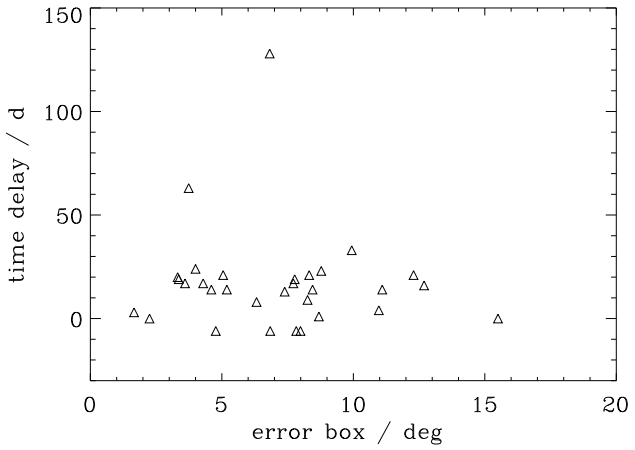

Figure 4.3: BATSE error boxes and time delays for the GRB/SN sample. The time delay is between the SN discovery date and the GRB event.

suggesting that such method does not select a random subsample of BATSE GRB.

4.4 Global properties

Based on the properties of GRB 980425 it has been suggested (see e.g. Bloom et al. 1998a) that, if there is a physical connection between a subsample of GRB and SN, such GRB might exhibit distinct characteristics. Therefore we have compared the global properties of the GRB/SN sample with those of the entire BATSE sample.

No qualitative (nor statistical) differences are found as far as duration (represented by T_{90}), spectral hardness (HR32) ratio and total burst fluence are concerned (see Fig. 4.4, top and bottom panels), as both the range and shape of the GRB/SN distributions are indistinguishable from those of the rest of GRB in the BATSE catalog.

As expected from the typical worsening of the positional accuracy with decreasing photon statistics (see Kippen et al. 1998), the GRB identified by the catalogs cross–correlations are mostly weak GRB, with typical peak (50-300 keV) flux < 1.5 phot cm^{-2} s^{-1} (see Fig. 4.4).

While no peculiarity is found for the above quantities in the GRB/SN sample, in the next Section we present a more detailed analysis of their GRB temporal profiles and

spectra[4]. Notice that the bias on the flux as well as the selection criteria of the GRB/SN sample result in a "non optimal" statistics for the temporal and spectral analysis. This in turn requires a careful selection of a BATSE GRB "control sample", as clearly previous analysis of BATSE GRB have been typically performed on brighter samples.

4.5 Light curves analysis

In this Section we present the analysis of the temporal profiles of the GRB/SN sample and compare the results with the (known) properties of larger GRB control samples.

4.5.1 Analysis

For most of the GRB (16/36) we analyzed the time profiles from the BATSE concatenated 64-ms data derived from the eight BATSE LADs (see Section 3.2); these data represent the detector count rates in 4 energy channels (25-50, 50-100, 100-300 and >300 keV). We fitted both the energy–integrated flux and the individual 4 energy channel light curves, according to the count statistics available for each event. The duration of 6 events was shorter than 2 sec: in these cases we could thus analyze the TTE data with 2-ms time resolution (see Section 3.2))[5]) integrated over the 4 energy channels. In the analysis of these data type we also accounted for the ≈30 ms offset between trigger time and TTE data load time. For the remaining 14 GRB/SN events either no reprocessed light curves were found in the public archive (9 cases) or the low statistics of the light curve did not allow any reasonable fit (5 cases).

First we determined for every GRB the background count rate selecting two time intervals not containing the burst[6], and modeled it with a 2nd order polynomial. We then built a pulse model by adding the best fit background model to the lognormal pulse profile (Brock et al. 1994) and fit the light curve as:

[4]Note that in the following the GRB/SN events reported in each case/figure is different, depending only on the quality of the available data.

[5]http://cossc.gsfc.nasa.gov/batse/batseburst/tte/index.html

[6]http://cossc.gsfc.nasa.gov/batse/batseburst/sixtyfour_ms/ bckgnd_fits.html

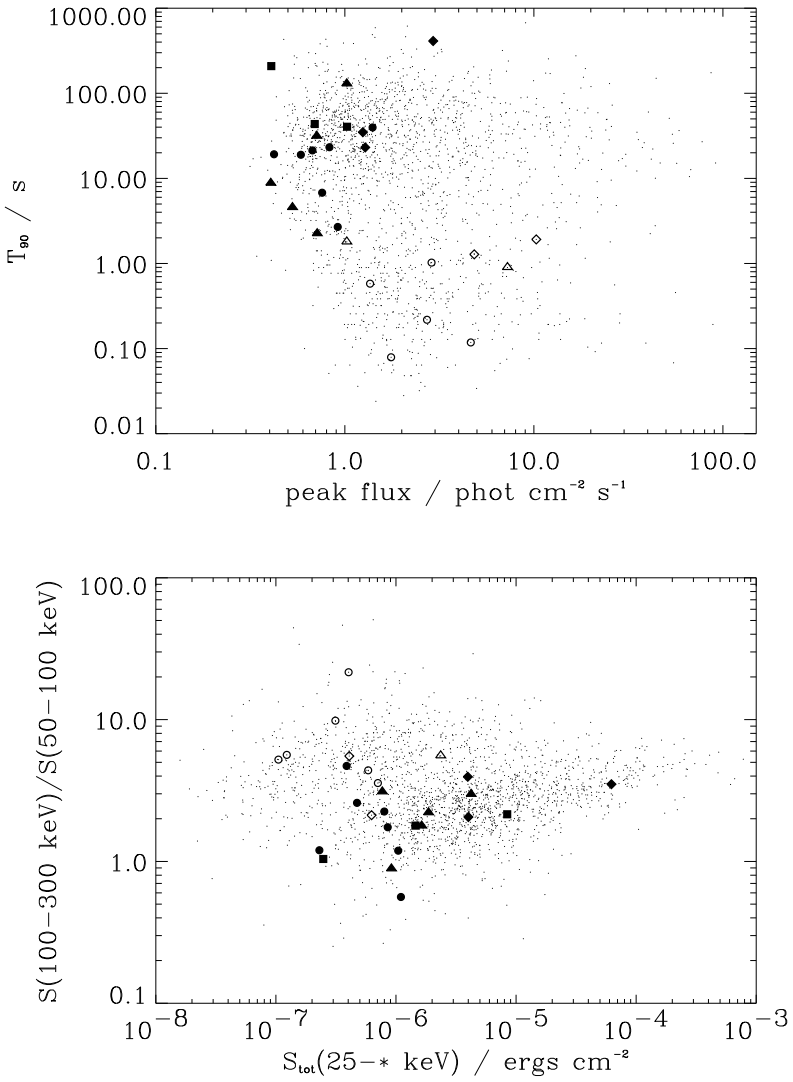

Figure 4.4: Comparison of the durations T_{90}, peak fluxes, hardness ratios (i.e. HR32) and total fluences of the GRB/SN and the entire BATSE samples. Triangles, squares and circles indicate the tentative associations found by Wang & Wheeler (1998), Hudec et al. (1999) and this work, respectively. Diamonds are the GRB with an indication of a SN event in the afterglow. Filled symbols represent long GRB (T_{90} >2 s).

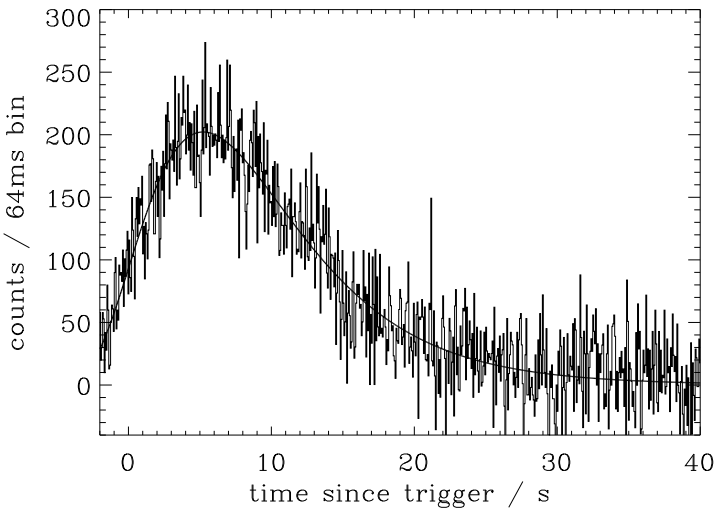

Figure 4.5: Lognormal model fit to the light curve (energy range: 30-1800 keV) of GRB 980425. The background was fitted with a quadratic polynomial and subtracted from the total count number. The parameters of the lognormal model are: A_{max}=202.2, t_0=7.5, μ=1.10 and σ=0.18; the χ^2_r of the fit is 1.02 for 730 d.o.f.

$$I(t) = \begin{cases} A_{\max}\ exp\left[-\frac{1}{2}\left(\frac{\log(t-t_0)-\mu}{\sigma}\right)^2\right], & t > t_0 \\ 0 & \text{otherwise} \end{cases}$$

where μ and σ are the mean and standard deviation, respectively, and the time is scaled to the pulse onset t_0 [7]. Two are the reasons behind this choice of profile: 1)most of the GRBs in the sample appear as single-peaked on the 64 ms and 2 ms timescale for long and short bursts, respectively (e.g. Norris et al. 1999 examined the sample of long, single-pulse gamma–ray bursts searching for bursts resembling the GRB 980425 and used the model by Brock et al. 1994 as adequately representing single-pulse events); 2) it allows a direct comparison with the results of previous studies (e.g. Norris et al. 1999, Quilligan et al. 2002). The best fits ($\chi^2 \sim 0.83$ – 1.18) are obtained for the integrated light curves, and in 11 (out of total 22) cases an acceptable fit was obtained for individual channel light curves. An example of the lognormal fit to a single-peaked GRB event is shown in Fig. 4.5.

[7] The lognormal pulse model is skewed to the right (as determined by σ).

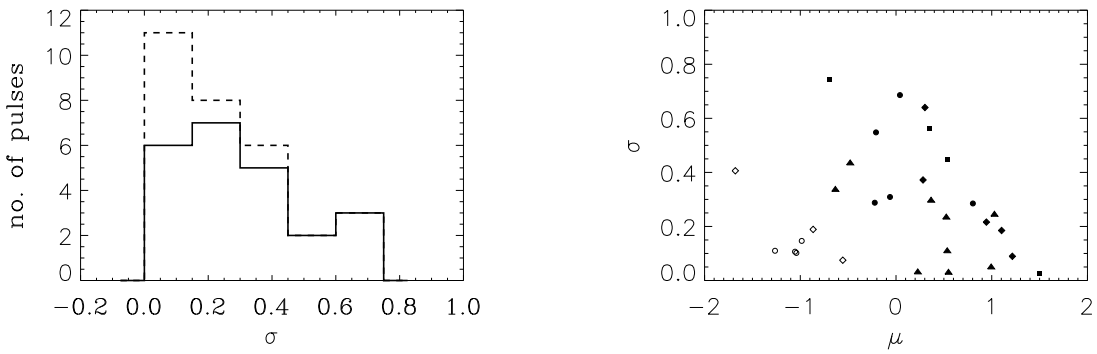

Figure 4.6: Left: Distribution of σ for the lognormal pulse model. The solid and dashed lines represent the parameters for long bursts and the contribution of short bursts. All the pulses in the time history are represented. Right: σ vs μ, i.e. the mean in log time. Symbols as in Fig. 4.4

4.5.2 Results

The resulting distribution of σ is shown in Fig. 4.6 (left panel) for all the pulses in the light curves of the 22 GRBs for which the fit was performed. The distribution of σ vs. μ is reported in the right hand panel. As expected short bursts are characterized by σ lower than long ones and their pulses are less asymmetric. While the statistics is rather poor, we note a global tendency for an anti–correlation between σ and μ both in long and short GRB/SN: there is no pulse with large μ (i.e. long rise time) and large σ (i.e. very asymmetric), namely they are typically FRED-like (see Section 3.3).

In order to compare the GRB/SN pulse properties with a control sample we examined also the distribution of their FWHM (64 ms time resolution). In Fig. 4.7 (left) this is shown together with the distributions derived by Norris et al. (1999) and Quilligan et al. (2002). The latter, referring to the brightest (long) 319 BATSE GRB, is very broad, peaking around 0.7 s, and significantly different from that of the GRB/SN sample. Interestingly, however, the FWHM distribution for the subset of long GRB/SN events (solid line in Fig. 4.7) appears to be similar to that derived by Norris et al. (1999) from the analysis of a sample of long, single-peaked GRB. Indeed a K-S test [8] returns (for long, single-peaked

[8]While formally the results by Norris et al (1999) refer to fits of count rates from channels CH2+3, typically the signals in CH1 and CH4 are weaker, thus not significantly affecting the comparison.

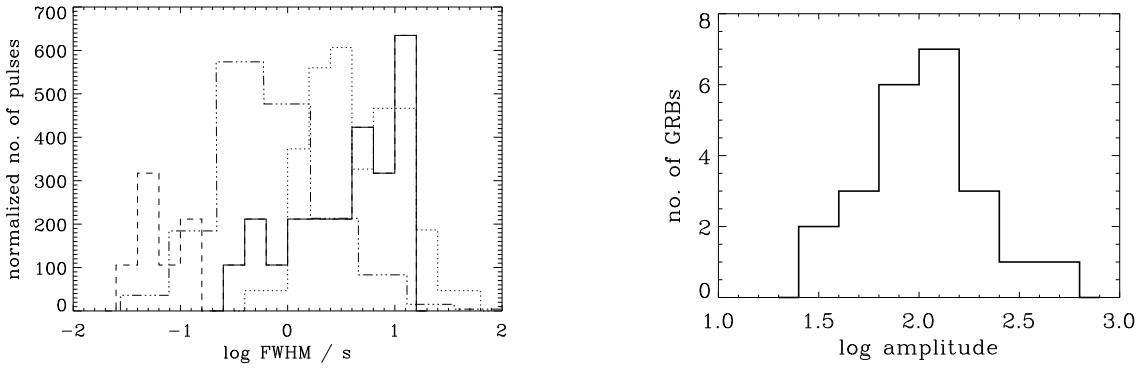

Figure 4.7: Left: Distributions of the full widths at half maximum. The solid/dashed lines represent the contribution of long/short GRB. The dotted line refers to the single-peaked bursts analyzed by Norris et al (1999), while the dash-dotted line are the bright, long bursts analyzed by Quilligan et al (2002). For clarity the distributions are normalized to the maximum number of data points (i.e. long bursts of Quilligan et al 2002). Right: distribution of pulse amplitudes on the 64 ms time scale. Short bursts are not included as they were analyzed at 2 ms resolution.

GRB/SN) a probability P_{KS}=0.98 that the two data sets originate from the same parent distribution. The comparison of the amplitude distributions (Fig. 4.7, right). cannot be properly done because it is biased by the brightness of the events.

In Fig. 4.8 (left panel) the pulse amplitudes (only for the 64 ms resolution timescale) vs. FWHM are displayed. Quilligan et al. (2002) find a weak negative correlation between these parameters. While there is no evidence for a trend for the whole GRB/SN sample, an anti-correlation (Spearman rank correlation coefficient of -0.65 and probability 0.3%) is present among the GRB/SN selected on the basis of the cross-correlation only. The interpretation of this is not clear: it might be simply due to the bias toward low fluxes in GRB/SN selected from the catalog cross–correlation and/or indicate that indeed the latter are largely spurious associations, not representing (atypical) properties of GRB physically associated with SN events.

A tendency for wider pulses to have larger time lags appears instead for the GRB/SN sample (Fig. 4.8, right). There the spectral lag (i.e. the delay between the peaks of the low with respect to high energy channel) is plotted against the FWHM of the fitted pulse. This behavior is consistent with what reported by Norris et al. (1996) on the

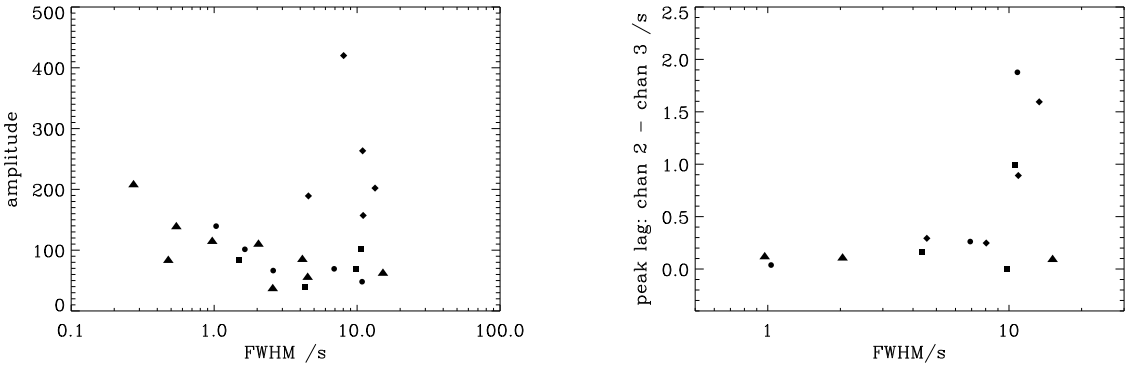

Figure 4.8: Left: Amplitude (fitted at 64 ms resolution) vs. FWHM as obtained from the fit to the total counts in the four channels. Right: Time lag between fitted peaks (in CH2 and CH3) vs. FWHM. Only long bursts are shown. Symbols as in Fig. 4.4

basis of a sample of 46 bright, long bursts: they found that the lag results mostly from the shift in the pulse centroid and thus the correlation is induced by the narrowing of the pulses toward higher energy. Different interpretations have been proposed for such property (e.g. Salmonson 2000, Schaefer 2004) and very recently it has been suggested that it might be accounted for in the jet-viewing-angle scenario (Ioka & Nakamura 2001) where both (small) pulse amplitude and (long) spectral lag are related to (large) viewing angles of the jet. As shown in the panels of Fig. 4.8, in the case of the GRB/SN sample (but excluding the 7 GRB/SN determined by the light curve bumps) small amplitude pulses could correspond to large spectral lags.

To summarize: within the limited statistics and differences in the selection criteria of the GRB/SN sample, the GRB/SN events appear to be broadly similar to the whole of the BATSE GRB population. However, the analysis of the FWHM distributions highlighted one intriguing possibility, namely that the GRB/SN events behave more typically like single–peaked GRB. Although aware that the bias toward weak GRB in the sample might be responsible for the above finding – Norris et al. (1999) already cautioned that dim bursts might have a multiple pulse structure which is difficult to detect – we explored this aspect in detail.

4.6 A connection between single-peaked GRB and SN?

As already mentioned, Bloom et al. (1998) suggested that GRB associated with SN might have distinctive temporal and spectral properties, similar to those of GRB 980425, namely a smooth, single peaked, long-duration (T_{90}=34.8 s) light curve and faint emission above 300 keV. Norris et al. (1999) considered this issue and searched the BATSE catalog with these criteria, but no other event similar to GRB 980425 and spatially/temporally correlated with any known SN was found. In our GRB/SN sample we instead found that the large majority ($\sim$ 80 %) of GRB are single peaked. Of those not selected by the catalog cross–correlation 5 out of 7 GRB are single-peaked events. It is worth stressing that of the other two spectral associations, GRB 031203 shows a single peaked light curve (Soderberg et al. 2004), while GRB 030329 presents different temporal properties, i.e. a profile with two peaks of similar intensity (Vanderspek et al. 2004).

In order to quantitatively test whether the GRB/SN sample comprises an unusually high number of single–peaked GRB (1) it has been necessary to determine an objective way of characterizing the "single-peakedness" and (2) due to the limited size of the GRB/SN sample (29 GRB with 64 ms data) the probability of finding a similar large percentage of single–peaked events had to be computed via random extractions of GRB subsamples from the BATSE catalog.

4.6.1 Method

We thus built an algorithm that identifies single–peaked bursts in the BATSE catalog. As the time profiles of GRB differ to great extent it is difficult to have a unique approach applicable to every burst: eventually we imposed conditions just to determine whether the burst has one or more than one peak.

Li & Fenimore (1996) proposed a method for identifying peaks in GRB time histories, and a modification of this was also applied by Nakar & Piran (2002) in the temporal analysis of short bursts. It consists of defining a count bin $C_{\rm p}$ at time $t_{\rm p}$ as a candidate peak if it satisfied the condition:

$$C_{\rm p} - C_{1,2} \geq N_{\rm var}\sqrt{C_{\rm p}}, \tag{4.1}$$

where $C_{1,2}$ are neighboring count bins at times $t_{1,2}$. $N_{\rm var}$ determines how rigorous the search is: too large $N_{\rm var}$ might clearly result in an algorithm insensitive to faint peaks; too low $N_{\rm var}$ could identify statistical variations as peaks. The previous works showed that the choice of $N_{\rm var}$=5 optimizes the algorithm.

The search was performed on the background-subtracted light curves, and thus a linear background was fitted to data before and after the burst trigger, and subtracted. The resulting time histories were binned to 128 ms resolution.

As one of the problems encountered was that sharp structures in the time history could be mis-identified as peaks, we applied a wavelet analysis for determining the dominant modes of variability. Wavelet transform is convenient to use when the analyzed signal consists of short spikes, that are not well approximated when doing a Fourier analysis: the wavelet coefficients resulting from the convolution of the signal with the wavelet functions represent the signal variation at a particular resolution (or scale) (e.g. Kolaczyk 1997, Quilligan et al. 2002). An example is shown in Fig. 4.9, where we present the results of the convolution of the data and the appropriately scaled and shifted wavelet function (higher scales correspond to the most "stretched" wavelets). We reconstructed the original signal by keeping only the maxima of the wavelet transforms; a very limited number ($\sim$ 25) of the wavelet coefficients was used to reproduce the signal. Although this does not guarantee the generation of a smooth light curve, with this approach the unique peak finding condition could be applied for the whole set of GRB.

The search for peaks was limited to the burst region, excluding periods before the burst which may contain a precursor. We tested several choices for the condition of peak finding, optimizing it to recognize what would be visually identified as a single-peaked GRB, and implemented slightly modified peak-finding conditions: a) adopted the value $N_{\rm var}$=7, and b) added the condition for a peak to have at least 20 % more flux than the neighboring 'valleys'.

4.6.2 Results

We applied the algorithm to the GRB/SN sample and this defined 23 (out of 29) single–peak bursts: this differs by less than 10% from the number we find by visual

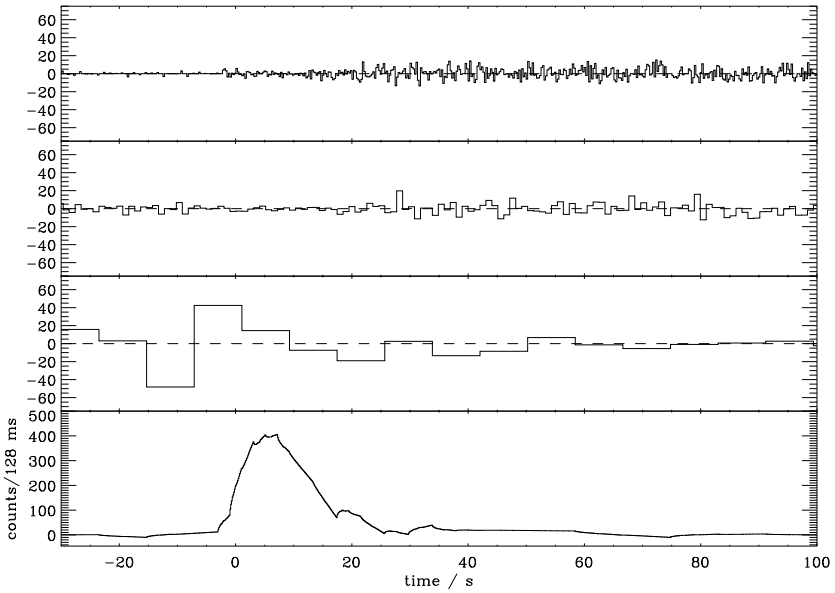

Figure 4.9: The wavelet reconstruction of the GRB 980425 light curve. Three top panels: wavelet coefficients for the original data decomposition (i.e. the binned photon counts of the gamma–ray burst shown in Fig. 4.3) decomposition; the scales $s=2^{1,3,6}$ are shown. The finer scales are dominated by noise and therefore only the maxima of the wavelet transform were used to reconstruct the light curve. Bottom panel: the GRB 980425 light curve reconstructed by retaining the 17 maximum wavelet coefficients.

inspection.

To establish the chance probability of such occurrence, we selected GRB from the BATSE catalog having fluences in the range span by the GRB/SN events (between 6.9×10^{-8} and 8.4×10^{-6} erg cm^{-2}), ending up with 1587 GRB, and systematically applied the algorithm to their 64-ms resolution data (for 142 out of them the algorithm did not identify any peak, as a consequence of the rigorous conditions imposed). We then randomly extracted subsamples of the same size ($\mathcal{N}$=29) of the GRB/SN sample, repeating the extraction n times. In Fig. 4.10 we show the distribution of the fraction of single–peak GRB for n=50, 150 and 250.

We fitted a lognormal function to the probability distribution[9], i.e:

$$P(x) = \frac{1}{\sqrt{2\pi}\sigma x} e^{(-(\ln(x)-\mu)^2/2\sigma^2)}, \tag{4.2}$$

for the case n =250 and find a 0.4 % probability of having 23/29 single-peaked bursts. If the number of single–peaked bursts in the sample were 10% lower (i.e. 20 or more events) the probability of observing it would still be $\sim$ 5%. Note that the distribution has a maximum for $\sim$15 single–peaked bursts; this is consistent with the result by Norris et al. (1999) who found 68/116 bursts with at least one pulse – suggesting however that it is difficult to assign an exact number of pulses as they observe a continuum of lower emissions superposed on otherwise single–peaked events.

The homogeneous treatment of the GRB/SN and random control subsamples should ensure that the above result is unbiased against effects that may vary the number of detected pulses in the GRB time history, such as the rigorous conditions on peak candidates, the fluence range, the (still present) spikes mis-interpreted as pulses and the presence of short GRB which in fact appear to be multi-peaked when seen at 2 ms resolution (there was 23% of short bursts in the sample).

[9]Lognormal distributions have been already used to describe the distributions of various GRB properties (see e.g. Li & Fenimore 1996, Quilligan et al. 2002)

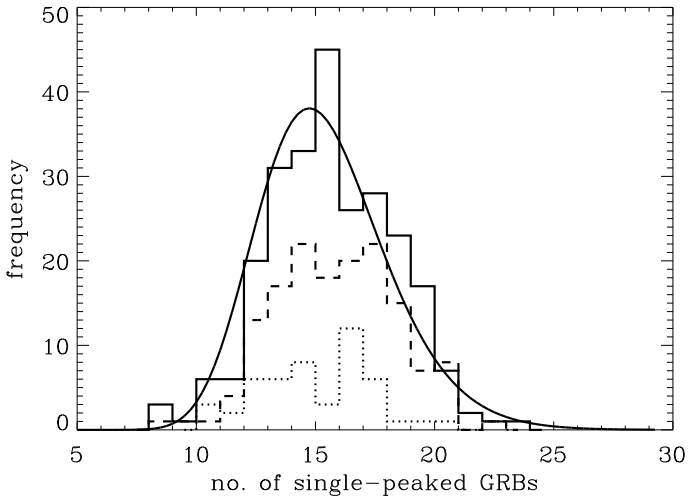

Figure 4.10: Distributions of the number of single–peaked GRB in subsamples of $\mathcal{N}$=29 GRB. The dotted, dashed and solid histograms represent the distributions for respectively n=50, 150, 250 extractions out of the total sample of 1445 bursts. The lognormal fit corresponds to the case n=250.

4.7 Spectral analysis

Let us now consider whether GRB/SN show any peculiarity in terms of spectral properties. We recall that the spectrum of GRB 980425 is 'unusual', peaking at $\sim$ 100 keV (Jimenez et al. 2001), below the typical 300 keV peak energy. Also GRB 030329 is characterized by a similar low peak energy (Vanderspeck et al. 2004), while GRB 031203 has a larger peak energy ($>$ 212 keV, Sazonov et al. 2004).

GRB spectra in the BATSE energy range (25-1800 keV) are usually described via the phenomenological Band representation (Band et al. 1993, see Section 3.4). Despite of a non–negligible dispersion of the fitted parameters, the typical values for the low and high energy power-laws photon indices are $\alpha \sim -1$ and $\beta \sim -2.5$, respectively, and the spectral peak energy $E_{\rm peak}$ is around a few hundred keV (Preece et al. 2000). The Band model in general successfully represents both the time integrated as well as the time resolved spectra (Ford et al. 1995).

Following the widely adopted methodology described by Preece et al. (2000), we analyzed the GRB/SN spectra obtained by integrating the signal over the burst duration (a

time resolved spectral analysis was possible only in a few cases due to the low signal–to–noise ratio).

4.7.1 Analysis

The spectral analysis was heavily limited because in many cases the GRB signal was too low for any reasonable spectral fit. For just over half of the bursts (16) we used the HERB data (see Section 3.2) from the most brightly illuminated BATSE LAD (128 energy channels). For short bursts or in those cases with no good time coverage with the HERB data we analyzed the MER data (see Section 3.2) (5 cases).

The background spectrum was extracted and averaged from two time intervals, before and after the burst trigger. The spectrum was eventually re-binned in energy in order to have enough statistics to apply the χ^2 goodness-of-fit test .[10]

The spectra were analyzed using the XSPEC v.11.1.0 package, performing the fitting with the Band model in the $\sim$30 – $\sim$1700 keV energy range. In some GRB this model fit resulted in unconstrained spectral parameters and/or unacceptable reduced χ^2 (18 cases): if mainly due to the low statistics at high energies we tested as alternative models the cutoff-power law (CPL; for 1 GRB) and broken power–law (BPL; 6 GRB) spectral functions, while if due to a low signal in most channels, we adopted the simpler single power-law model fit (11 GRB). The same set of models was applied to larger samples of bright bursts (Preece et al. 2000): we stress that our aim is to characterize the spectra of the GRB/SN sample rather than establish which model preferentially fit them (in fact the choice of a particular model may not be unique even for bright bursts, e.g. Ghirlanda et al. 2002). We considered the model fit acceptable when a reasonable χ^2 (ranging from 0.8 to 1.3) and non systematic residuals were obtained. All the models (except for the single power–law) are characterized by a low energy power–law $\propto E^{\alpha}$, a high energy power–law (Band and BPL models) $\propto E^{\beta}$ and the characteristic energy $E_{\rm peak}$.

[10] We binned in order to obtain a minimum of 5 counts/bin. This (minimal) choice has been tested by re-binning the data for a minimum of 10 and 20 counts/bin (e.g. Bevington & Robinson 1992) and the corresponding fits did not yield either significantly different χ^2 nor significantly different fit parameters.

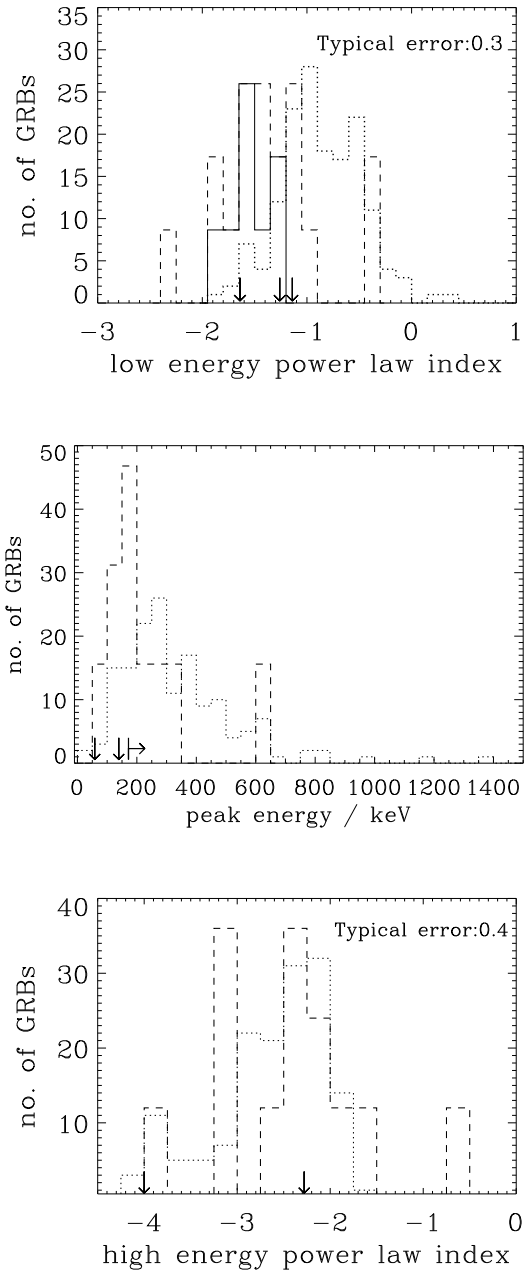

Figure 4.11: Spectral parameter distributions obtained for the GRB/SN (dashed lines) and GRB examined by Preece et al. (2000) (dotted lines). For clarity the number of GRB/SN events is normalized to the total number of GRB in the larger control sample by Preece et al. (2000). In the top panel the results obtained by fitting single power law model are indicated separately (solid line). A high energy power–law index $\beta = -4$ refers to the exponential function fit. Errors for the peak energy range from 20 to $\sim$ a few hundred keV. The arrows in each panel indicate the values (or limits) corresponding to GRB 980425, GRB 030329 and GRB 031203. Note that the highest values in the three distributions refer to GRB 990810 and GRB 971221, found by catalog cross–correlation.

4.7.2 Results

The distributions of the spectral parameters are shown in Fig. 4.11 for the GRB/SN and the Preece et al. (2000) samples. [11]

For the GRB/SN sample the average spectral index is $\alpha \sim$–1.5, with almost no bursts with $-1 < \alpha < 0$, which are instead found in the comparison sample. This suggests that on average GRB/SN events have low energy spectra softer than typical GRB. Note that GRB 980425 and GRB 030329 have spectra fitted with $\alpha \sim$–1.2 (Vanderspek et al. 2004) and GRB 031203 is modeled with a single power law with $\alpha \sim$–1.6 (Sazonov et al. 2004). It is also important to note that the single power law models (fitted to $\sim$ half of GRB) in general gives a value of α lower than that inferred from 'convex' models (Band, CPL or BPL). A K-S test performed on the α values obtained by fitting the 'convex' models only yields that the GRB/SN sample is significantly different from that reported by Preece et al. (2000), with P_{KS}=0.03.

The distributions of $E_{\rm peak}$ (for the 10 GRB/SN events that had spectrum fitted by Band, CPL or BPL) are reported in the middle panel of Fig. 4.11. The typical peak energy for GRB/SN is $\sim$ 220 keV, lower than that of bright BATSE GRB (from Preece et al. 2000) with P_{KS}=0.04. As mentioned, 2 out of 3 GRB with spectroscopic evidence of association lie in the lowest bin of this distribution (see Fig. 4.11).

Finally we report in Fig. 4.11 (bottom panel) the distributions of β. Within the large errors (β is usually not well constrained because the S/N decreases in the high energy channels), there is no evidence of deviations with respect to bright long bursts.

4.8 Redshift estimates

Clearly a crucial test on the physical connection of our GRB/SN pairs would be the determination of the GRB redshifts. Up to date, redshifts are known only for $\sim$ 42 GRB via the optical emission lines of their host galaxies or absorption lines in the optical transient spectra. Due to the high γ-ray flux, unaffected by extinction, and to the limited

[11] For the comparison the results of the time-resolved spectral analysis by Preece et al. were averaged, as for most GRB/SN it was possible to analyze only time integrated spectra.

number of afterglow detections, several attempts have been made in order to find a reliable method for deriving distances from the prompt γ–ray emission only. Unfortunately the large diversity in the temporal and spectral properties of GRB and the related uncertainties in turn result in significant uncertainties in any such method. For our purposes however even an indication of the GRB distance could rule out or reinforce an association.

Several correlations have been proposed to infer the GRB energetics on the basis of observable temporal and spectral γ-ray properties. Fenimore & Ramirez-Ruiz (2000) (see also Reichart et al. 2001) found a correlation between the luminosity and a variability indicator for a few GRB with measured z: smoother bursts appear to be intrinsically less luminous. Another distance indicator was identified by Norris et al. (2000) as a correlation between GRB luminosities and spectral lags. These correlations have then been used to estimate redshifts for a large sample of GRB (Fenimore & Ramirez-Ruiz 2000). Another interesting correlation has been found by Amati et al. (2002) (see also Lloyd-Ronning & Ramirez-Ruiz 2002) between the intrinsic peak energy $E_{\rm peak}$ and the isotropic total radiated energy $E_{\rm rad}$. Alternative methods to determine z have been proposed: Atteia (2003) identified a method by combining the spectral parameters and GRB duration; Bagoly et al. (2003) suggested a correlation between the peak flux ratios and z. The robustness of some of these correlations in representing the properties of BATSE GRBs will be further discussed in Chapter 6..

It is worth noticing that the calibration of all these relations is based on GRB with known z, but always excluding GRB 980425 due to its peculiar energetics and temporal/spectral properties. Also GRB 031203 turned out to be an outsider of some of those correlations. Caution should be thus considered in using the above results for candidate GRB/SN events, which might indeed be most similar to GRB 980425 and GRB 031203.

In the following we focus on two of such methods, for which we could infer more reliably the corresponding GRB parameters, namely the Lag-Luminosity correlation (Norris et al. 2000) and Peak Energy–Energy correlation (Amati et al. 2002).

4.8.1 Lag-Luminosity correlation

Norris et al. (2000) found that the spectral time lag τ is anti-correlated with the isotropic peak luminosity $L_{\rm iso}$, namely $\rm L_{iso,53} \approx 1.3 \times (\tau/0.01\ s)^{-1.15}$ for a sample of 6 bursts with known z. In order to derive the lag measure for the GRB/SN the same methodology was applied. The spectral lags were computed using a cross-correlation method similar to that described by Band (1997); there the cross correlation function was defined that measures the temporal correlation of two time series v_1 and v_2 as

$$CCF(\tau; v_1, v_2) = \frac{< v_1(t)\ v_2(t+\tau) >}{\sigma_{v1}\sigma_{v2}} \tag{4.3}$$

where $\sigma_v =< v^2 >^{1/2}$ and τ is the 'lag'. For example, if v_2 leads v_1 by t_0 (e.g. $v_1(t) = v_2(t-t_0)$), then the cross correlation function peaks at $\tau = -t_0$. In particular (see Fig. 4.12): i) we calculated the cross correlation functions (CCF) of the time histories in two different energy channels (see also Band 1997), i.e. CH1 and CH3, adding the apodization intervals before and after the burst (apodization intervals had a constant count number, computed as average value in adjacent time bins); ii) the analysis was limited to light curve regions with count rates larger than 10% of the peak luminosity; iii) the time series were binned in order to have higher S/N (64 ms data were binned to 128 ms; for short GRB TTE data were binned to 4 ms); iv) we fitted a linear background to every channel separately in the non-burst portions of the data and subtracted it from the total counts; v) finally the CCF were fitted with a third order polynomial around their peaks in order to derive an estimate of the time lag, then corrected by [12] a factor $1/(1+z)$. We derived the peak luminosity in the 50-300 keV energy range directly by integration of the GRB fitted spectrum for each possible redshift.

The results are presented in Fig. 4.13 (top panel). Unfortunately it was possible to estimate time lags for only 3 bursts (16 GRB/SN have both spectral data and four-channels time histories available and of those most have negligible signal in CH1; also in 3 cases the obtained time lags were negative and thus not further considered). The curves represent the intrinsic (i.e. corrected for z) $L_{\rm iso}$ and τ assuming a range $z = 0.01$ - 4 for the possible

[12] Note that both time dilation and channel energies should be corrected for z (see e.g. Fenimore & Ramirez-Ruiz 2000).

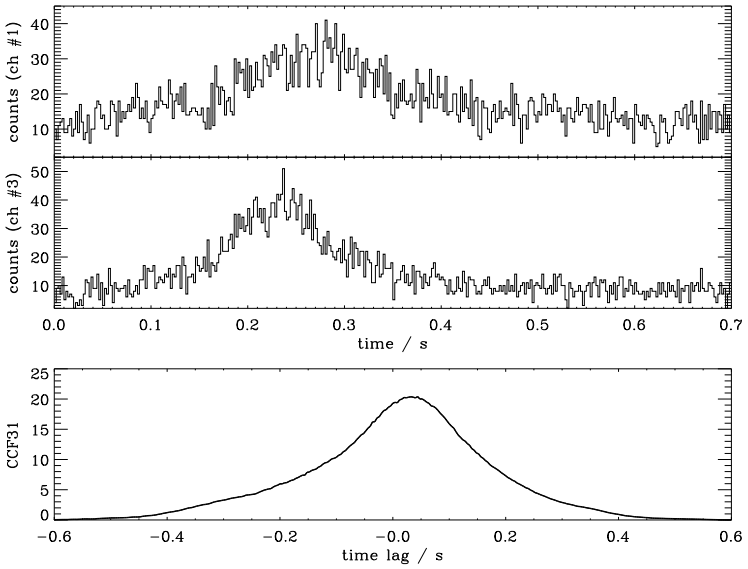

Figure 4.12: Top: the light curves of GRB 991002 for BATSE channel #1 (20-50 keV) and channel #3 (100-300 keV), derived from TTE data. Bottom: the cross correlation function (see text for details). The maximum, at τ=0.035 s, was found by fitting a 3rd order polynomial.

redshift. The points on them indicate the values of $L_{\rm iso}$–τ corresponding to the redshift of the putative associated SN, when known. It appears that the GRB/SN events could be consistent with the Lag-Luminosity correlation only if they were placed at high z (>1.5) indicating that the association are spurious. Alternatively, these GRB might not obey such correlation and thus could still be located at the SN redshift. The latter (intriguing) possibility does in fact get some credit from the fact that these GRB would then mimics the characteristics of 2 out of 3 spectroscopic GRB/SN (i.e. GRB 980425 and GRB 031203), possibly forming a separate class.

4.8.2 Peak Energy–Energetics correlation

The Peak Energy–Isotropic Energy correlation (Amati et al. 2002) has the form $E_{\rm peak} \propto E_{\rm rad}^{0.52}$. Similarly to the procedure described above we computed for the GRB/SN the total bolometric fluence (see Amati et al. 2002) by integrating (1-10^4 keV) the best fit spectrum (11 GRB/SN events). The results are presented in the $E_{\rm peak}$–$E_{\rm rad}$ plane in

Fig. 4.13 (bottom panel). The position of the symbols again indicate the corresponding values for the SN redshift, while the curved lines show the values for the interval z=0.01-4. The GRB/SN events for which only lower/upper limits of the peak energy could be estimated are shown only at the z of the possibly associated SN. We also mark the values for the 3 spectroscopic associations. Only two of the GRB/SN could be consistent with the Amati et al.'s relation: GRB 980703 (at z=0.967, Djorgovski et al. 1998), and GRB 971221 which might be associated with a SN at $z \approx 0.58$ (see Table 1). The properties of the rest of GRB/SN are not consistent with those predicted by such relation, but most importantly in 10 cases (5 of which with well determined parameters) could not obey the correlation (within its scatter) for any z. As known GRB 980425 and GRB 031203 are also clear outliers of the Amati et al.'s relation (whereas GRB 030329 is consistent with it).

To conclude, within the limitations given by the (small) fraction of the GRB/SN sample we interestingly find that these events do not follow the Lag-Luminosity and the Peak Energy-Isotropic Energy correlations, in some cases for any assumed z. The possible explanation is that these spectral relations simply do not hold for all the gamma–ray bursts and that the selection effects play an important role. However, the possibility is left open – supported by the similarity with the behavior of GRB 980425 and GRB 031203 – that at least a few GRB/SN events form a separate class with respect to the majority of long GRB.

4.9 Summary and discussion

We presented a detailed analysis of the temporal and spectral properties of a sample of BATSE GRB with an indication to be associated with a SN event, with the aim of determining whether these reveal any peculiar property with respect to the bulk of the detected GRB.

The "GRB/SN sample" was obtained combining GRB associations based on the presence of re-brightening in the afterglow light curves which might be interpreted as SN signatures and (more tentative) on positional/temporal coincidence from the cross correlation of GRB and SN catalogs. The latter ensemble was expanded with respect to previous

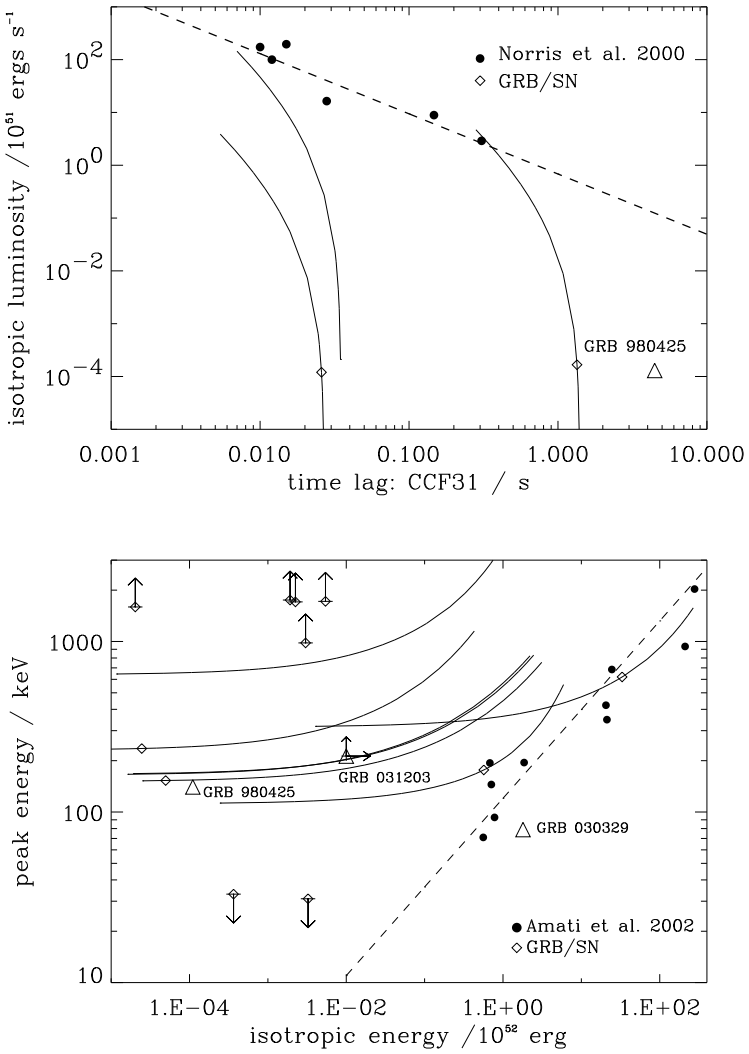

Figure 4.13: Top panel: Relation by Norris et al. (2000). Bottom panel: Relation by Amati et al. (2000). In both panels, the GRB/SN events are marked (diamonds) at the values corresponding to the redshift of the associated SN, while the trajectories represent the values corresponding to different redshifts, in the range 0.01-4. The dashed lines indicate the correlations as determined by Norris et al. (2000) and Amati et al. (2002). GRB/SN events which had only upper or lower limits on their peak energy are shown only for the values corresponding to the redshift of the coincident SN as arrows.

works, by including the most recent and complete GRB and SN catalogs. The whole set comprises 36 GRB. For GRB with public data we performed a systematic analysis and compared their temporal and spectral properties with those of larger, "control" samples of BATSE GRB.

The analysis of the temporal profiles revealed that in most cases (~ 80 %) the light curve presents a *single peak*. This property has been already considered by different authors (also on theoretical grounds) as a possible distinctive feature of GRB associated with SN events (Bloom et al. 1998a, Norris et al. 1999). The chance probability of finding the same fraction of single peaked bursts from a random extraction from the BATSE archive turned out to be ~ 0.4 %.

We further analyzed the time profiles fitting a lognormal model and correlated the pulse parameters. Dim bursts turned out to have *time lags* larger than bright ones, as possibly explained by a larger viewing angle (Ioka & Nakamura 2001). This interpretation has also been invoked in the case of GRB 980425/SN 1998bw and GRB 031203/SN 2003lw to account for their low luminosity compared to the bulk of GRB (Waxman 2004).

In terms of the spectral properties the GRB/SN sample shows *softer* spectra (both in terms of low energy spectral index and peak energy) with respect to typical GRB. This might be a distinctive feature of GRB associated with SN as 2 out of 3 spectroscopic associations also share an atypical low peak energy.

Finally, in the attempt to estimate their redshift, we considered two of the intrinsic correlations proposed for the population of long bursts, namely the Lag–Luminosity (Norris et al. 2000) and the $E_{\rm peak}$–$E_{\rm rad}$ (Amati et al. 2002) relations. While some GRB/SN might be consistent with them if not associated to the putative SN, some events do not obey such correlations for any redshift. This might indicate that they are effectively different or that these correlations only hold for particular sub-samples of GRB (e.g. bright long bursts - see also Ghirlanda et al. 2004 who find that short bursts mostly populate a region 'above' the $E_{\rm peak}$–$E_{\rm rad}$ correlation). In particular, the properties of this handful of GRB/SN again closely resemble those of 2 out of 3 spectroscopic associations which are also outliers of those relations.

As discussed in 4.2, previous results as well as the large positional uncertainties and

wide time window for the selection of GRB/SN via catalog cross–correlation in fact point toward a low probability of finding true associations via this method. However, the lack of the knowledge on progenitors and the low number of spectroscopic associations suggested us to investigate the statistical properties of a (non-homogeneous) GRB/SN sample as a whole, without imposing the further constraints. Indeed, the above results are suggestive of distinctive properties of GRB/SN sample. We find that it comprises (with respect to the whole of the BASTE events) an unusually high fraction of single peaked bursts, with softer spectra and some of those do not follow two of the proposed correlations for GRB. Most of these properties are mimicking those of the spectroscopic GRB/SN associations.

Further strong support to the reality of some of the GRB/SN associations found by catalog cross-correlation is provided by the following fact. If the sample of supernovae coincident with gamma–ray bursts were random, one expects that the relative number of different types of supernovae selected in this way would reproduce the percentages found in the whole SN catalog. That is, the frequency of Type Ib/c supernovae in the SN catalog is 6/100 (e.g. Valenti et al. 2005) and this would correspond to 1.6 SNe Type Ib/c in the sample of 26 supernovae (that is the number of SNe associated to gamma–ray bursts by catalog cross-correlation, with determined Type). However the GRB/SN sample comprises 8/26 Type Ib/c SNe ($\sim$ 31%) thus again indicating that the associations are not purely random, even with respect to the SN population.

Although it is not obvious how to assess individual GRB/SN associations, in order to determine any intersection among GRB/SN having 'unusual' characteristics, in Table 4.1 and 4.2 we schematically listed the three 'unusual' properties for each GRB/SN (single–peakedness, spectrum and consistency with the $E_{\rm peak}$–$E_{\rm rad}$ relation). In 19 GRBs (other than GRB 980425) there are at least 2 properties which set the event as GRB 980425-like: 10 GRB/SN have 2 or 3 (3 of those are short GRBs and only 1 is not selected by the catalog cross-correlation); 6 GRB have 2 but not the third one (5 are short and 2 not selected by the catalog cross-correlation).

While the uncertainty on the reality of a single association remains high, these results indicate that: 1) there is a population significantly larger than that detected so far

of GRB 980425-like events associated with SNe; 2) the corresponding GRBs have "atypical" temporal and spectral properties; 3) they appear underluminous in their observed γ–ray emission (at the level of 0.1-1 %) with respect to "standard" GRBs.

All three aspects give statistical and physical information on the nature of GRB 980425-like events. The finding of a significant number of these underluminous nearby bursts (e.g. viewed off axis) might in fact indicate from statistical arguments that these comprise the majority of GRBs (e.g. Sazonov et al. 2004). From the physical point of view, one promising scenario accounting for a qualitatively softer spectrum, a smooth, single–peak light curve and an apparently under-energetic event could be envisaged if the line of sight makes a large angle with respect to the jet axis and the observed GRB emission is in fact prompt emission reprocessed (reflected) at such angles by circumburst material. Fig. 4.14 shows the light curves expected in such case for two different viewing angles. They were calculated taking into account time arrival delays from different scattering distances, where we assumed the material to be located at distance R from the burst site and distributed in a shell with finite width $\Delta R \sim R$. Indeed the smooth light curve observed in GRB 980425 can be well reproduced. A detailed study of the spectral and temporal properties expected in this model is ongoing.

Estimates of the bolometric energetics of GRB (e.g. Soderberg 2004) and the improved statistics which will be allowed in the HETE-II, INTEGRAL and starting Swift era offer the most obvious possibilities to test these results.

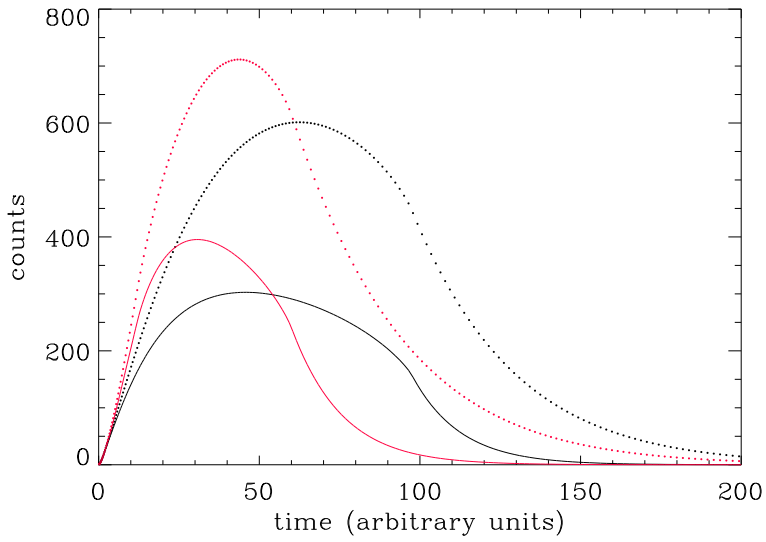

Figure 4.14: The light curves of gamma–ray bursts as expected if the prompt emission is reprocessed by circumburst material. It is assumed that the burst emission is collimated within an opening angle $\theta_j \sim 4.6^0$. The red curves refer to a viewing angle $\theta_v \sim 1.7^0$, and the black curves to $\theta_v \sim 3.4^0$; the dotted lines are the light curves produced if the width ΔR is halved. A typical distance of the scattering material $R \sim 10^{15}$ cm and a column density $< n > \Delta R \sim 10^{24}$ cm^{-2} were adopted.

GRB	RA	DEC	Error box (deg)	T_{90} s	Single peak*	α	SN	RA	DEC	Discovery date	Type	z[@]	Follow $E_{peak} - E_{\rm rad}$	Catalog cross-corr.
920321[2]	184.5	5.7	3.6	-	N	$-1.06^{+0.14}_{-0.13}$	1992Q	182.0	-1.6	920407	-	-	N	Y
920613[1]	312.9	-55.6	4.6	129.0	N	-	1992ae	322.1	-61.6	920627	Ia	0.075	N	Y
920708[1]	308.3	-49.9	3.3	3.2	Y*	$-1.41^{+1.54}_{-0.17}$	1992al	311.5	-51.4	920727	Ia	0.014	N	Y
920628[1]	317.8	-27.3	7.7	4.5	Y	-	1992at	321.8	-37.0	920717	Ia	-	-	Y
920925[1]	129.7	-58.7	5.0	-	Y	-	1992bg	115.5	-62.5	921016	Ia	0.036	-	Y
951107[2]	148.8	39.8	4.0	43.5	Y*	$-1.62^{-0.11}_{-0.10}$	1995bc	147.7	40.3	951201	II	0.048	N	Y
960221[1]	47.8	-31.2	4.3	31.3	Y	-	1996N	54.7	-26.3	960310	Ib	-	-	Y
961029[2]	59.3	-52.6	3.3	40.4	Y	-	1996bx	59.7	-53.3	961118	Ia	0.069	-	Y
970508[3]	132.4	80.6	2.3	23.1	Y	$-1.46^{+0.10}_{-0.23}$	-	-	-	-	-	0.835	Y[+]	N
970514[4]	67.6	-60.9	3.7	1.3	Y	-	1997cy	68.0	-61.7	970716	II	0.0642	-	N
971218	116.1	16.7	5.2	6.8	Y	$-1.25^{+0.31}_{-0.58}$	1998B	116.5	18.7	980101	Ia	0.045	N	Y
971221	73.7	4.7	6.3	1.0	Y	$-2.35^{+0.57}_{-1.56}$	1997ey	74.2	-2.6	971229	Ia	0.58	Y	Y
980326[5]	133.3	-18.6	2.1	-	Y*	$-1.90^{+0.26}_{-0.20}$	-	-	-	-	-	0.9–1.1	Y[+]	N
980425[6]	291.9	-53.1	1.6	34.8	Y	$-1.14^{+0.22}_{-0.21}$	1998bw	293.7	-52.8	980428	Ic	0.0085	N	N
980525	157.6	-17.8	6.8	39.6	N	$-1.69^{+0.18}_{-0.19}$	1998ce	152.6	-25.8	980519	II	-	-	Y
980703[7]	359.1	12.0	0.5	411.6	N	$-1.01^{+0.10}_{-0.12}$	-	-	-	-	-	0.967	Y	N
980910[8]	195.1	-21.1	6.8	-	-	-	1999E	199.3	-18.5	990115	IIn	0.025	-	N
990527	199.9	49.3	7.7	18.9	Y	$-1.65^{+0.33}_{-0.40}$	1999ct	198.3	46.2	990613	Ia	0.18	-	Y
990810	358.1	1.7	4.3	0.1	Y	$-0.32^{+0.40}_{-0.40}$		multiple	(2)	associations			N	Y
991002[9]	25.1	3.7	2.2	1.9	Y	$-1.12^{+0.49}_{-0.26}$	1999eb	25.7	3.7	991002	IIn	-	N	N
991015	11.6	8.9	7.8	2.7	Y	-	1999ef	14.7	12.7	991009	Ia	-	-	Y
991123	157.2	26.9	4.7	-	Y	-	1999gj	10.5	26.1	991117	Ia	0.018	-	Y
000114	121.6	39.5	7.9	0.58	Y	$-1.42^{+0.21}_{-0.21}$	2000C	114.2	35.2	000108	Ic	0.012	N	Y
000415	199.4	-29.9	7.4	0.22	Y	$-0.39^{+0.74}_{-0.49}$	2000ca	203.8	-34.1	000428	Ia	0.024	N	Y

Table 4.1: The GRB/SN sample – part I; GRBs have BATSE error boxes smaller than 8 deg (*) refers to a single-peaked GRB with substructure. There is no SN reported when there was only a SN bump present in the afterglow or in case of multiple (#) associations. [@] IAUC SN catalog. [+] Already in the Amati et al. (2002) sample; [1] Wang & Wheeler (1998); [2] Hudec et al. (1999); [3] Piro et al. (1999); [4] Germany et al. (2000); [5] Bloom et al. (1999); [6] Galama et al. (1998); [7] Holland et al. (2001); [8] Rigon et al. (2003); [9] Terlevich et al. (1999).

GRB	RA	DEC	Error box (deg)	T_{90} s	Single peak*	α	SN	RA	DEC	Discovery date	Type	z[@]	Follow $E_{peak} - E_{\rm rad}$	Catalog cross-corr.
910423[1]	196.7	-5.2	11.1	208.5	Y	$-1.88^{+0.40}_{-0.51}$	1991aa	190.5	-6.0	910507	Ib	-	-	Y
950917[2]	339.9	-1.47	8.2	-	Y	-	1995ac	341.4	-8.8	950926	Ia	0.05	-	Y
960925[2]	29.3	-13.9	8.4	1.8	Y	-	1996at	17.1	-1.0	961009	Ib/c	0.09	-	Y
961218[2]	97.7	-21.7	12.7	8.7	Y*	-	1997B	88.3	-17.9	970104	Ic	0.01	N	Y
970907[2]	346.9	11.2	8.3	0.9	Y	$-1.26^{+0.14}_{-0.16}$	1997dg	355.1	26.2	970928	Ia	0.03	N	Y
971013[2]	167.0	2.7	8.8	12.3	Y	-	1997dq	175.2	11.5	971105	Ib	0.003	-	Y
971120[2]	155.7	76.4	9.9	2.2	Y	-	1997ei	178.5	58.5	971223	Ic	0.011	-	Y
980530	148.3	-27.3	8.7	21.3	Y	$-1.51^{+0.14}_{-0.15}$	1998ck	145.2	-29.1	980531	Ia	0.038	N	Y
990719	224.5	10.8	10.9	23.2	N	-	1999dg	227.8	13.5	990723	Ia	-	-	Y
990902	58.2	62.5	15.5	19.2	Y	-	1999dp	67.3	69.5	990902	II	0.016	-	Y
991021	346.3	-30.9	12.3	-	Y	-	1999ex	334.0	-36.8	991109	Ic	0.011	-	Y
000319	172.7	-13.8	9.8	0.08	Y	-		multiple	(5)	associations		-	-	Y

Table 4.2: The GRB/SN sample - part II; GRBs with BATSE error boxes larger than 8 deg. (*) refers to a single-peaked GRB with substructure. There is no SN reported when there was only a SN bump present in the afterglow or in case of multiple (#) associations. [@] IAUC SN catalog; [1] Wang & Wheeler (1998); [2] Hudec et al. (1999).

Chapter 5

Extremely hard GRB spectra: evolution and thermal character

5.1 Introduction

As mentioned in Section 2.3.2, the standard scenario for the observed prompt spectrum involves synchrotron/inverse Compton radiation of relativistic electrons accelerated in internal shocks within a relativistic outflow. The majority of present date observations is well interpreted by this model and efforts have been made in order to explain the observed spectral parameters and the correlations among them. However, a non negligible fraction of bursts does not follow the predictions of the synchrotron emission model in terms of observed spectra and inferred parameters describing the details of the emission process. It should be noticed that the understanding of the emission process is not only related to the inferences on the physical conditions in the fireball, but even to a more fundamental issue related to the inefficiency of internal shocks in dissipating energy. This remains an open and crucial point in the understanding of GRBs, as in fact the low efficiency of such mechanism contradicts the relatively higher radiative efficiency of prompt vs afterglow phases.

In this chapter the evidence for a thermal emission phase in gamma–ray bursts is discussed and the case of the extremely hard low energy spectrum of GRB 990413 is presented. In Section 5.2. the most popular emission models for the prompt gamma–ray

burst spectra are reviewed; the difficulties encountered in the 'standard' interpretation of the observed hard low energy slopes are the subject of Section 5.3. The case of the burst GRB 990413 showing an extremely hard low energy component is discussed in Section 5.4. This burst exhibited also strong temporal variability, which results to be connected with a variable contribution of two different emission components (thermal vs. non–thermal). The variability level of this burst and its comparison with a sample of bursts with similar brightness is examined in Section 5.5. The possible emission processes responsible for such phenomenology in GRB 990413 are discussed in the last Section.

5.2 Emission models for the prompt GRB spectrum

The extreme diversity of the GRB time profiles, the apparent non-thermal spectrum and the lack of a clear signature of the radiation process involved makes it difficult to model the gamma–ray burst emission; the observed non-thermal spectrum with a complex temporal structure is usually interpreted within the framework of the internal shocks scenario (Rees & Mèszàros 1994), which relates the observed gamma–ray burst emission to the radiation from shock-heated plasma. The emitting region - the shocked material - moves relativistically at small angles with respect to the line of sight. The process by which the energy dissipated in the shocks is radiated clearly depends on the energy distribution of electrons/positrons in the shocked material and on the values of the comoving particle density and magnetic field.

5.2.1 Synchrotron model

The main radiation mechanism invoked to interpret prompt GRB spectra is synchrotron emission. It has been shown that the optically thin synchrotron spectrum (Katz 1994, Tavani 1996) could represent a good fit to GRB spectra; varying the parameters and assumptions involved in the derivation of the synchrotron spectrum may accommodate a (limited) range of the observed low energy spectral characteristics (e.g. Lloyd & Petrosian 2000).

There are several important physical assumptions that determine the emission

process: (i) the electrons/positrons are assumed to be stochastically accelerated, e.g. via the Fermi mechanism in the relativistic shocks to a power-law distribution in energy:

$$N(\gamma_e) \propto \gamma_e^{-p} \quad \text{for} \quad \gamma_e > \gamma_{min} \tag{5.1}$$

(ii) the total energy U that goes into electron/positron random motions is parametrized as a fraction $\epsilon_e = U/e$ of the total internal energy e in the shocked region, and (iii) the unknown strength of the magnetic fields in the shocked region is also parametrized by the ratio of the magnetic field density to the total energy, $\epsilon_B = B^2/8\pi e$. These parameters in principle should be determined from the microscopic physical process that takes place in the shocks. Given our ignorance on such process(es), the attempt is to constrain them by requiring the model to reproduce the observed spectral features of gamma–ray bursts. The minimum Lorentz factor of the electron distribution, γ_{min}, is related to the electron energy density U and the number density n_e as:

$$\gamma_{min} = \frac{p-2}{p-1}\frac{U}{n_e m_e c^2} \tag{5.2}$$

Typically $p > 2$ is adopted which is consistent with most of the observational data (Preece et al. 2000); the value of the upper energy cutoff does not play a critical role in the spectrum as it radiates at energies much higher than peak energy and it does not significantly affect the energetics (for $p > 2$).

Synchrotron cooling time scale

The characteristic photon energy emitted by a randomly oriented single electron with Lorentz factor $\gamma_e \gg 1$ in a tangled magnetic field due to synchrotron radiation is (in the observer frame):

$$(h\nu_{syn})_{obs} = \frac{\hbar q_e B}{m_e c}\gamma_e^2 \Gamma \tag{5.3}$$

where Γ is the Lorentz factor of the emitting material and q_e the electron electric charge. The power emitted in the fluid frame is:

$$P_{syn} = \frac{4}{3}\sigma_T c U_B \gamma_e^2 \tag{5.4}$$

where $U_B = B^2/8\pi = \epsilon_B e$ is the magnetic energy density and σ_T is the Thomson cross section. Thus the cooling time of the electron in the local frame is $\gamma_e m_e c^2/P_{syn}$ and the observed time scale is shorter by a factor of Γ:

$$t_{syn}(\gamma_e) = \frac{3m_e c}{4\sigma_T U_B \gamma_e \Gamma} \tag{5.5}$$

that gives (substituting eq. 5.3) $t_{syn}(\nu) \propto \nu^{-1/2}$. This characteristic cooling time sets a lower limit to the GRB variability time scale: the spikes in the light curve can not be shorter than the cooling time (Sari, Narayan & Piran 1996). That is, the individual subpeaks within a temporal profile of a GRB possibly represent the cooling curves of episodically heated electrons.

Synchrotron spectrum

The instantaneous synchrotron spectrum of a single electron with energy $\gamma_e mc^2$ can be approximated with a power law $F_\nu \propto \nu^{1/3}$ up to $\sim \nu_{syn}(\gamma_e)$ and an exponential decay above it (Rybicki & Lightman 1979).

In order to calculate the overall spectrum from an assembly of particles that have been accelerated in the shocks and loose their energy via synchrotron emission, the synchrotron spectrum for a single electron needs to be convolved over the particle energy distribution. We consider the electron distribution as discussed in Section 5.1. As the cooling time of an electron is inversely proportional to its Lorentz factor γ_e, electrons with a Lorentz factor higher then a critical Lorentz factor γ_c cool on the relevant timescale t'. To estimate γ_c we compare t_{syn} (eq. 5.5) with the t' (in the observer's rest frame):

$$\gamma_c = \frac{3m_e c}{4\sigma_T U_B \Gamma t'} \tag{5.6}$$

Thus two characteristic energies will have a significant role in the properties of the integrated synchrotron spectrum: $\nu_m \equiv \nu_{syn}(\gamma_{min})$ and $\nu_c \equiv \nu_{syn}(\gamma_c)$.

Two radiative regimes are possible: (1) the *fast cooling* regime occurs if $\gamma_c < \gamma_{min}$ and all the electrons cool rapidly, and (2) if $\gamma_c > \gamma_{min}$ only the high energy tail of the

distribution (those electrons above γ_c) cool and the system is in the *slow cooling* regime. The most energetic electrons will be always cooling rapidly and the highest portion of the spectrum will satisfy:

$$F_\nu = N[\gamma(\nu)]m_e c^2 \gamma(\nu) d\gamma/d\nu \propto \nu^{-p/2}. \tag{5.7}$$

Similarly, if the low energy electrons are slow cooling, the lowest part of the spectrum will behave like $F_\nu \propto \nu^{1/3}$.

In the GRB prompt phase the condition of fast cooling is expected for the typical conditions forseen. Indeed the relativistic shocks must emit their energy effectively, and furthermore, the temporal variability could not be reproduced if the cooling time is too long. Thus the integration time for the prompt phase is much longer than the cooling time, and the observed spectrum has to be computed by integrating the instantaneous spectrum taking into account the effect of cooling.

In the case of fast cooling all the electrons will cool down roughly to γ_c and the flux at the observer is given by (e.g. Sari, Piran and Narayan 1998):

$$F_\nu \propto \begin{cases} (\nu/\nu_c)^{1/3} F_{\nu,max}, & \nu_c > \nu \\ (\nu/\nu_c)^{-1/2} F_{\nu,max}, & \nu_m > \nu > \nu_c \\ (\nu_m/\nu_c)^{-1/2} (\nu/\nu_m)^{-p/2} F_{\nu,max}, & \nu > \nu_m \end{cases}$$

where $F_{\nu,max}$ is the observed peak flux. The typical spectrum corresponding to fast cooling is shown in Fig. 5.1. The light curve depends on the hydrodynamic evolution, that in turn determines the time dependence of ν_m, ν_c and $F_{\nu,max}$.

Synchrotron self-absorption

One of the simplifications in standard synchrotron models applied to gamma–ray bursts is that the emission region is optically thin. That is because synchrotron self-absorption requires extreme physical conditions to be effective at gamma–ray energies, namely the magnetic energy density must be extremely high (e.g. Crider & Liang 1999 argued that the low energy spectral break in GRB 970111 may be due to synchrotron

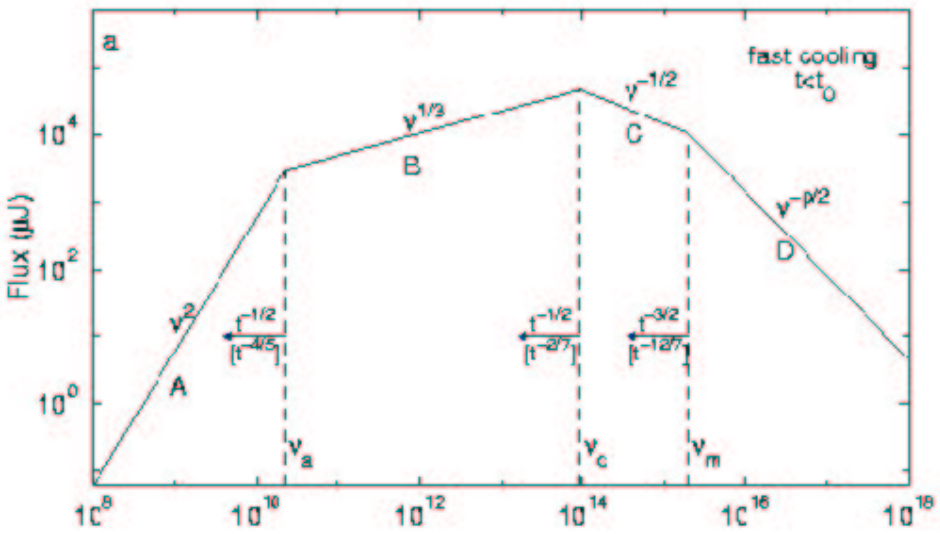

Figure 5.1: Synchrotron spectrum from a power-law electron distribution in the fast cooling regime. The frequencies ν_m, ν_c and ν_a decrease with time as indicated; the scalings above the arrows correspond to an adiabatic evolution, and the scalings below (in square brackets) correspond to a fully radiative evolution. From Sari, Piran & Narayan 1998.

self-absorption. Assuming $\Gamma \approx 1000$, $E_{abs} \approx 70$ keV and $\tau_T \approx 1$, they estimate B=4×10^7 G).

When synchrotron self-absorption is important the spectrum exhibits an additional break at the synchrotron self-absorption frequency ν_a and a steep cutoff in the low energy spectrum. The self-absorption frequency is given by the condition that the optical depth is of the order unity; the absorption coefficient for a power law distribution of particles is given by (Rybicki & Lightman 1979):

$$\alpha_{\nu'} = \frac{(p+2)}{8\pi m_e \nu'^2} \int_{\gamma_{min}}^{\infty} d\gamma_e P'_{\nu'}(\gamma_e) \frac{n(\gamma_e)}{\gamma_e}. \tag{5.8}$$

The self absorption frequency satisfies: $\alpha_{\nu'} R/\Gamma = 1$; it can be estimated once we have a model for the hydrodynamics and know how R and γ vary with time. The spectrum below ν_a depends on the electron distribution. One obtains $F_\nu \propto \nu^2$ (Sari et al. 1998) for $\nu < \nu_a$ since almost all the low-frequency radiation is emitted by electrons with a typical synchrotron frequency much higher than ν_a (Fig. 5.1).

5.2.2 Inverse Compton emission

The inverse Compton process (IC) can be viewed as a transfer of energy between electrons and photons, that is, the boosting up of the synchrotron photons when they scatter on high energy electrons. IC scattering depends on the Comptonization parameter $Y = \gamma_e^2 \tau_T$ and in the fast cooling regime (that is interesting for the prompt GRB emission) becomes important for $Y = \sqrt{\epsilon_e/\epsilon_B} > 1$ (Sari, Narayan & Piran 1996, Sari & Esin 2001). Even if the IC scattered photons result too energetic and therefore their energy is beyond the observed energy range, the inverse Compton process affects the observed spectrum in two ways: firstly, it shortens the cooling time since the emitting electrons are cooled by the synchrotron and IC processes, and secondly, it influences the overall energy budget and reduces the efficiency of the energy conversion into the observable range.

In the case of relativistic electrons, the photon energy is boosted in inverse Compton scattering by a factor γ_e^2 (Rybicki & Lightman 1979); after a single IC scattering the photon's energy is so high that in the electron's rest frame it is in the Klein-Nishina energy

regime and the decrease of the cross section makes a second scattering very unlikely. The typical IC scattered photons will be observed at the energy:

$$(h\nu_{IC})_{obs} = \frac{\hbar q_e B}{m_e c}\gamma_e^4\Gamma \tag{5.9}$$

The Lorentz factors of the order of a thousand (in the fluid rest frame) imply that - if the observed gamma–ray emission is produced by synchrotron in the internal shocks - the IC emission would generate a second peak in the GeV energy range (Zhang & Mészáros 2001). Böttcher & Dermer 1998 considered several other high energy spectral components (e.g. synchrotron by protons) besides the IC component and predict ∼10 MeV - 100 GeV fluxes at a level that may have been observed with EGRET (in bright GRBs) and could be detected by GLAST, whose sensitivities are $\approx 8\times 10^{-8}$ photons (>100MeV) $\mathrm{cm}^{-2}\mathrm{s}^{-1}$ and $\approx 2\times 10^{-9}$ photons (>100MeV) $\mathrm{cm}^{-2}\mathrm{s}^{-1}$, respectively.

5.3 Hard GRB spectra

The spectral parameter (e.g. in the Band's parametric representation, Band et al. 1993) which is most constraining for the emission models of gamma–ray bursts is the low energy power law photon index α. As recalled above, the optically thin synchrotron spectrum from a power law distribution of relativistic electrons with a sharp minimum energy cutoff and with an isotropic pitch angle distribution predicts a limiting value of $\alpha = -\frac{2}{3}$ (Katz 1994), while there is a significant number of events with harder α (Preece et al. 2000). Moreover, the time–resolved spectral analysis revealed that the spectrum evolves with time (Ford et al 1995, Preece et al. 2000); the evolution of the low energy photon spectra in GRBs (Crider et al. 1997) showed that in the flux rise phase the spectrum can be much harder than the limiting slope $E^{-2/3}$. This might indicate that the physical conditions of the emitting plasma evolve and that various emission processes dominate at different times and/or that the spectral evolution is directly related to the central engine physics.

More recently Ghirlanda et al. (2003), focusing on the time resolved spectral analysis of a handful of extremely hard GRB spectra, enlightened the difficulties of non-

thermal models in accounting for them, showed that some of the spectra could be consistent with black body emission and thus suggested that in some bursts the initial emission phase could have a thermal character. Recently Ryde (2004) studied a few gamma–ray bursts with very hard spectra, discussing the observed emission in terms of two components: a black body and a non-thermal one, with relative strengths variable throughout the burst duration.

The alternative scenarios invoked for the non-negligible percentage of observations inconsistent with the predictions of the simplest synchrotron model include the following:

Synchrotron emission. (i)Lloyd & Petrosian 2000 found that the entire range of observed behaviors can be accounted for by the optically thin synchrotron model if some (simplified) assumptions are relaxed. In particular, a more realistic smooth (rather than sharp) cutoff in the electron distribution tends to soften the low energy spectral behavior (see Fig. 5.2). However, the electron distribution must fall off below some turnover energy, otherwise the optically thin model would predict too many bursts with α smaller than about $-\frac{3}{2}$; (ii) by considering a distribution of ultrarelativistic electrons in a highly non-uniform, small scale magnetic field (i.e. with length scales smaller than the electron gyro-radius), Medvedev 2000 showed that low energy power law indices as large as α=0 can be produced ('jitter' radiation theory). Lloyd & Petrosian 2000 obtained a similar result by assuming a highly anisotropic pitch angle distribution of the accelerated electrons (small pitch angle model) (Fig. 5.2).

Compton emission. (i) models have been proposed that predict hard low energy portion of the spectrum based on the Comptonization of soft (e.g. self-emitted cyclo-synchrotron) photons to gamma–ray energies (Liang et al. 1997, Ghisellini & Celotti 1999). The typical spectrum is flat, $F_\nu \propto \nu^0$; (ii) another scenario was proposed by Lazzati et al. 2000. It postulates that the prompt GRB emission is produced by the Compton drag process, which is caused by the interaction of a relativistic fireball with a dense soft photon ambient bath, such as that expected to be present if the progenitor is a massive star. They consider a relativistic fireball propagating in a funnel inside a massive star; as the funnel walls emit a quasi-blackbody spectrum, and the photons are boosted by the square of the Lorentz factor

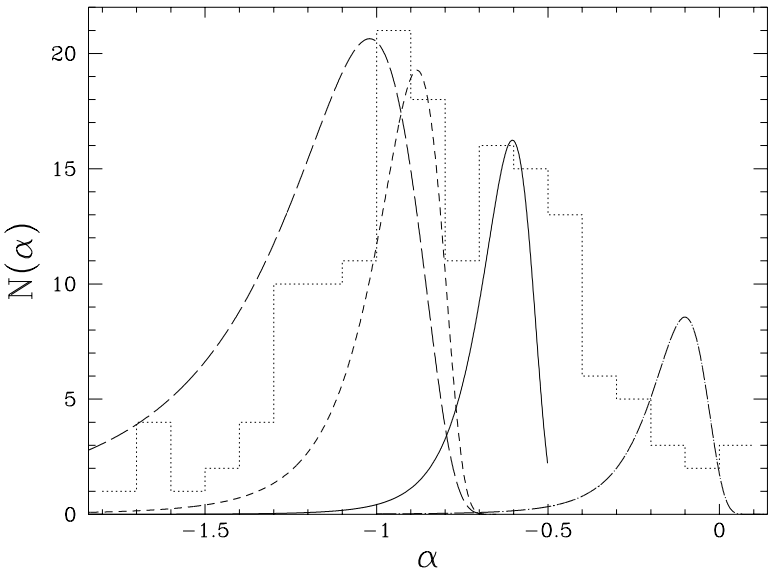

Figure 5.2: Predicted α distributions. The three left-hand curves are for an isotropic pitch angle distribution for a $q \to \infty$, $q = 2$ and $q = 0$, where q characterizes the cutoff in the electron distribution - sharp, intermediate and flat respectively ($N(\gamma) \sim (\gamma/\gamma_{cut})^q/(1 + (\gamma/\gamma_{cut})^{p+q})$ with γ_{cut} representing some critical energy below which the electron distribution changes from p to q). The rightmost curve (dot-dashed) corresponds to the small pitch angle distribution for an intermediate cutoff. The dotted histogram is the observed distribution taken from Preece et al. 2000. The simulated curves have been separately normalized to the height of this observed distribution. From Lloyd & Petrosian 2000.

Γ of the fireball, the local spectrum has a blackbody shape at a 'temperature' enhanced by Γ^2. The observed spectrum is a convolution of all the locally emitted spectra; Ghisellini et al. 2000 showed that it has a complex shape with power-law segments that correspond to the decrease in temperature inside the funnel, the deceleration of the fireball and the dilution of the radiation energy density as the fireball propagates outside the star envelope. The lowest energy part of the spectrum is described by $F_\nu \propto \nu^2$ ($\alpha = 1$).

Photospheric emission. Direct thermal emission is expected as the first signal from an expanding fireball as it becomes optically thin and before non-thermal particle acceleration takes over. (i) Mészáros and Rees (2000) examined the dependence of the relative importance of photospheric emission on the physical parameters of the fireball. They considered 'standard' synchrotron radiation, Comptonization of the photospheric photons, as well as

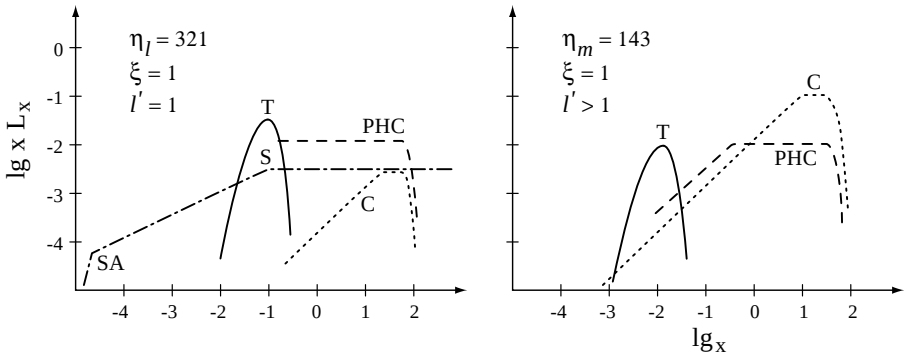

Figure 5.3: Two examples of the predicted spectra when photospheric emission is important. The thermal contribution results in hard slopes of the low energy portion of the spectrum. The different emission components are labeled: T stands for the thermal photosphere; C for the shock pair-dominated Comptonized; S for the shock synchrotron; PHC for the photospheric Comptonized component. Energy is given in the units $x = h\nu/m_e c^2$. From Mészáros and Rees 2000.

the role of copious pair production, occurring for high comoving synchrotron luminosities. They predict that a dominant contribution from the photosphere with respect to the internal shock dissipation is expected for very low baryon loading, weakly varying outflows or low shock efficiencies - the thermal component may provide low-energy slopes as hard as $F_\nu \propto \nu^2$. The high-energy power law spectra still require a strong synchrotron component, or blackbody photons Comptonized to higher energies. The peak of the photospheric component is shifted to lower energies (Fig. 5.3) for relatively low values of the baryon loading, when the fireball transparency occurs in the coasting regime. In such case the thermal emission becomes prominent when the contribution of shock synchrotron photons is low. Copious pair production, via $\gamma\gamma \rightarrow e^{\pm}$, can be important as it increases the opacity and the cooling of the photosphere. In these conditions (corresponding to a compactness parameter exceeding unity) shocks occur at large optical depths and their radiation is thermalized and adds to the purely thermal (T) and non-thermal (PHC) components emerging from the photosphere. (ii) Daigne and Mochkovitch (2002) compared the time profile and spectrum of the emission from internal shocks with the photospheric thermal emission (Fig. 5.4). They considered the emerging spectrum as function of the arrival times of the photons from a sequence of shells of different Lorentz factor Γ in the relativistic wind. The ratio of the count rate due to photospheric emission over that due to internal shock clearly shows the

observable presence of a thermal component either in the X-ray or gamma–ray range. Still - as the presence of a bright thermal component was not supported by observations at the time - they concluded that the "standard" fireball model assumes a too hot and luminous photosphere.

A final remark worth making is that the strong arguments for synchrotron emission produced in internal shocks were based on the observations of a non-thermal spectrum and the variability properties of the prompt emission. However a significant contribution from thermal emission (from the photosphere or from Comptonization of other soft photons) provides a way of addressing the observations of the hard low energy spectral slopes.

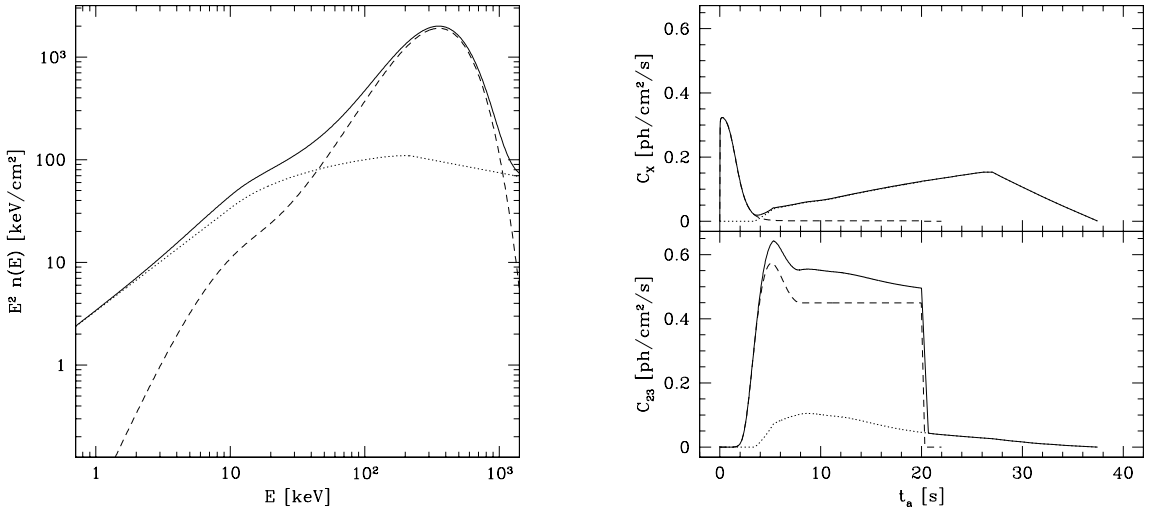

Figure 5.4: Predicted spectrum and light curves. Left: the spectrum $E^2N(E)$ as a function of photon energy. A redshift z=1 was assumed. Right: count rates as a function of arrival times in the 3.5-8.5 keV band (top) and in the 50-300 keV band (bottom). The dashed line corresponds to the photospheric emission, the dotted line to the non-thermal emission from internal shocks and the solid line to the total emission. The spectrum is dominated by the luminous contribution from the photosphere peaking at ∼370 keV. From Daigne & Mochkovitch 2002.

5.4 The case of GRB 990413: further insight into the thermal phase

Within the problematic discussed above we present the results relative to a new case, GRB 990413, which showed to have a very hard spectrum with a low energy spectral component $\alpha = 1.49$ which is well fitted by a black body model with characteristic temperature ~ 70 keV. We find that the temperature/luminosity evolution is consistent with that found in other "thermal" GRBs (Ghrilanda et al. 2003). Interestingly the time resolved spectral analysis reveals the presence of a second non–thermal component contributing (for about 1 sec) up to 30% of the total flux. The evolution of the thermal/non–thermal spectral components is strongly correlated with the flux variations observed in the light curve, which shows a higher variability compared to other thermal bursts. Thus the spectral time evolution of this burst may reveal the temporal transition and interconnection between the two radiation regimes, thermal and non-thermal one.

GRB 990413

The GRB 990413 total fluence[1] is $(6.813 \pm 0.449) \times 10^{-6}$ ergs/cm^2 integrated over energies > 25 keV. The duration of the burst is $T_{90} = 12.73 \pm 0.45$ s. Its peak flux (over the range 50-300 keV) is 3.77 ± 0.29 phot/cm^2 s and it was reached ~ 2.8 s after the trigger. BATSE 64 ms resolution time profile (at energies above 25 keV) integrated over the four BATSE energy channels (Fig. 5.6, top) consists of two separate broad peaks with superimposed substructures with width $\approx 10\%$ of the main peaks width. The broad peaks (visually examined) span over the time interval 0-8 s and 10-14 s after the trigger. The duration and peak flux of GRB 990413 are consistent with the typical values found for the population of long BATSE GRBs (e.g. Paciesas et al. 1999).

5.4.1 Black-body spectrum

For the GRB spectral analysis we used initially the High Energy Resolution Burst (HERB) BATSE data (see Section 3.4). The spectra from the most illuminated LAD (#5)

[1] http://cossc.gsfc.nasa.gov/batse/BATSE_Ctlg/index.html

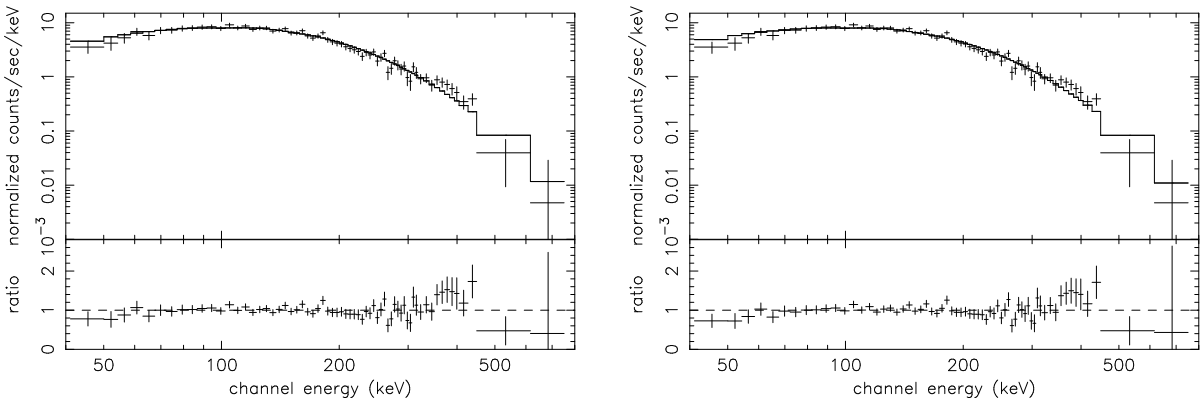

Figure 5.5: COMP and BB model fits to the time integrated (14 sec) count spectrum (left and right panel, respectively). The inserts show the model to data ratio.

were selected in order to have the highest signal to noise ratio; for this detector (over the total usable energy range) the S/N was ≈ 55, or $\approx 2\sigma$, for the time integrated spectrum (see e.g. Preece et al. 2000). The background spectrum was estimated as the average spectrum over two time intervals (2070 s and 19 s) before and after the burst trigger. The energy data bins were grouped in order to have the minimum of five counts per channel after the background subtraction. As a check, the fits were re-done with a minimum of 10 and 20 counts per channel (eg. Bevington & Robinson 1992), with results consistent within the parameters' confidence intervals. The spectrum was analyzed using the XSPEC v.11.1.0 package.

The burst count spectrum, integrated over its total duration of 14 sec since the burst trigger, was fitted by Band model (Band et al. 1993, see sect. 3.4). This model fit resulted in an extremely hard low energy spectral slope, i.e. $\alpha = 1.52^{+0.32}_{-0.30}$, but the high energy power law photon index was unconstrained due to the low signal above ~ 600 keV.

A better fit (i.e. reduced $\chi^2_r = 1.25$ for 96 d.o.f) was obtained with the COMP[2] model (Fig. 5.5), i.e. a power law with a high energy exponential cutoff, $N(E) = K(E/1\mathrm{keV})^{\alpha} e^{-E/E_b}$. The COMP model fit revealed a very hard low-energy spectral component, with photon spectral index $\alpha = 1.49^{+0.34}_{-0.27}$, and an e-folding energy of the exponential

[2]The fit energy range was 43 - 1787 keV; the low energy end is not the standard 30 keV as we had large energy channel width (8 keV) at 32 keV after we applied channel grouping to obtain higher S/N ratios

cutoff of $E_b = 75.1^{+5.0}_{-5.0}$ keV, which corresponds in the $E\mathrm{F}_E$ spectrum to a peak energy $E_{\rm peak} \approx 260$ keV. As a possible test of the synchrotron model, we also fitted the COMP model with frozen low energy spectral photon index $\alpha = -2/3$, i.e. the limiting value of the optically thin synchrotron model (see Section 5.2.1). This fit clearly deviated from the data at the low energy end and it resulted in a reduced $\chi^2_r \sim 4$ for 97 d.o.f. that excludes the model at 99.9% confidence level.

Given the extreme hardness of the low energy spectral component of the COMP fit, we fitted the time integrated spectrum of GRB 990413 with a Black Body model (BB). We find a temperature $kT = 67.9^{+2.3}_{-2.3}$ keV for a reduced χ^2_r=1.27 (for 97 d.o.f). The EF_E peak energy is $E_{\rm peak}$ ∼196 keV. This value is consistent with the few hundred keV peak energy found in the other 10 GRBs with thermal spectra (Ghirlanda et al. 2003 and Ryde 2004). We also note that, although the GRB spectrum is well fitted by a BB model, its low energy slope is slightly steeper than the Rayleigh–Jeans extrapolation in the low energy domain (i.e. $\alpha = 1$) as shown by the best COMP fit which gives $\alpha \sim 1.5$. Both in terms of χ^2_r and model-to-data ratios the COMP and BB fits appear to be equivalent.

In order to assess the robustness of our results, we tested against several sources of uncertainty (see Ghirlanda et al. 2003): 1) we performed the fits reducing the fitting energy range at the high energy end to test whether the characteristic exponential cutoff energy of the COMP model might determine a hard low energy spectral component and we found that instead α did not significantly change within the confidence interval centered around the above best fit value; 2) we examined the (null) influence of different background spectra by choosing different time intervals to compute the average background; 3) we fitted the data with the response matrix of the second LAD most normal to the burst direction, and this test gave a still positive, but less steep $\alpha = 0.29^{+0.07}_{-0.28}$ (the energy of the exponential cutoff was $153.8^{+41.0}_{-8.3}$ keV). However, in the latter case because of the very low S/N ratio, χ^2_r was 1.61 for 97 d.o.f.; 4) as a check on the detector response, we fitted the data using the response matrix of the most illuminated detector (LAD 5) but on another burst at approximately the same position of GRB 990413 and found $\alpha = +1.11^{+0.27}_{-0.19}$ with χ^2_r=1.26 for 97 d.o.f. We conclude that the result that GRB 990413 has an extremely hard low energy spectrum consistent with a BB model is indeed robust.

5.4.2 Time resolved spectral analysis

As established by different authors (e.g. Ford et al 1995, Preece et al 2000, 1998) the GRB spectrum typically evolves with no unique behavior. The spectral evolution is evident in all of the three spectral parameters, i.e. low and high energy spectral slope and a peak energy. For instance, the asymptotic α evolves in 58 % of the bursts (Crider et al 1997). Also the GRBs with a thermal spectrum show evidence of a spectral evolution which is well described by the best fit temperature. Ghirlanda et al. 2003 find that the BB temperature in their 5 GRBs after an initial constant phase (of few tenths of a second) evolves as $\sim t^{-1/4}$. A slightly steeper decay $\sim t^{-2/3}$ is found in 4 other thermal bursts by Ryde 2004. The luminosity evolution instead does not demonstrate a unique behavior.

We performed a time resolved spectral analysis using HERB data, covering the time interval 0.05−14 s after the trigger time with a total of 5 spectra with similar integration time of 1.2 sec each. We fitted these spectra with both the COMP and the BB model and compare the results in Table 5.1. The reduced χ^2_r is acceptable in almost all cases (a possibly larger value is found only for the last spectrum which is indeed characterized by a lower S/N). The typical values of the COMP model low energy spectral index are similar to those found from the analysis of the time integrated spectrum (i.e. $\alpha \sim 1.5$ - sect. 5.4.1). We find that only the second spectrum shows a slightly softer low energy spectral component. The peak spectral energy, i.e. $E_{\rm peak} = E_{\rm b}(\alpha + 2)$ decreases from an initial value of ~ 296 keV to ~ 222 keV in the late time spectrum, indicating a typical hard-to-soft evolution.

In Fig. 5.6 (middle and bottom panel) we report the spectral evolution as found from the fit of the BB model (see kT_{BB} in Table 5.1). The BB flux (integrated in the fit energy range) is nearly constant up to 2.36 sec since the trigger and then decreases approximately as $\propto t^{-1}$. The temperature evolution is instead well described by $kT \propto t^{-1/4}$ (solid line in the bottom panel of Fig. 5.6). This behavior fully agrees with what found by Ghirlanda et al. 2003 and Ryde 2004 for their set of "thermal" GRBs.

The 10 BATSE GRBs that have been found so far to show a thermal spectrum appear to have a smooth light curve (see Ghirlanda 2003 and Ryde 2004, Fig.3 and Fig.1 respectively). GRB 990413 instead has a quite variable light curve characterized by "dips"

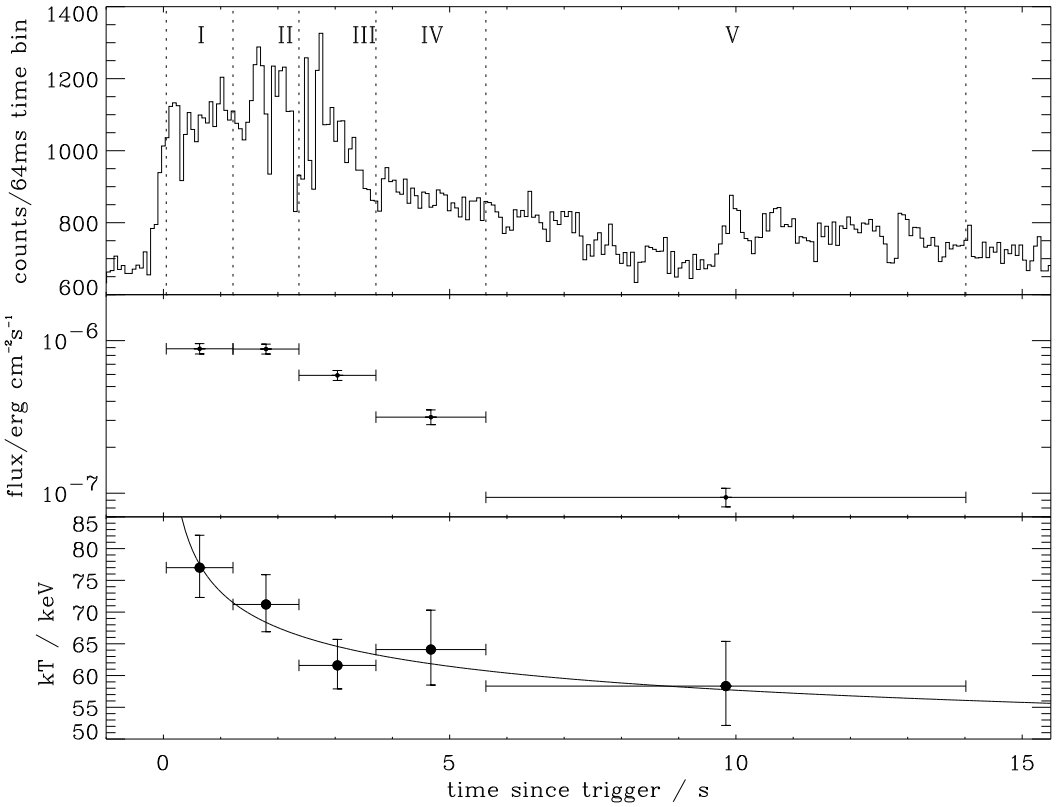

Figure 5.6: Top: GRB 990413 light curve summed over the four BATSE energy channels (i.e. for energies > 25 keV). The five time intervals for which the time-resolved spectral analysis was performed are indicated (see Table 5.1). Middle: Best fit BB model flux integrated in the energy fit range. Bottom panel: black body temperature evolution and the fit of a kT $\propto$ t$^{-1/4}$ function (solid line).

Δt_{fit} s	model	α	E_{break} keV	kT$_{BB}$ keV	χ^2_r/d.o.f.
0.05–1.21	comp	$1.50^{+0.47}_{-0.53}$	$84.7^{+15.7}_{-8.3}$		1.17/88
	bb			$77.0^{+5.1}_{-4.7}$	1.17/89
1.21–2.36	comp	$0.81^{+0.42}_{-0.50}$	$109.1^{+43.6}_{-21.6}$		1.04/73
	bb			$71.2^{+4.7}_{-4.3}$	1.10/74
2.36–3.71	comp	$1.51^{+0.74}_{-0.56}$	$67.8^{+19.3}_{-8.4}$		0.85/87
	bb			$61.6^{+4.1}_{-3.7}$	0.85/88
3.71–5.63	comp	$1.53^{+0.58}_{-0.68}$	$69.7^{+24.4}_{-10.3}$		1.04/99
	bb			$64.1^{+6.2}_{-5.6}$	1.03/100
5.63–14.01	comp	$1.55^{+0.47}_{-0.17}$	$62.5^{+8.2}_{-5.8}$		1.36/104
	bb			$58.3^{+7.0}_{-6.2}$	1.36/105

Table 5.1: Time resolved spectral analysis of GRB 990413. The COMP and BB best fit spectral parameters are reported for each time resolved spectrum. Errors on the parameters correspond to the 90% confidence level. Δt_{fit} is the time interval over which the fits were performed. The energy fit range is approximately 40-1800 keV for all the spectra except for the second spectrum which was analyzed on the reduced energy range 40-900 keV, due to the extremely low count number in the high energy channels.

(Fig. 5.7) during which the count rate is reduced by a factor 3 with respect to its value at the peaks. It is, therefore, interesting to study the spectral evolution on (shorter) timescales comparable to the light curve variability. However, the LAD data that we presented in this Section have a maximum (signal to noise limited) time resolution > 1 sec. For this reason we analyzed the Medium Energy Resolution (MER) data (see Section 3.4). We integrated the spectra for the analysis keeping the track of the "peaks" and the "dips" in the light curve; the selected time intervals are shown in Fig. 5.7, top panel, and reported in the first column of Table 5.2.

We aimed at examining whether the flux changes seen in the light curve reflect the changes in the spectral evolution, paying attention in particular to the time intervals in which the sudden variations in the flux occur. For all the spectra in 15 selected time intervals we tested three models: black body, a single power law and a combination of the two. The single power law was modeled to characterize a possible non-thermal contribution. The motivation for this choice is twofold: primarily, the gamma–ray bursts in which the thermal phase was observed also exhibited an evolution in time from initial thermal phase

$\Delta\ t_{\rm fit}$ [s]	p	kT$_{\rm BB}$ [keV]	$\chi^2_{\rm r}$ / d.o.f.	peak/dip
0.12 – 0.29	–	$78.6^{+8.8}_{-7.7}$	1.51/11	peak
0.63 – 1.25	–	$80.1^{+3.4}_{-4.2}$	1.73/11	peak
1.57 – 1.78	$-1.5^{+0.3}_{-1.2}$	$89.9^{+10.6}_{-9.4}$	1.31/9	peak
1.86 – 1.91	$-1.6^{+0.4}_{-0.4}$	–	0.46/10	dip
1.94 – 2.26	$-1.2^{+0.3}_{-0.3}$	$72.9^{+8.5}_{-6.8}$	0.78/9	peak
2.28 – 2.37	$-1.5^{+0.2}_{-0.3}$	–	1.26/9	dip
2.37 – 2.45	$-1.6^{+0.2}_{-0.3}$	–	0.77/11	dip
2.50 – 2.57	–	$66.5^{+9.2}_{-7.9}$	0.99/11	peak
2.59 – 2.68	$-1.6^{+0.2}_{-0.2}$	–	1.45/11	dip
2.71 – 2.82	–	$62.2^{+6.1}_{-5.4}$	1.43/11	peak
2.95 – 3.69	–	$71.3^{+4.6}_{-4.2}$	1.57/11	peak
3.85 – 4.66	$-1.5^{+0.5}_{-3.2}$	$87.6^{+11.1}_{-10.3}$	0.29/9	peak
5.06 – 5.92	–	$72.0^{+9.5}_{-8.2}$	1.78/11	peak
6.02 – 6.93	–	$71.4^{+8.9}_{-7.7}$	1.37/9	peak
9.93 – 11.30	$-1.3^{+0.4}_{-0.4}$	$54.2^{+17.7}_{-11.1}$	0.33/9	peak

Table 5.2: Results of the spectral analysis with high temporal resolution for a BB and PL models fitted to the MER data of GRB 990413. When only kT is reported, the spectrum was best fitted by a BB component alone. $\Delta t_{\rm fit}$ is the time interval over which the spectra were integrated. The energy fit range is approximately 36-1548 keV for all spectra. p is the single power law photon spectral index defined as $N(E) \propto E^p$.

to the late non-thermal one (e.g. Ghirlanda et al. 2003); secondly, identifying the presence of the two contributions to the emission (thermal/non-thermal) may be expected in the gradual transition between photospheric emission and the development of internal shocks, and therefore the production of the non-thermal component (e.g. Fig. 5.4, Daigne & Mochkovitch 2002). For all the spectra we first tested the BB model, and found that it does still fit all the spectra but those corresponding to the 4 "dips" identified in the light curve. In these cases in fact we found that the spectrum is non-thermal and best fitted by a single power law model. Apparently this is suggesting the presence of a second spectral non–thermal component in the GRB spectrum. The GRBs with thermal spectra also exhibited an evolution in time from an initial thermal phase to a late non-thermal one (Ghirlanda et al. 2003) and a double model fit, i.e. BB+PL, has been used to model these spectra (Ryde

2004).

We thus analyzed all the 15 spectra with both the BB and the PL model and report the results in Table 5.2 and show them in Fig. 5.7. The four spectra obtained in the dips of the light curve (integrated for 48 ms, 96 ms and the last two of 80 ms) are best fitted with a PL model without a thermal contribution. The power law photon spectral index is the same in all the 4 dips, i.e. $\alpha \sim -1.6$. If this corresponds to the typical non–thermal spectrum found in long bright GRBs (e.g. Preece et al. 2000), the peak energy should be > 1500 keV i.e. the upper energy limit of the fit window. We note that this spectral slope is consistent with the expected synchrotron emission from a cooling population of relativistic electrons (such as those accelerated in the internal shocks). Moreover, we find that the spectrum corresponding to the peak preceding the first dip and between the first and the second dip is better fit by a BB+PL model.

In the spectra where both components (thermal and non-thermal) contribute to the total photon number, we find that still the thermal component dominates. When the underlying power law component is present, black body radiation still comprises >80% of the total emission during the first peak and >60% in the second peak (Fig. 5.8). The prevailing contribution of the thermal component is also apparent in Fig. 5.11 - 5.12 where the νF_ν spectra are shown in a time sequence.

5.5 Variability estimate

In the previous section it has been shown that the spectral components (thermal and non–thermal) present in GRB 990413 appear to be correlated to the variability of its light curve. The light curves of the other 10 thermal bursts appear smooth compared to that of GRB 990413 which indeed is similar to the majority of GRBs. In this section we quantitatively compare the variability of GRB 990413 with that of typical non–thermal bursts and with the small sample of the thermal GRBs. In order to quantify the observed high variability of GRB 990413 with respect to other GRBs with hard low energy spectral component, we applied the simplified method of Fenimore & Ramirez-Ruiz (2000). We computed the variability as

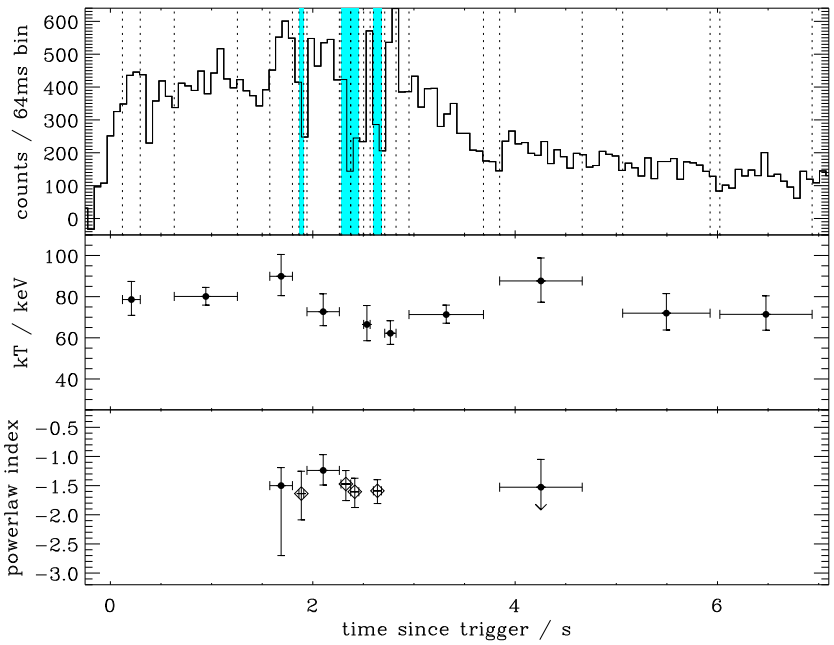

Figure 5.7: Time-resolved spectral analysis of the first peak of GRB 990413. For clarity, only the first pulse and its "decay" phase are presented. The second peak is integrated in only one spectrum in the interval 9.9–11.3 sec (due to the lower signal to noise) and is reported in Tab. 2. Top panel: count rate integrated over the four BATSE energy channels. The shadowed regions highlight the "dips" of the light curve where the non–thermal spectrum appears. Middle and bottom panels: temporal evolution of the spectral parameters. Diamonds correspond to the parameters of the spectra integrated in the time intervals where the "dips" in the light curve occur. When kT of the black body fit and the (decaying) power law index are reported for the same time interval, the two-component model gave the best fit.

$$V = \frac{1}{N} \sum_i \frac{(c_i - < c >_w)^2 - (b_i + c_i)}{c_p^2} \tag{5.10}$$

where c_i are the source photon counts in 64 ms resolution; N is the number of time bins that we used in our estimate having the source counts at least 5σ above the background; c_p is the number of peak counts used in normalization. $<c>_w$ are the counts smoothed with a boxcar window of width w ; the choice of the time interval for smoothing was determined by the average (observed) thermal phase duration. That is, we applied the time window for smoothing of length comparable or shorter than the interval in which the thermal spectra were observed. We performed several tests to determine the optimum choice (longer time

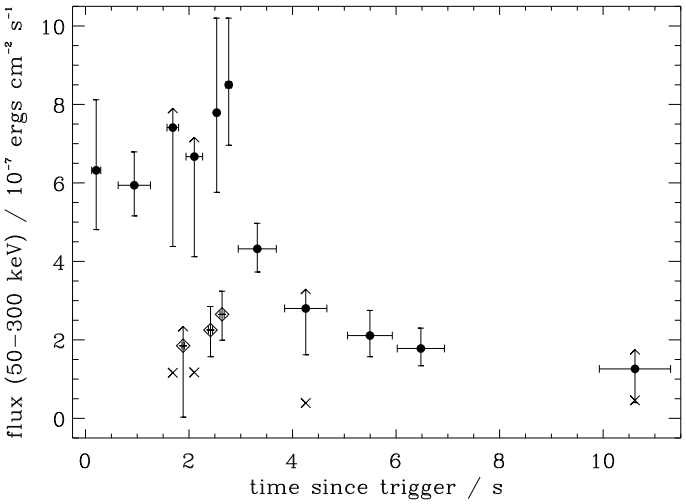

Figure 5.8: Flux in the 50-300 keV energy band; circles refer to the flux integrated in the time intervals in which the "peaks" in the light curve occur and the diamonds correspond to the fluxes in the "dips" of the light curve. The flux in the interval 2.28-3.37 s is not shown because the error interval for the flux was not confined. The crosses indicate the contribution of the power law component to the total flux in the case when a black body was fitted superimposed to a power law component.

scales for smoothing, e.g. $w \propto T_{90}$ would not reflect the fast alternations that we wanted to "measure") and the best choice of time w was found to be $w = 3$ s. As the observed time history should be corrected for the cosmological time dilation, we verified also how our result changes if the burst was placed at a typical redshift z=1 (Fig. 5.9); we found - applying the correction as defined in Fenimore& Ramirez-Ruiz 2000 - that the variability would change by less than 10 per cent (the major changes are produced by varying the smoothing time window). We estimated the errors on variability (see Reichart et al. 2001 for the detailed procedure) by assuming that the terms in the sum are statistically independent and neglecting the error in the averaged normalization factor (Nc_p).

As the uncertainties of the measured variability strongly depend on the brightness of the burst, for the comparison of GRB 990413 with a larger set of GRBs we computed the variability of the sample of 237 gamma–ray bursts from the BATSE catalog of comparable durations (T_{90} >10 s) and brightness (3.7 photons s^{-1} cm^{-2} < P_{64ms} < 30.7 photons s^{-1} cm^{-2}). This range of peak fluxes includes the fluxes measured for GRB 990413 and for

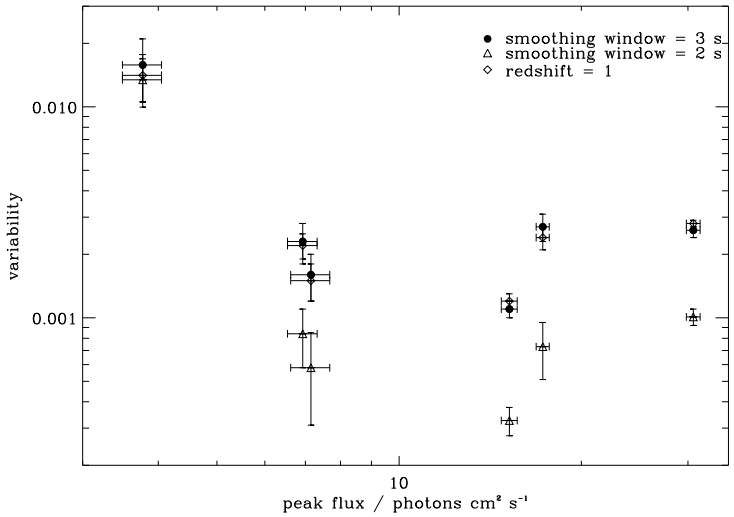

Figure 5.9: Variability estimate using various smoothing time window scales w and with the correction for the redshift z=1 (using w=3 sec), as function of the observed peak photon flux. The GRB 990413 and the bursts analyzed by Ghirlanda et al. 2003 are shown. GRB 990413 (with peak flux 3.8 photons $\mathrm{cm}^{-2}\mathrm{s}^{-1}$ in the 50-300 keV range) has apparently higher variability with respect to other 'thermal' GRBs.

the bursts analyzed by Ghirlanda et al. 2003. The results are shown in Figure 5.12: GRB 990413 clearly cannot be distinguished from most of the GRBs in the sample in terms of variability, while the rest of the "thermal" bursts (from Ghirlanda et al 2003) are in the lower part of the distribution. We verified again our result for different choices of the smoothing time window, indeed finding that the variability of GRB 990413 increases proportionally to the length of the smoothing timescale with respect to the other hard-thermal bursts. The 5 GRBs analyzed by Ryde 2004 have lower peak fluxes and for the given smoothing time scale (w=3 s) their variability (although with large uncertainties due to the low signal) resulted to be lower than GRB 990413.

5.6 Summary and discussion

We highlighted the problems encountered when trying to interpret the gamma–ray burst prompt spectrum within the widely adopted models for its emission, that is, synchrotron/inverse Compton radiation from relativistic electrons accelerated within the

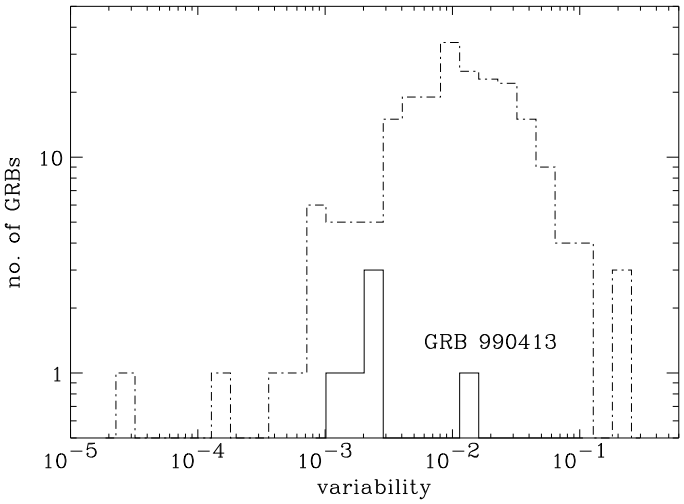

Figure 5.10: Variability measure for a smoothing time window w=3 s; the dot-dashed histogram represents the sample of GRBs within the same range of peak fluxes and durations as the GRBs examined by Ghirlanda et al 2003 and GRB 990413 (solid line).

nonuniform highly relativistic blast wave. The evidence of the thermal nature of some of GRB spectra and particularly the hard-to-soft evolution of the spectra during the course of the burst point toward the inadequacy of the solely non-thermal radiation component in explaining all the aspects of observations in a convincing manner. We discussed the proposed models and the range of spectral behaviors they can account for; however invoking a thermal photon/particle distributions (e.g. Compton drag model or quasi-thermal Comptonization models) as a source of the observed radiation appears inevitable to account for the observed hard low energy slopes in prompt GRB spectra.

We presented the time integrated and the time resolved spectral analysis of the long duration (14 sec) double peaked BATSE burst 990413 that was found to have an extremely hard spectrum. Our analysis indicates that (a) GRB 990413 shows, on average a thermal spectrum with typical temperature $kT \sim 70$ keV comparable to the other 'thermal' bursts, and (b) the spectral evolution of this component is consistent with what found for the 'thermal' bursts analyzed by Ghirlanda et al. 2003, i.e kT $\propto t^{-1/4}$.

We find that a second non–thermal component contributes to the spectrum, during the main peak and particularly in connection to the highest variability episodes of the burst.

A combined model (thermal + non–thermal) has been applied in fitting the spectra. Our results show that (i) the non–thermal component is detectable only for about 1 sec during a long (14 sec) burst, (ii) it is hard and does not evolve with time and (iii) it dominates the flux only in correspondence of the minima ("dips") of the GRB light curve, while the thermal component dominates for all of the burst duration.

This "sequential" occurrence of the two emission mechanisms can account for the initial thermal to late non–thermal evolution observed in the 10 GRBs studied by Ghirlanda et al. 2003 and Ryde 2004. GRB 990413, besides having a very hard (with respect to typical GRBs) spectrum consistent with black body emission, revealed a non–thermal component already during the possible photospheric phase. Moreover, this component is associated to the rapid temporal variability (V=0.016) that is attributed, in the internal shock scenario, to the velocity distribution of the colliding shells within the relativistic outflow. Therefore, the model that could account for the spectrum of GRB 990413 needs to allow the possibility of developing internal shocks while still inside the photosphere, and have to consistently reproduce the evolution of their relative contribution.

In recent work Rees and Mészáros (2005) considered the possibility that the observed peak energy of a GRB spectrum may be the Comptonized thermal radiation from the photosphere, as already discussed in sect. 5.3; in this scenario dissipation of energy (via processes such as magnetic reconnection, neutron decay or internal shocks) in the photosphere would increase greatly the pair production and enhance the radiation from thermal Comptonization. Thus the observable photospheric luminosity would be boosted by the energy converted from the fireball kinetic energy.

The presence of rapid dips during a thermal dominated phase is also interesting. Among the possible causes two appear quite plausible: (i) there might be inhomogeneities in the fireball optical depth (at the time of transparency); (ii) the dips directly trace the central engine intermittence in energy injection and launching of the fireball (the dips duration still largely exceeds the typical timescales associated with the fireball formation). Rees and Mészáros (2005) notice that actually rapid variations in the photospheric emission could be at least as important as the associated internal shocks in causing rapid variability in GRBs.

Indeed Ryde 2005 argues that all types of spectral evolution and spectral shapes

that have been observed can be described with the same model consisting of the thermal and nonthermal (synchrotron) component. The value of the low-energy power law index α is in this case simply the outcome of the relative strengths of the thermal component and the slope of the nonthermal one.

As GRB 990413 was found independently of its spectral properties it may well be that this phenomenology is more common than known so far. A detailed numerical calculation of the 'transition' to transparency and the formation of internal shocks might clarify the relative roles of the two different radiative regimes and provide information on the fireball physical parameters (Lorentz factor distribution of the shells, baryon loading).

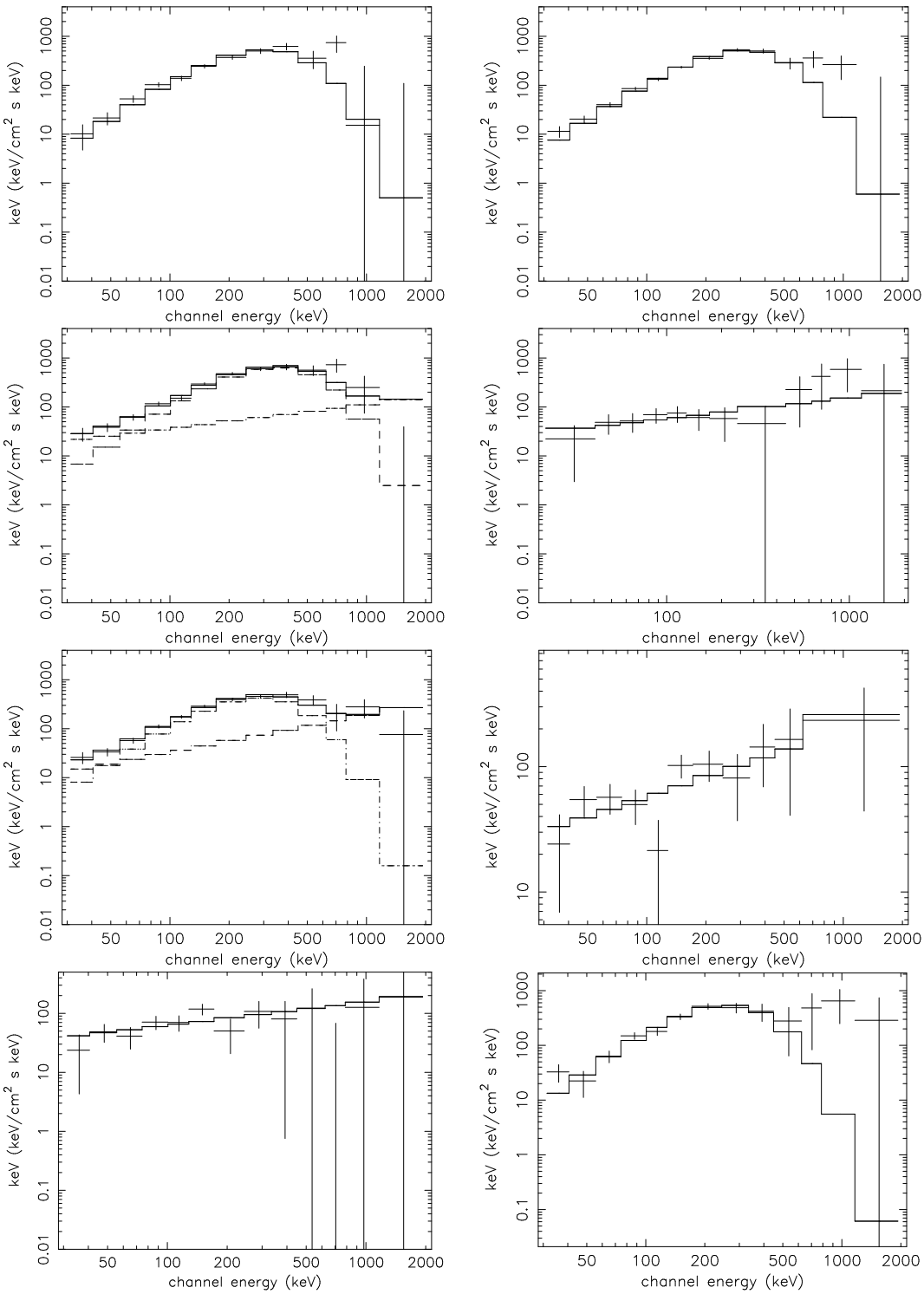

Figure 5.11: Spectral evolution of GRB 990413. First raw: BB spectra integrated in time intervals 0.12-0.29, 0.63-1.25 s. Second raw: spectra integrated in the interval 1.57-1.78 s (a superposition of a BB and a single power law) and 1.86-1.91 s (single power law fit corresponding to a 'dip'). Third raw: spectra integrated during 1.94-2.26 s (a superposition of a BB and a single power law) and 2.28-2.37 s (single power law fit corresponding to a 'dip'). Fourth raw: single power law spectrum for 2.37-2.45 s ('dip') and BB spectrum for 2.5-2.57 s.

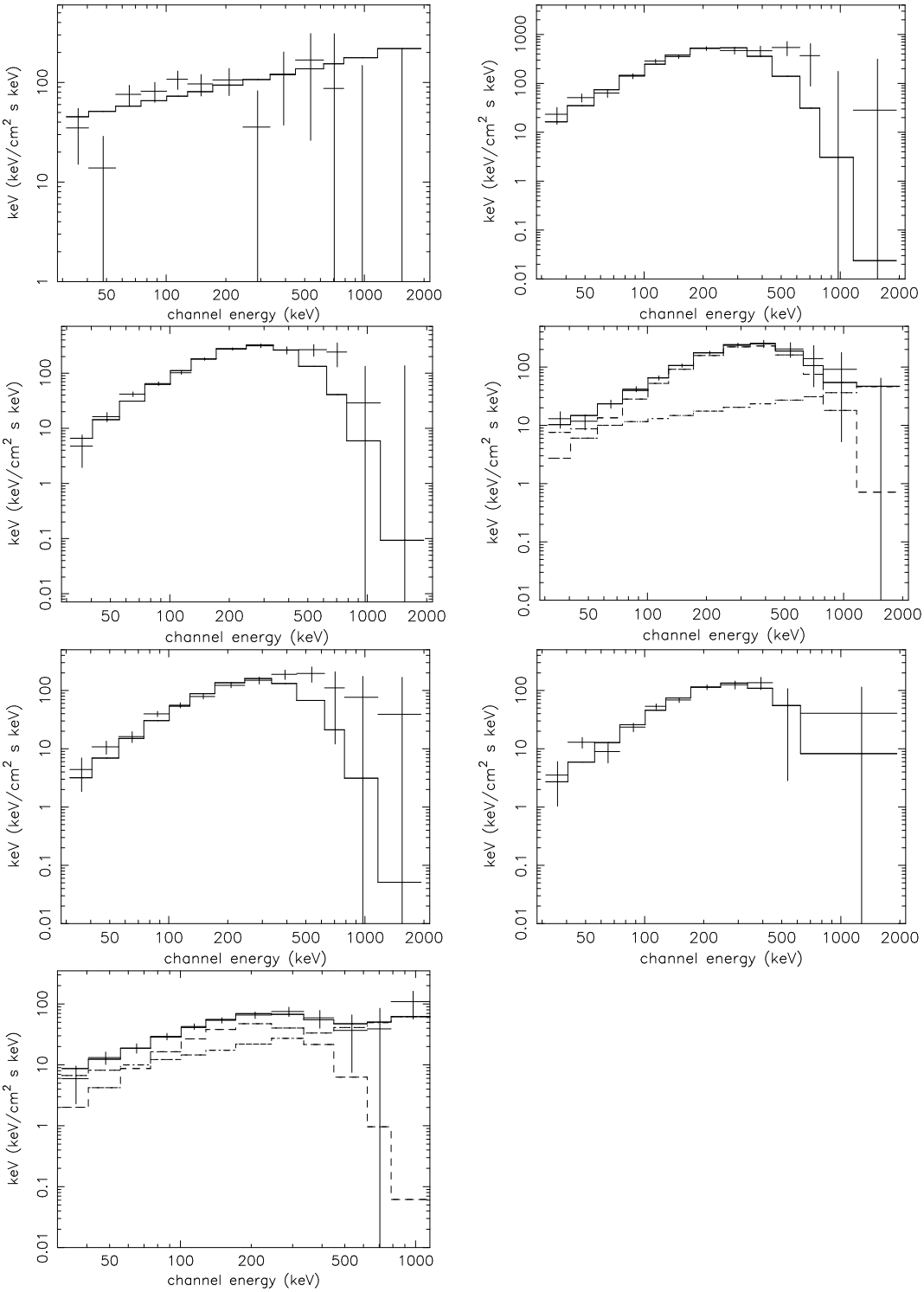

Figure 5.12: Spectral evolution of GRB 990413 (continued). First raw: single power law spectrum integrated in the time interval 2.59-2.68 s ('dip') and BB spectrum fitted in 2.71-2.82 s. Second raw ('decay' of the first pulse): BB spectra integrated in the interval 2.95-3.69 s and a superposition of a BB and a single power law in the interval 3.85-4.66 s. Third raw: BB spectra integrated during 5.06-5.92 s and 6.02-6.93 s. Fourth raw (second pulse): a superposition of a BB and a single power law spectrum in the interval 9.93-11.3 s.

Chapter 6

Gamma–ray bursts and cosmology

6.1 Introduction

As already anticipated in Section 2.2.5, gamma–ray bursts constitute potentially excellent probes for cosmological investigations at high redshifts, since the detection of gamma–rays is not subjected to the constraints on dust attenuation as it is the case with SN Ia. The recently proposed empirical correlations for the energetics of gamma–ray bursts allow the determination of luminosity distances for each GRB, and in a way similar to SN Type Ia with the light-curve correction can be standardized to high enough precision to probe in detail the energy content of the universe.

In this chapter we describe the method used for assessing whether these correlations are statistically consistent with the observed peak energy vs fluence distributions of a large sample of long (BATSE) GRBs, until redshifts can be determined for a significantly larger number of events. The only assumption is that these events follow the cosmological star formation rate redshift distribution. Although a statistical consistency is not a proof of the reality of such correlations, it would support the view that they might indeed represent intrinsic properties of long GRBs. We review briefly the up-to-date proposed empirical correlations used for the estimate of the intrinsic GRB energetics in section 6.2; we detail the assumptions and procedure in Section 6.3, present the inferred properties of BATSE gamma–ray bursts in Section 6.4 and discuss them in Section 6.5.

6.2 GRB energetics and empirical correlations

It has been suggested (Lloyd–Ronning, Petrosian & Mallozzi 2000; Amati et al. 2002 [A02 hereafter]; Sakamoto et al. 2004; Lamb et al. 2004; Atteia et al. 2004) that the apparent isotropic energy of the prompt phase, $E_{\gamma,\rm iso}$, correlates with the intrinsic peak energy of the integrated emission $E_{\rm peak}$, with a dependence $E_{\rm iso} \propto E_{\rm peak}^{0.5}$. A similar correlation has been claimed between $E_{\rm peak}$ and the peak luminosity (Yonetoku et al. 2004). Recently Ghirlanda, Ghisellini & Lazzati (2004a) (GGL04 hereafter), by correcting for the putative fireball opening angle – estimated from the (achromatic) break time in the afterglow light curve (Sari, Piran & Halpern 1999; Frail et al. 2001; Bloom, Frail & Kulkarni 2003) – argued that an even tighter correlation holds between the actual prompt energetics, E_γ, and $E_{\rm peak}$, namely $E_\gamma \propto E_{\rm peak}^{0.7}$. Such correlations have been determined from and calibrated on a limited number of GRBs, i.e. at most the ~ 40 long GRBs for which redshift information is currently available. No unique and robust interpretation of such results has been found so far (e.g. Zhang & Meszaros 2002; Schaefer 2003; Liang, Dai & Wu 2004; Eichler & Levinson 2004; Yamazaki, Ioka & Nakamura 2004; Rees & Meszaros 2005). However it is clear that if these correlations were to hold for the whole GRB population (see Friedman & Bloom 2004; Nakar & Piran 2004; Band & Preece 2005 for dissenting views), they could provide powerful clues on the physical origin of the prompt emission and have important repercussions on the potential cosmological use of GRBs.

6.3 Simulations of the GRB population

In order to test whether the observed peak energy and fluence distributions are consistent with the correlations proposed by A02 and GGL04, we considered the sample of BATSE GRBs analyzed by Preece et al. (2000) (referred to as the 'bright' BATSE sample hereafter), consisting of 156 events for which $E_{\rm peak}$ has been estimated. We then simulated – via a Monte Carlo – the fluence distribution for a population of GRBs characterized by the corresponding $E_{\rm peak}$ distribution. The procedure we adopted is the following:

- assumed that the GRB rate follows the star formation rate (as estimated by Madau

& Pozzetti 2000), namely when computing the observed rate of GRBs as a function of redshift,

$$\frac{dN}{dt\ dz} = \frac{dV(z)}{dz}\frac{R_{\rm GRB}(z)}{1+z} \tag{6.1}$$

we adopted:

$$R_{\rm GRB}(z) \propto R_{\rm SN}(z) = 0.3 h_{65} \frac{\exp(3.4z)}{\exp(3.8z)+45} {\rm M}_\odot {\rm yr}^{-1} {\rm Mpc}^{-3} \tag{6.2}$$

This star formation rate increases rapidly between z=0 and 1, peaks between z=1 and 2, and gently declines at higher redshifts. Porciani & Madau 2001 provide three models of the cosmic SFR up to redshifts $\sim$ 5; we will show later that no significant changes in the results are found among these three models. Our assumption is based on the present observational evidence of (long) gamma–ray burst progenitors; the lowest initial stellar mass that is able to produce a hypernova (HN) appears to be $\sim$20 $M_\odot$ (only a fraction of about 5% of observed SNe Type Ic are HNe, Podsiadlowski et al. 2004)[1]. Thus the constant of proportionality includes the formation mass fraction of the progenitors and it is a free parameter of the model;

- adopted the observed $E_{\rm peak}$ distribution of the bright BATSE GRBs, as obtained by averaging the results of the time resolved spectral analysis by Preece et al. (2000) (see Fig. 3.1, Section 3.4); it is important to note that the GRBs comprised in their analysis were bright bursts only from the BATSE catalog – the selection criterion was a total fluence larger than 4×10^{-5} ergs cm^{-2} integrated over all energies or peak flux exceeding 10 photons cm^{-2} s^{-1} on the 1024 ms integration timescale in the BATSE energy band (50-300) keV);

- randomly assigned a redshift and a characteristic intrinsic peak energy $(1+z)E_{\rm peak}$ to each event, where $E_{\rm peak}$ is randomly extracted from the observed distribution;

- adopted the A02 correlation (with its spread, see Section 6.4.3) to estimate the corresponding energetics $E_{\gamma,iso}$;

[1] See also a comment on GRB/HN rate in Section 2.4

- by applying the cosmological corrections[2] estimated the corresponding fluence in the 50-300 keV energy range (for a typical Band's spectral representation with $\alpha = -1$ and $\beta = -2.25$, see Preece et al. 2000). Thus the observed fluence (in ergs cm^{-2}) was computed for the BATSE channels #2 and #3 (50-300 keV):

$$P = \int_{50}^{300} EN(E)dE \tag{6.3}$$

  where N(E) is the photon spectrum and has the units of phot/cm^2 keV (see Section 3.4). It was normalized from the source-frame "bolometric" isotropic energy $E_{\gamma,iso}$ obtained by integration of the model spectrum over the energy range 1 keV-10 MeV; the integration required the correction for the band redshift effect:

$$E_{\gamma,iso} = \frac{4\pi d_L^2}{(1+z)} \int_{1/1+z}^{10^4/1+z} EN(E)dE \tag{6.4}$$

- compared the simulated fluence distribution with that of bright BATSE GRBs. The comparison of fluences clearly avoids, with respect to fluxes, any further assumption about GRB durations.

The consistency between the simulated and observed fluence distributions has been quantitatively assessed by estimating the maximum difference D in the cumulative distributions $S(P)$, as in the Kolmogorov-Smirnoff (KS) test,

$$D = \max |S_1(p) - S_2(p)| \tag{6.5}$$

The parameter D has been used to compare the degree of agreement of the different models with data (i.e. for different assumptions/parameters). We adopted as a limit for a qualitatively satisfactory agreement a value $D < 0.07$, although formally the corresponding associated probability of two distributions being drawn from the same parent one would be only $P_{\rm KS}$= 0.002.

As mentioned above, the observed $E_{\rm peak}$ distribution is (obviously) considered at $z = 0$, i.e. it is implicitly assumed to evolve with redshift. Although this might not be

[2]We adopt a 'concordance' cosmology $\Omega_\Lambda = 0.7$, $\Omega_{\rm M} = 0.3$, and $H_0 = 65$ km s^{-1} Mpc^{-1} ($H_0 = 70$ km s^{-1} Mpc^{-1} for the GGL04 case).

necessarily true, it provides the simplest (and only possible) self-consistent hypothesis on the intrinsic distribution.

An analogous test for the GGL04 relation is clearly less straightforward, as it requires information on the GRB opening angle distribution. The latter is however constrained only by 16 GRBs for which an estimate on the opening angle can been determined from the break time of the afterglow light curve (see GGL04). We approximated such a distribution as a log-normal function and constrained it by requiring that the observed fluence distribution can be reproduced. We can then only verify its qualitative consistency with the values inferred for those 16 GRBs and treat it as a prediction to be tested when more estimates of opening angles will be available.

6.4 Results

The robust finding of this analysis is that the assumption that the A02 correlation holds for bright BATSE GRBs leads to a fluence distribution in agreement with the observed one. The comparison of the predicted and observed distributions is shown in Figure 6.1 and their formal consistency is confirmed by a KS test (probability $P_{\rm KS}= 0.06$).

The observed fluences can be satisfactorily reproduced ($P_{\rm KS}= 0.18$) also by adopting the GGL04 relation for an log-normal opening angle distribution peaking around $\sim 4-5^o$. Indeed this appears to mimic the distribution of the (few) estimated opening angles (see Figure 6.2).

6.4.1 The BATSE long GRB population

The above results would be strongly strengthened if it were possible to extend them to the whole BATSE long GRB population. However, this is hampered by the fact that the corresponding $E_{\rm peak}$ distribution is not determined.

However, the interesting consideration in this respect is that the fluence distribution of all BATSE GRBs extends down in fluence more than two orders of magnitudes with respect to the bright BATSE sample. If the GRB rate does follow the start formation rate redshift distribution, this implies that the bulk of GRBs has much lower E_γ than the

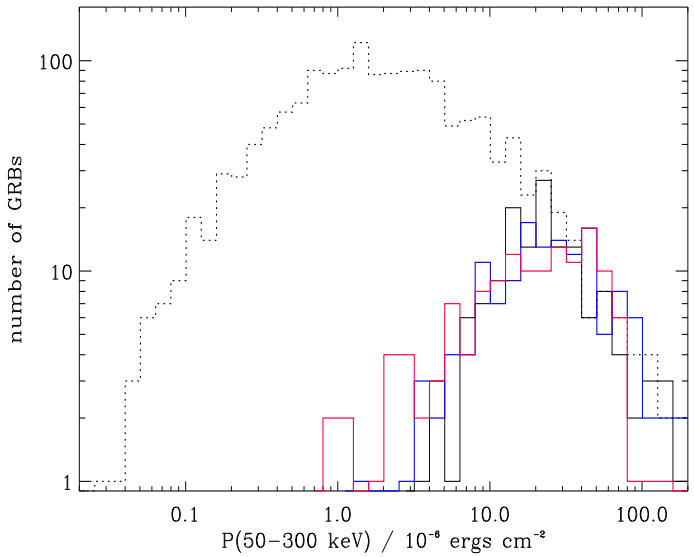

Figure 6.1: Fluence distributions. Observed ones: 'bright' BATSE GRBs (Preece et al. 2000) (black solid line); the whole BATSE long GRB population (dotted line). Simulated ones, under different assumptions: the A02 relation + the 'bright' BATSE $E_{\rm peak}$ distribution (red solid line); the GGL04 relation + the 'bright' BATSE $E_{\rm peak}$ distribution + the opening angle distribution for the 'bright' GRBs shown in Fig. 6.2 (blue solid line).

bright ones. In other words, the cosmological distance cannot be responsible for such spread in fluences. It is clearly possible that effects such orientation with respect to the line of sight play a major role. In any case observationally this corresponds to the existence of a significant population of (apparently) less powerful events. Indeed HETE-2 observations show direct evidence for a trend of decreasing peak energy with decreasing GRB fluence (Sakamoto et al. 2005, see Fig.2.2; Lamb, Donaghy & Graziani 2005).

Given the above results at this stage it is meaningful to determine the $E_{\rm peak}$ distribution which allows to reproduce the fluence distribution of all BATSE GRBs if the A02 correlation were to hold for all events. The point here is that – if tightly constrained – the inferred $E_{\rm peak}$ distribution provides a prediction to be tested against observations without requiring the determination of the redshift for a consistent number of GRBs.

To this aim we considered the fluences of the whole BATSE GRB population [3] comprising $\sim$ 1500 events, and repeated the above procedure for different extrapolations

[3] http://cossc.gsfc.nasa.gov/batse/BATSE_Ctlg/flux.html

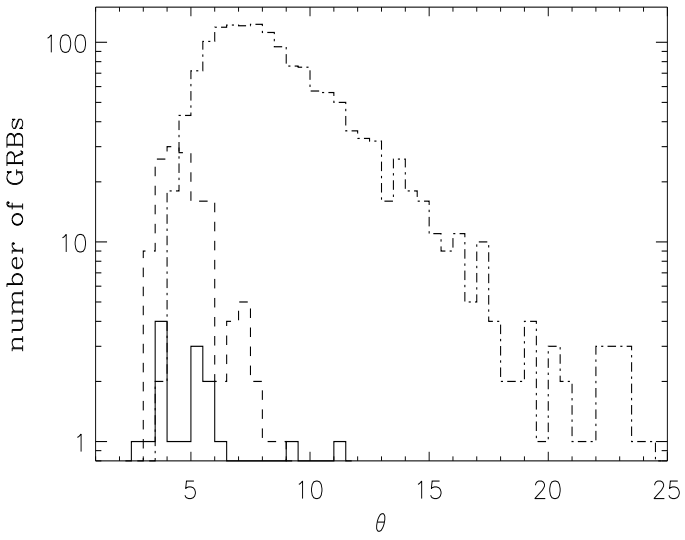

Figure 6.2: Opening angle distributions, as constrained by the request that the GGL04 correlation is representative of bright BATSE GRBs (dashed line) and the whole of the BATSE GRB population (dot-dashed). Reported are also the values inferred from the break time of the afterglow light curves in a small number of GRBs (solid histogram, data from GGL04).

of the $E_{\rm peak}$ distribution of bright GRBs. In Figure 6.3 we report the $E_{\rm peak}$ distribution which – assuming the A02 relation — allows to satisfactorily reproduce the overall fluence distribution (as shown in Figure 6.4, top). This broadly peaks around $\sim$ 80 keV. The parameter D (see Section 6.3) was within the defined limits for the consistency of the observed and simulated distribution (D=0.07 corresponding to $\rm P_{KS}$=0.002).

Whether this 'exercise' has any meaning depends on how tightly such extrapolation is constrained. We considered other smooth extrapolations of the bright GRB $E_{\rm peak}$ distributions, and for illustration we mention a couple of them, namely a distribution extending even further down in energy (shown in Fig. 6.3), peaking around $\sim$ 60 keV, and one peaking around 100 – 200 keV. These alternatives resulted in inconsistent fluence distributions, over and under estimating the dimmest GRBs, respectively (the result for the latter case is shown in Figure 6.4, top). We conclude that this analysis is quite sensitive to the shape and extent of such extrapolation.

Interestingly, we realized a posteriori that information on GRBs with intermediate

fluences (between the bright and whole BATSE samples) are available. Yonetoku et al. (2004) considered BATSE GRBs at fluence levels lower than the 'bright BATSE sample and performed a spectral analysis on them. Thus the properties of such sample are ideal to provide an independent cross-check on the predicted $E_{\rm peak}$ distribution. Indeed, the $E_{\rm peak}$ and fluence distributions for the Yonetoku et al. (2004) sample are perfectly consistent with the $E_{\rm peak}$ distribution we constrained (see Figure 6.3) with their distribution peaking around 100-200 keV.

Finally we considered the GGL04 correlation (Figure 6.4, bottom). In this case, the extrapolation to lower $E_{\rm peak}$ shown in Figure 6.3 cannot account by itself for the fluence distribution if the (narrow) distribution of angles inferred for bright GRBs is adopted. As shown in Figure 6.4 (bottom), the corresponding fluence distribution in such case results to be a factor ~ 5 higher and narrower than the observed one. Within this scenario such discrepancy can be accounted for if all BATSE GRBs include a large fraction of bursts with wider opening angles: Figure 6.2 reports the inferred (log-normal) opening angle distribution which yields a satisfactory agreement for the fluences. This peaks around 6-8^o and extends to about 20-25^o. [4] It should be stressed that also such opening angle distribution is quite constrained, both in shape and in extension. The statistical parameters describing the overall agreement of the two distributions confirmed that they are consistent: D=0.04 with the corresponding probability $\rm P_{KS}$=0.16.

6.4.2 Inferred properties of BATSE GRBs

Under the above assumptions, the redshift distribution and luminosity function of (BATSE) GRBs can be inferred.

Given that the cosmological distance (up to $z \sim 5$) is not the primary driver for the spread in fluences (see Fig. 6.5), the GRB rate basically follows the assumed star formation rate redshift distribution. For the very same reason, the results are basically insensitive (within a factor 2 in fluences) to a star formation rate $\sim$ constant above $z \sim 2$ (case 2 in Porciani & Madau 2001).

[4] The larger central value of the angles has to be considered as a representative parameter, which could in principle mimic other effects, like possible absorption.

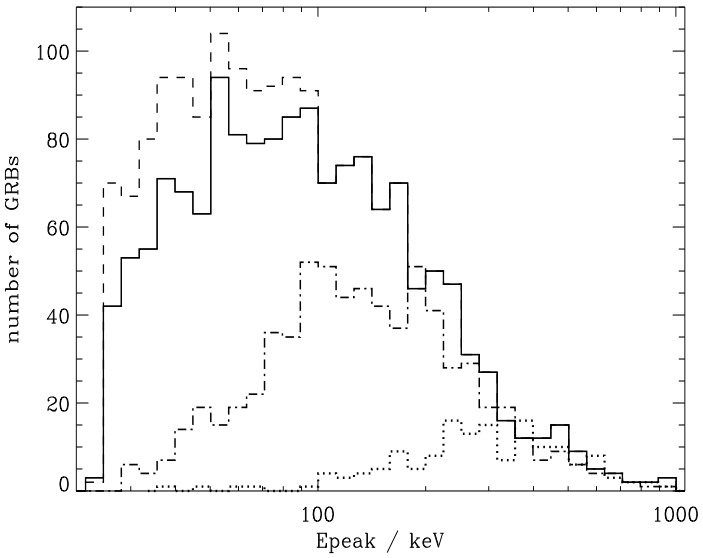

Figure 6.3: $E_{\rm peak}$ distributions for the bright BATSE GRBs (dotted line; Preece et al. 2000), for the sample examined by Yonetoku et al. (2004) (dot-dashed line) and that constrained by this work for the whole BATSE long GRB sample (solid line). The dashed line shows another $E_{\rm peak}$ distribution tested (see text).

In Figure 6.5 we show the redshift distributions for three subsets of simulated GRBs comprising an equal number of bursts (≈ 500). Bursts are divided into groups according to their fluence and the corresponding average fluences are 0.4, 2.1 and 21.2 $\times$ 10^{-6} erg cm^{-2}, respectively. We find that there is no significant difference among their redshift distributions: all three distributions span over the whole range of considered redshifts $z < 5$ and in average differ by $\Delta z < 0.2$. Indeed this confirms the negligible role of distance in selecting GRBs by fluence.

The inferred 'luminosity' function, expressed in terms of E_γ, is reported in Figure 6.6. It clearly reflects the $E_{\rm peak}$ distribution. Interestingly, this well agrees with the 'luminosity functions' constrained from number counts. In fact, it is consistent with the findings by Sethi & Bhargavi (2001) and Schmidt (2001) in terms of the parameters (peak luminosity, width and decline at low E_γ) of a log-normal function for an average GRB duration of $\sim$ 100 s. It is also qualitatively consistent with the characterization as a broken power–law at the higher energies reported by Guetta, Piran & Waxman (2004) (see Fig-

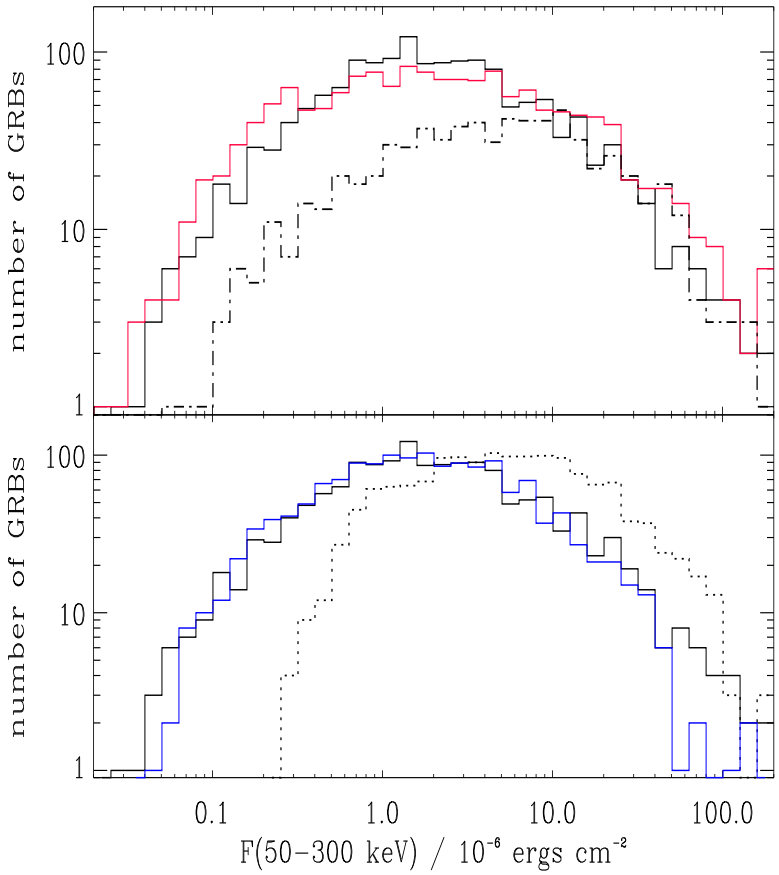

Figure 6.4: Fluence distributions. Observed one for the whole BATSE long GRB population (black solid line, top and bottom panels). Simulated ones, under different assumptions: the A02 relation + the extrapolated $E_{\rm peak}$ distribution shown in Figure 6.3 (red line, top panel); the A02 relation + an extrapolated $E_{\rm peak}$ distribution peaking around 100-200 keV shown in Figure 6.3 (dot-dashed line, top panel); the GGL04 relation + the extrapolated $E_{\rm peak}$ distribution shown in Figure 6.3 + the opening angle distribution for the 'bright' GRBs shown in Figure 6.2 (dotted line, bottom panel); the GGL04 relation + the extrapolated $E_{\rm peak}$ distribution shown in Figure 6.3 + the opening angle distribution for the whole BATSE population shown in Figure 6.2 (blue line, bottom panel);

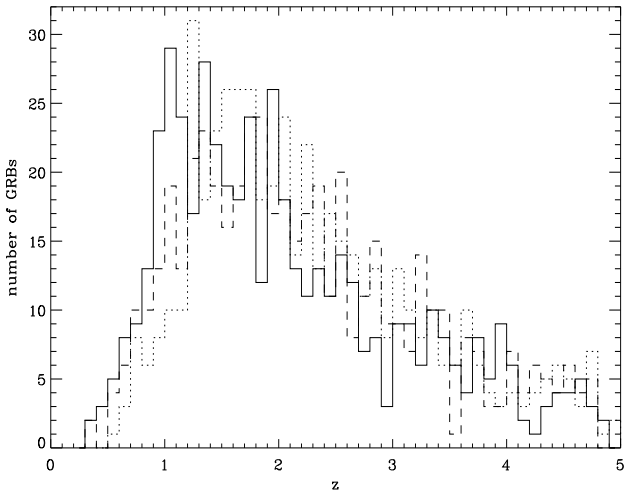

Figure 6.5: The redshift distribution for three sub-sets of the simulated sample comprising an equal number of GRBs ($\sim$ 500) with average fluences 0.4 (dotted line), 2.1 (dashed line) and 21.2 (solid line) $\times$ 10^{-6}erg cm^{-2} respectively. The total fluence distribution is shown in Fig. 6.4, top.

ure 6.6). That is, following Schmidt 1999, for a non evolving luminosity function described as a broken power law,

$$\Phi_0(L) \propto \begin{cases} (L/L^*)^{\alpha} & L^*/\Delta_1 < L < L^* \\ (L/L^*)^{\beta} & L^* < L < \Delta_2 L^* \end{cases}$$

where L^* is a characteristic luminosity while $1/\Delta_1$ and Δ_2 determine the lower and upper limits of the broken power law, they find reasonable fits to the observed peak flux distribution for the parameters $-0.6 < \alpha < -0.1$ and $-3 < \beta < -2$.

Such agreement provides a self-consistency check on the assumptions and an independent support to the validity of the extrapolation in $E_{\rm peak}$ constrained above. It should be stressed that the decline at low E_γ might be simply due to incompleteness near the BATSE fluence sensitivity limit.

6.4.3 Spread of the correlations

While the above results do support the existence of a connection between energetics and $E_{\rm peak}$, it is of great relevance to quantitatively determine any intrinsic spread of such

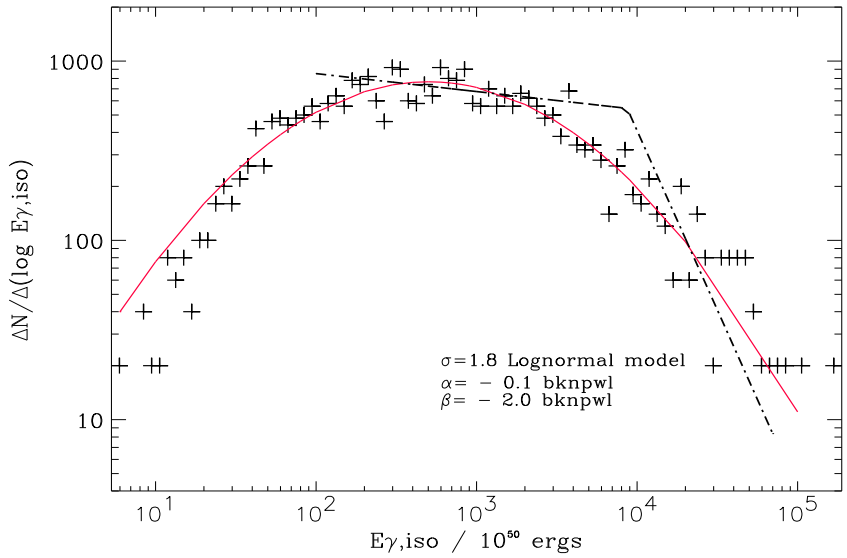

Figure 6.6: 'Luminosity' (E_γ) function of the BATSE GRBs simulated in this work. Also reported is the log-normal fit to such distribution and the slopes inferred by Guetta et al. (2004) for a broken power-law representation of the high luminosity end (dot-dashed line).

relations, both for the understanding the robustness of the physical process behind these correlations and for the possible use of GRBs for cosmological studies.

Indeed Nakar & Piran (2004) have recently argued that the A02 correlation might be the result of selection effects, as a large number of GRBs (at least 50 per cent in the sample they considered) do not appear to follow it. Similar findings have been reported by Band & Preece (2005) who performed a more refined analysis and concluded that 88 per cent of BATSE bursts are inconsistent with the A02 relation, and only at most 18 per cent could be consistent with it. Whether these findings imply that the correlations are totally spurious - contrary to our indications - or that they are significantly broader than estimated so far, has to be determined.

To this aim we simply considered a variable spread (σ) around the A02 correlation, whose shape was approximated as a Gaussian in logarithmic energy. The comparison of the simulated and observed fluence distributions constrains such spread to be centered at $E_0 \simeq E_{\rm A02}$ ($\log(E_0/E_{\rm A02}) = 0.05$ for the bright GRB sub-sample) with $\sigma = 0.17$. This value of σ is fully compatible with the actual spread in the A02 correlation (see GGL04). While

a smaller spread is acceptable, a very strong upper limit $\sigma < 0.3$ is imposed in order not to exceed the fluence distribution both at high and low values. This result argues against the possibility that the A02 correlation is in fact just an envelope (see Nakar & Piran 2004; Band & Preece 2005).

Nakar & Piran 2004 adopted a criterion for an observed burst to follow the spectral correlations we investigated; this is analog to that we used in Section 4.8.2 to estimate the unknown redshifts for gamma–ray bursts associated with SNe. The condition that the 'trajectory' for different z of a particular GRB in (E_{iso}, E_p) plane intersects the spectral correlation (A02 or GGL04) is given by:

$$\frac{A_k}{4\pi D^2}\frac{E^k_{\rm peak,obs}}{F} = \frac{r_c^2(z)}{(1+z)^{k-1}} \tag{6.6}$$

where $D \equiv c/H_0$, $r_c(z)$ is the dimensionless comoving distance to redshift z and F is the bolometric fluence; the spectral correlation is described as $E_{\gamma,iso} = A_k E^k_{\rm peak}$. Thus the parameter d_2 ($k \approx 2$ in the A02 relation) which defines the minimal 'distance' of the 'trajectory' from the spectral correlation is given by:

$$d_2 = 8 \times 10^{-1} \frac{(E_{\rm peak,obs}/1{\rm keV})^2}{F/{\rm erg\ cm^{-2}}} \tag{6.7}$$

Nakar & Piran 2005 argue that - strictly speaking - the bursts for which $d_2 > 1$ do not satisfy the A02 relation, and those for which $d_2 > 2$ as outliers to the A02 correlation. However these conditions can be also considered an estimate of the spread in such (empirical) correlations. We thus estimated such parameter for the simulated GRBs. In Fig. 6.7 the cumulative distribution of bursts for different d_2 is displayed (as defined by eq. 6.7). It is evident that: (1) the fraction of the bursts with parameter $d_2 > 2$ in our sample is $\sim$20%; (2) this fraction falls rapidly for larger values of d_2 and less than 10% of simulated GRBs have $d_2 > 4$. Thus the simulated population can not account for the properties of the GRBs considered by these authors.

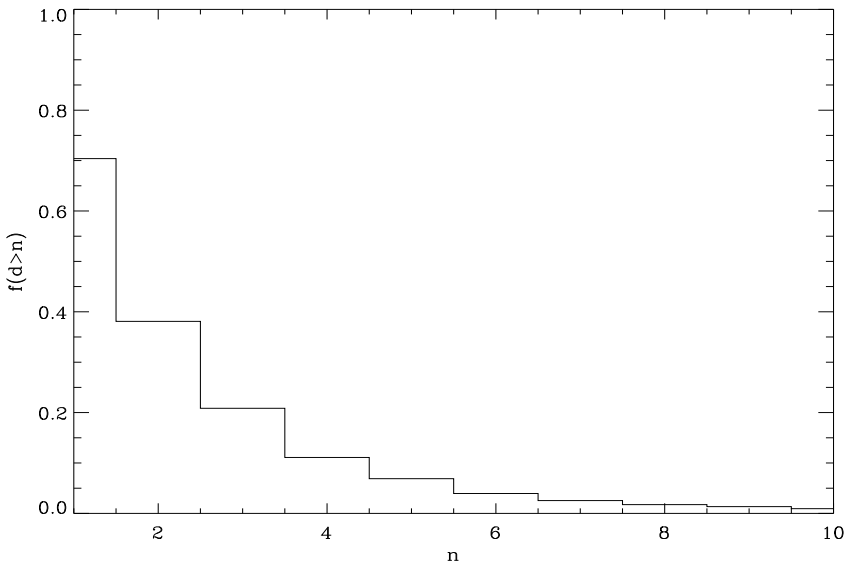

Figure 6.7: The fraction of GRBs with parameter d_2 >n (see the text for details) for the simulated burst population.

6.5 Discussion and Conclusions

The main result we found is that the properties of the whole 'bright' BATSE GRBs sample (Preece et al. 2000) can be accounted for under the assumptions that (a) there is a link between the energetics and the typical spectral peak energy of the prompt phase, as described by the correlations proposed by A02 and GGL04, and (b) GRBs follow the star formation rate redshift distribution.

The fluences of dim GRBs cannot be ascribed to their cosmological distribution, and in our hypothesis they are due to an extension of the $E_{\rm peak}$ distribution toward lower energies (and thus the results are rather insensitive to the actual GRB redshift distribution at high z).

The condition that under the above two assumptions the fluence distribution of the whole of the BATSE population (long GRBs) can be reproduced, tightly constraints the extrapolation of the $E_{\rm peak}$ distribution to low energies.

The inferred extrapolation, partly overlapping with the range of definition of X-ray rich bursts, predicts a rising number of events at decreasing $E_{\rm peak}$, slowly declining below

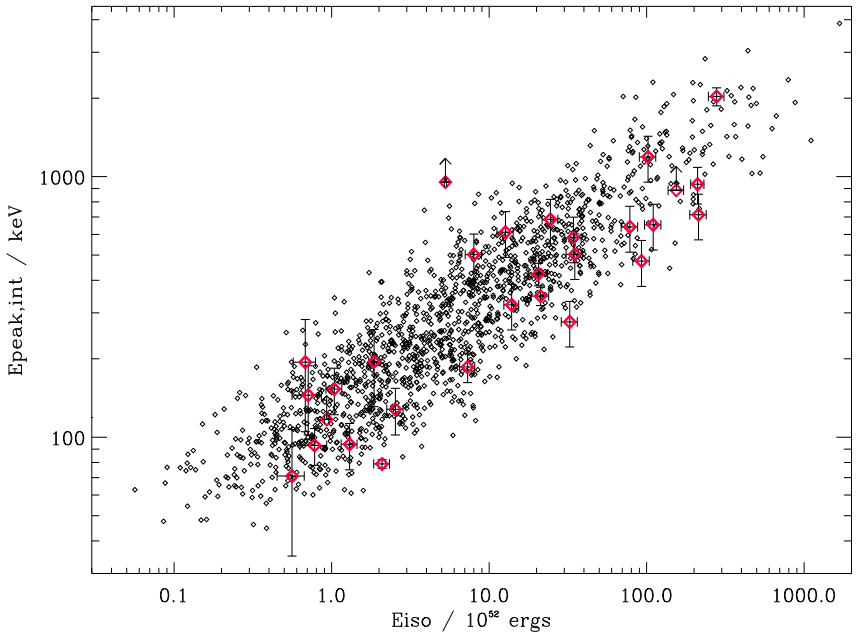

Figure 6.8: Distribution of the simulated GRBs in the intrinsic peak energy vs $E_{\rm iso}$ plane, including the spread around the A02 correlation. The larger red symbols indicate the GRBs considered by GGL04.

$\sim$ 80 keV. This turned out to be consistent with the $E_{\rm peak}$ and fluence distributions of the GRBs at intermediate fluences analyzed by Yonetoku et al. (2004), and implies a luminosity function in agreement with those constrained from the GRB number counts.

The bright GRB fluence distribution can be reproduced also adopting the GGL04 relation, for an opening angle (log-normal) distribution peaking around $4-5^o$ and extending to $\sim 8^o$, consistent with the $\sim$ 15 estimated angles. Consistency with the whole BATSE sample does instead require a broader opening angle distribution, peaking around $\sim 6-8^o$ and extending to $\sim 25^o$. This reflects the fact that the A02 and GGL04 distributions have a different slopes, i.e. the indication of a connection between the average GRB opening angle and energetics E_γ (and/or $E_{\rm peak}$). However, our analysis does not allow to exclude an A02 correlation with slope similar to the GGL04 one, i.e. an opening angle distribution independent of energy.

While the found consistencies cannot prove the reality of an intrinsic tight link between GRB energetics and spectral properties, they significantly corroborate such possi-

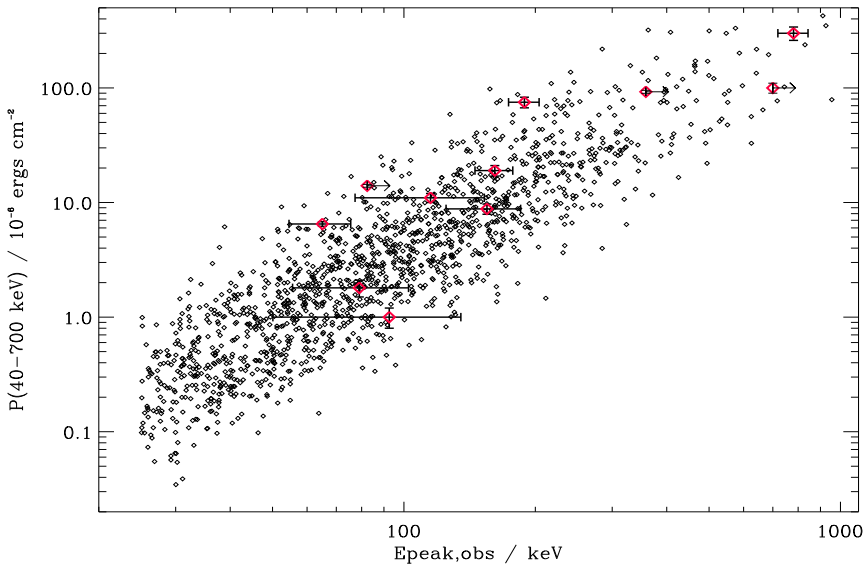

Figure 6.9: Fluence vs $E_{\rm peak}$ distributions as inferred from the model in 40-700 keV energy band. The diamonds (larger red symbols) indicate the GRB events considered by GGL04 and A02 (for the same energy band).

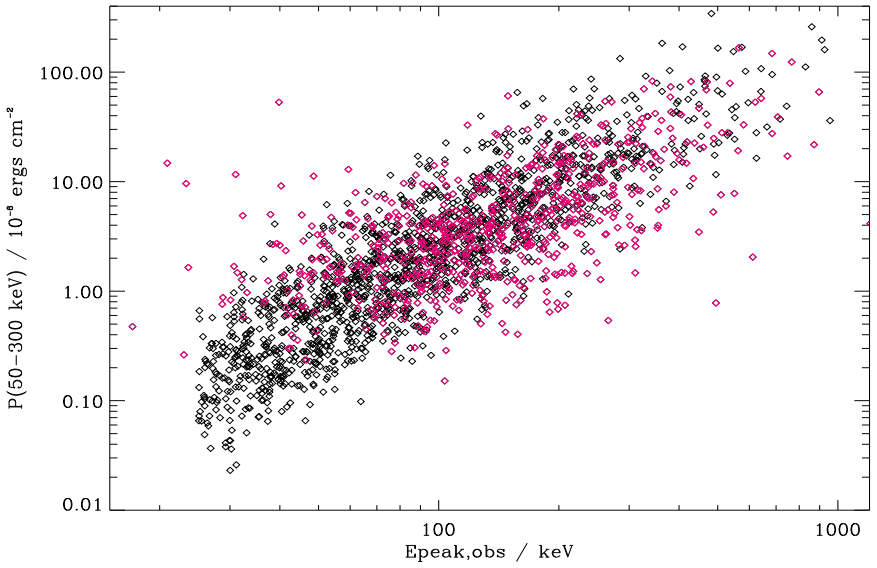

Figure 6.10: Fluence vs $E_{\rm peak}$ distributions as inferred from the model in 50-300 keV energy band (BATSE energy channels #2 and #3). The red symbols represent the fluences (for the same energy band) of the bursts examined by Yonetoku et al. (2004), i.e. the GRBs with the energy distribution presented in Fig. 6.4. top, dot-dashed histogram.

bility. The scenario tested appears to be fully consistent. The spread in the above correlations has to be similar to the observed one. This provides an indication of the strength of a physical connection in the prompt emission and constrains the statistics required for the use of GRBs as cosmological distance indicators.

It should be stressed that the above inferences only refer to GRBs observable and observed by the fluence and energy range sensitivity of BATSE. Selection effects even within the BATSE sample (related to the determination of redshift and opening angle) have being claimed to be responsible for the A02 (and GGL04) correlations by Nakar & Piran (2004) and Band & Preece (2005), on the basis of events inconsistent with them [5]. Well known 'outliers' of such correlations include two of the GRBs with evidence of an associated Supernova (see Chapter 4 for more cases), as well as short GRBs (Ghirlanda, Ghisellini & Celotti 2004). Nakar & Piran (2004) and Band & Preece (2005) argued that a large fraction of the whole GRB population does violate the above relations.

We cannot identify the reason of the discrepant results. Clearly, it is possible that the agreement we find with the BATSE fluence distributions is fortuitous.

Alternatively, one could ascribe the discrepancy to a significant spread in the above correlations. However an estimate of the distribution of the parameter '$d_{\rm k}$' for our simulated sample is inconsistent with their findings within the spread 'allowed' by our analysis. We find proportionally more GRBs with low '$d_{\rm k}$'. In Figure 6.8 we report the simulated GRBs in the $E_{\rm peak}$ vs $E_{\rm iso}$ plane, together with the bursts considered by GGL04, and in Figure 6.9 the analogous information is plotted in the fluence vs $E_{\rm peak}$ plane. A further support to the validity of our hypothesis is the comparison of the fluence vs $E_{\rm peak}$ inferred in our simulations and the same quantities reported in the BATSE catalog for the bursts analyzed by Yonetoku et al. 2004 (Figure 6.10).

With respect to the possibility that the 'outliers' found by the above authors might represent the tail of a distribution, it is worth noticing the large fraction of high $E_{\rm peak}$ GRBs found by Nakar & Piran (2004). They estimated $E_{\rm peak} > 250$ keV for about 50 per cent of their events (i.e. corresponding to about 25 per cent of the whole BATSE long GRB

[5] Although it might be difficult to pinpoint a reason why the GGL04 correlation would be tighter than the A02 one.

sample). This fraction is inconsistent with the findings by Yonetoku et al. (2004) whose lower fluence GRBs are typically characterized by softer spectra, supporting our results. We stress that our analysis does not suffer from the constraints on the fluence (and z) imposed by the S/N requirement to estimate $E_{\rm peak}$. Unfortunately, the lack of detailed information on the GRBs considered by Nakar & Piran (2004) and Band & Preece (2005) does not allow a deeper investigation on the discrepancy at this stage.

The direct testing of the A02 and GGL04 correlations based on individual events requires the determination of redshift (and break time in the afterglow light curves) for a significant number of GRBs. Indirect support to their reality can however come from the determination of the $E_{\rm peak}$ distribution at lower energies, i.e. for X–ray rich GRB and X–ray flashes, as is going to be provided by HETE 2 and Swift.

Chapter 7

Summary and Conclusions

In recent years there has been great progress toward the solution of the GRB puzzle thanks to new observational pieces of evidence. Overall a theoretical framework has been formulated, which can account for most of the current observations. There is quite a good understanding and also extensive testing of some aspects, i.e. the afterglow emission which arises in the stage of the fireball evolution from which most of the information can be obtained. However, the more one moves backwards in time through the various stages of a gamma–ray burst event, the more uncertain the mechanisms at work are. The nature of the GRB progenitor(s) has been a matter of debate ever since their discovery, and only recently the increased evidence for supernovae events associated to GRBs has provided significant support to some of the proposed scenarios. A major open issue is the nature and interpretation of the GRB prompt gamma–ray emission itself.

The work presented in this Thesis discusses the clues provided by the spectral and variability characteristics of the prompt phase on the physics of GRBs.

In the first part, I report on the results concerning the association of gamma–ray bursts with supernovae, in connection with the GRB progenitor population. I analyzed the sample of BATSE gamma–ray bursts that have an indication to be associated with a SN event, on the basis of directional and temporal coincidences or photometric and spectroscopic evidence of SN emission in the late-time afterglow. The analysis revealed that:

in terms of temporal evolution the bursts associated with supernovae are (predominantly) *single–peaked* events; their spectra are *softer* with respect to typical GRBs; they are mostly outliers of the established empirical correlations. The properties of the GRB/SN sample thus appears to be intriguingly similar to the few firm cases of gamma–ray bursts associated to supernovae. The finding of a significant number of underluminous, single-peaked, soft bursts could be interpreted as due to prompt emission reprocessed by circumburst material (a kind of environment expected in case of a supernova explosion preceding the GRB), whose effect dominates at large angles between the line of sight and the GRB jet axis. Initial results on the expected GRB properties in such a scenario are promising and further developments are planned.

In the second part of the Thesis I focused on the origin of the prompt emission and discussed the radiation mechanisms that are likely to be at work in the prompt phase.

While many observed GRB spectra are consistent with the prompt emission being due to synchrotron radiation from shock-accelerated, relativistic electrons, this scenario encounters difficulties in accounting for hard low energy spectral indices, found in a sizable number of GRBs. I then presented observational evidence that the gamma-ray emission in GRB 990413 is consistent with being of thermal origin. The evidence for a thermal character of spectra in this -and other- GRBs and their hard-to-soft spectral evolution makes it inevitable to closely consider the initial thermal phase predicted by the standard model and assess whether such thermal emission is a fundamental and general property of the initial phase and/or under which conditions it becomes prominent. In this respect the temporal evolution of GRB 990413 provides interesting clues, as it shows rapid variability ('dips') that seems to reflect the spectral behavior. The short timescale ($\propto$ 10 ms) flux changes correspond to dominance of nonthermal emission: the two spectral components, thermal and nonthermal, prevail on each other during the course of the burst. As the nonthermal component is usually attributed (in the internal shock scenario) to the velocity distribution of shells, the alternation of two different emission processes can provide insight into the conditions within the relativistic wind when it becomes transparent and/or the temporal pattern of the shell/wind ejection from the central engine.

In the last part of my Thesis I examined the robustness of the correlations among the gamma-ray energetics and the spectral properties as proposed by Amati et al. 2002 and Ghirlanda et al. 2004. These indeed can be key to the understanding of the chief emission process. Furthermore they constitute a promising tool for the cosmological use of gamma–ray bursts, as they could provide an estimate of the burst energy accurately enough to effectively probe the dynamics of the intermediate redshift (z <10) Universe. As these correlations were inferred using only a small sample of (bright) events with known redshifts and spectral properties - possibly biased by selection effects - I considered whether their validity can be extended to a large sample of GRBs. Under the simple assumptions that (i) gamma–ray bursts follow the star formation redshift distribution, and (ii) the above correlations hold, I simulated the resulting distribution of long GRB fluences from the distribution of peak energies. The inferred fluence distribution appears consistent with the whole observed BATSE one if the typical spectral peak distribution is extrapolated to low energies with respect to that of bright events. More precisely the peak energy distribution is constrained to peak around $\sim$ 80 keV (much lower than $\sim$ 250 keV, typical of bright GRBs). The requirement that also the Ghirlanda et al. relation holds, constraints also the collimation/jet opening angle distribution. My analysis showed that for the whole BATSE population this should be broad, peaking around $\sim 6^0 - 8^0$ and extending to $\sim 25\ ^0$. Also the spread in the above correlations is limited by our analysis to be similar or smaller than the observed spread. The larger number of bursts with lower peak energies is actually corroborated indirectly by the observation of X–ray rich GRBs and X–ray flashes.

The nature of the GRB progenitor, the significance of thermal emission in gamma–ray bursts and the extension of the spectral-energetics correlations to the region of XRFs and XRR GRBs, are some of the key questions of gamma–ray burst physics discussed in this work; the clarification of these issues requires the study of a larger set of GRBs with known redshifts and afterglow observations, and the spectral analysis over a wider energy range. The new missions dedicated to study of gamma–ray bursts, the on-going HETE-II, *Swift* and *GLAST* - whose launch is scheduled for August 2007 - are expected to have the capability of addressing these problems.

Bibliography

[1] Amati, L., et al. 2002, A&A, 390, 81

[2] Andersen, M.I., et al. 2000, A&A, 364, L54

[3] Atteia, J.L. 2003, A&A, 407, L1

[4] Bagoly, Z., et al. 2003, A&A, 398, 919

[5] Band, D.L., et al. 1993, ApJ, 413, 281

[6] Band, D.L. 1997, ApJ, 486, 928

[7] Band D.L. & Preece R.D. 2005, ApJ, 627, in press (astro-ph/0501559)

[8] Bevington, P.R. & Robinson, D.K. 1992, Data reduction and error analysis for the physical science (2nd ed., McGraw-Hill)

[9] Bhat, P.N., et al. 1992, Nature,359, 217

[10] Bloom, J.S., et al. 1998, ApJ, 507, L25

[11] Bloom, J.S., et al. 1998a, ApJ, 506, L105

[12] Bloom, J.S., et al. 1999, Nature, 401, 453

[13] Bloom, J.S., et al. 2001, ApJ, 554, 678

[14] Bloom, J.S., et al. 2002, ApJ, 123, 1111

[15] Bloom, J.S., et al. 2003, ApJ, 594, 674

[16] Bosnjak Z., Celotti A., Ghirlanda G., Pian E. 2005, A&A, submitted

[17] Bosnjak Z., et al. 2004, in Proc. Texas Symposium at Stanford, in press

[18] Böttcher, M. & Dermer, C.D. 1998, ApJ, 499, L131

[19] Briggs, M.S., et al. 1999, ApJSS, 122, 503

[20] Brock, M., et al. 1994, in AIP Conf. Proc. 307, Gamma-Ray Bursts, ed. G.J. Fishman. J.J.Brainerd, & K.Hurley (New York:AIP), 672

[21] Cavallo, G. & Rees, M.J. 1978, MNRAS, 183, 359

[22] Christensen, L. et al. 2004, A&A, 425, 913

[23] Colgate, S.A. 1974, ApJ, 187, 333

[24] Connaughton, V. 2002, ApJ, 567, 1028

[25] Costa, E., et al. 1997, Nature, 387, 783

[26] Crider, A., et al. 1997, ApJ, 479, L39

[27] Crider, A. & Liang, E.P. 1999, AASS, 138, 405

[28] Daigne F. & Mochkovitch R. 2002, MNRAS, 336, 1271

[29] Della Valle, M., et al. 2003, A&A, 406, L33

[30] Della Valle, M. 2004, to appear in Gamma-Ray Bursts in the Afterglow Era, Conf. Proc. 4^{th} Rome Workshop, astro-ph/0504517

[31] Djorgovski, S.G., et al. 1998, ApJ, 508, L17

[32] Djorgovski, S.G., et al. 1999, GCN notice 289

[33] Djorgovski, S.G., et al. 2001, in proc. "Gamma-Ray Bursts in the Afterglow Era: 2nd Workshop", eds. N. Masetti et al., ESO Astrophysics Symposia, Berlin: Springer Verlag

[34] Eichler, D. et al. 1989, Nature, 340, 126

[35] Eichler D. & Levinson A. 2004, ApJ, 614, L13

[36] Fenimore, E.E. & Ramirez-Ruiz, E. 2000, astro-ph/0004176

[37] Fenimore, E.E. 1993, Nature, 366, 40

[38] Fenimore, E.E. et al. 1995, ApJ, 448, L101

[39] Fishman, G.J., et al. 1993, AASS, 97, 17

[40] Fishman, G.J. & Meegan, C.A., 1995, ARA&A, 33, 415

[41] Fishman, G.J., et al. 1994, ApJSS, 92, 229

[42] Ford, L.A., et al. 1995, ApJ, 439, 307

[43] Frail, D.A., et al. 1997, Nature, 389, 261

[44] Frail, D.A., et al. 2001, ApJ, 562, L55

[45] Friedman A.S. & Bloom J.S. 2004, ApJ, 627, 1

[46] Fruchter, A.S., et al., 1999, ApJ, 519, L16

[47] Fynbo, J.P.U., et al. 2004, ApJ, 609, 962

[48] Fynbo, J.P.U., et al. 2003, A&A, 406, L63

[49] Galama, T.J., et al. 1998, Nature, 395, 670

[50] Galama, T.J., et al. 1998a, ApJ, 500, L97

[51] Galama, T.J., et al. 2001, ApJ, 549, L209

[52] Gallant, Y.A., et al. 2000, 5th Huntsville Symposium, October, 1999. Editors: R. Marc Kippen, Robert S. Mallozzi, Gerald J. Fishman. AIP Conference Series, Vol. 526, p.524

[53] Garnavich, P.M., et al. 2003, ApJ, 582, 924

[54] Gehrels, N., et al. 1994, ApJSS, 92, 351

[55] Gehrels, N., et al. 2005, astro-ph/0505630

[56] Germany, L., et al. 2000, ApJ, 533, 320

[57] Ghirlanda, G., et al. 2002, A&A, 393, 409

[58] Ghirlanda G., et al. 2003, A&A, 406, 87

[59] Ghirlanda, G., et al. 2004a, ApJ, 616, 331

[60] Ghirlanda, G., et al. 2004b, ApJ, 613, L13

[61] Ghirlanda, G., et al. 2004, A&A, 422, L55

[62] Ghirlanda, G., et al. 2005, astro-ph/0502186

[63] Ghisellini, G. & Lazzati, D. 1999, MNRAS, 309, L7

[64] Ghisellini, G. & Celotti, A. 1999, ApJ, 511, L93

[65] Ghisellini G., et al. 2000, MNRAS, 316, L45

[66] Gonzalez, M.M. et al. 2003, Nature, 424, 751

[67] Goodman, J. 1986, ApJ, 308, L47

[68] Goodman, J. 1997, New Astronomy, 2, 449

[69] Granot, J., et al. 2000, ApJ, 534, L163

[70] Guetta, D., et al. 2004, astro-ph/0311488

[71] Guetta, D., et al. 2005, ApJ, 619, 412

[72] Hartmann, D. & Epstein, R.I. 1989, ApJ, 346, 960

[73] Heger, A. et al. 2003, ApJ, 591, 288

[74] Heger, A. & Woosley, S.E. 2002, AIP Conf.Proc. 662, 214

[75] Heise, J. et al., 2001, Gamma-Ray Bursts in the Afterglow Era, Proceedings of the International workshop held in Rome, October 2000. Edited by Enrico Costa, Filippo Frontera, and Jens Hjorth. Springer, 2001, p. 16.

[76] Hjorth, J., et al. 2003, Nature, 423, 847

[77] Holland, S., et al. 2001, A&A, 371, 52

[78] Hudec, R., et al. 1999, A&AS, 138, 475

[79] Hurley, K., Sari R. & Djorgovski, S.G. 2003, review article in "Compact Stellar X-Ray Sources", Editors W. Lewin and M. van der Klis, Cambridge University Press 2003.

[80] Inoue, S., et al. 2003, ApJ, 583, 379

[81] Ioka K. & Nakamura T. 2001, ApJ, 554, L163

[82] Iwamoto, K. et al., 1998, Nature, 395, 672

[83] Jimenez, R., et al. 2001, ApJ, 561, 171

[84] Katz J.I. 1994, ApJ, 432, L107

[85] Kippen, R.M., et al. 1998, ApJ, 506, L27

[86] Klebesadel, R.W., et al. 1973, ApJ, 182, L85

[87] Kolaczyk, E.D. 1997, ApJ, 483, 340

[88] Kouveliotou, C., et al. 1993, ApJ, 413, L101

[89] Kulkarni, S.R. et al. 1998, Nature, 393, 35

[90] Lamb D. Q., et al. 2004, New Astronomy Review, 48, 459464

[91] Lamb D. Q., et al. 2004a, Gamma–Ray Bursts: 30 Years of Discovery: GRB Symposium, AIP Conference Proceedings, Vol. 272, p.19

[92] Lamb D. Q., et al. 2005, 4th Workshop 'Gamma-Ray Bursts in the Afterglow Era', L. Piro, L. Amati, S. Covino, & B. Gendre eds., Il Nuovo Cimento, in press

[93] Lazzati D., et al. 2000, ApJ, 529, L17

[94] Le Floc'h, E., et al. 2003, A&A, 400, 499

[95] Levan, A., et al. 2004, astro-ph/0403450

[96] Li, H. & Fenimore, E. 1996, ApJ, 469, L115

[97] Liang, E. & Kargatis, V. 1996, Nature, 381, 49

[98] Liang, E., et al. 1997, ApJ, 479, L35

[99] Liang E. W., Dai Z. G., Wu, X. F. 2004, ApJ, 606, L29

[100] Link, B., et al. 1993, ApJ, 408, L81

[101] Lithwick, Y. & Sari, R. 2001, ApJ, 555, 540

[102] Lloyd, N.M. & Petrosian, V. 1999, ApJ, 511, 550

[103] Lloyd, N.M. & Petrosian, V. 2000, ApJ, 543, 722

[104] Lloyd, N. M., Petrosian, V., Mallozzi, R. S. 2000a, ApJ, 534, 227

[105] Lloyd N.M. & Petrosian V. 2002, ApJ, 565, 182

[106] Lloyd-Ronning N.M. & Ramirez-Ruiz, E. 2002, ApJ, 576, 101

[107] MacFadyen, A.I. & Woosley, S.E. 1999, ApJ, 524, 262

[108] Madau, P. & Pozzetti, L. 2000, MNRAS, 312, L9

[109] Malesani, D., et al. 2004, ApJ, 609, L5

[110] Mallozzi, R.S., et al. 1995, ApJ, 454, 597

[111] Matheson, T., et al. 2003, ApJ, 599, 394

[112] Mazets, E.P., et al. 1981, Nature, 290, 378

[113] Medvedev, M.V. 2000, ApJ, 540, 704

[114] Meegan, C.A., et al. 1992, Nature, 355, 143

[115] Meegan, C.A., et al. 1996, ApJSS, 106, 65

[116] Mèszàros, P. & Rees, M.J. 1992, ApJ, 397, 570

[117] Mèszàros, P. & Rees, M.J. 1993, ApJ, 405, 278

[118] Mèszàros, P. & Rees, M.J. 1997, ApJ, 476, 232

[119] Mèszàros, P. & Rees, M.J. 1997a, ApJ, 482, L29

[120] Mèszàros, P. & Rees, M.J. 2000, ApJ, 530, 292

[121] Metzger, M.R., et al. 1997, Nature, 387, 878

[122] Mochkovitch, R., et al. 1993, Nature, 361, 236

[123] Murakami, T., et al. 1988, Nature, 335, 234

[124] Nakamura, T. et al. 2001, ApJ, 550, 991

[125] Nakar, E. & Piran, T. 2002, MNRAS, 330, 920

[126] Nakar, E. & Piran, T. 2004, astro-ph/0412232

[127] Narayan, R., et al. 1992, ApJ, 395, L83

[128] Narayan, R., et al. 2001, ApJ, 557, 949

[129] Nemiroff, R.J., et al. 1994, ApJ, 423, 432

[130] Norris, J., et al. 1986, ApJ, 301, 213

[131] Norris, J., et al. 1996, ApJ, 459, 393

[132] Norris, J., et al. 1999, ApJ, 518, 901

[133] Norris, J., et al. 2000, ApJ, 534, 248

[134] Paciesas W.S. et al. 1999, ApJS, 122, 465

[135] Paczyǹski, B. 1986, ApJ, 308, L43

[136] Paczyǹski, B. 1991, Acta Astronomica, 41, 257

[137] Paczyǹski, B. & Rhoads, J.E. 1993, ApJ, 418, L5

[138] Panaitescu, A. & Kumar,P. 2001, ApJ, 554, 667

[139] Panaitescu, A., et al. 1998. ApJ, 503, 314

[140] Pendleton, G.N., et al. 1995, NIM A, 364, 567

[141] Pendleton, G.N., et al. 1999, ApJ, 512, 362

[142] Piran, T. 1999, Phys. Rep., 314, 575

[143] Piro, L., et al. 1999, ApJ, 514, L73

[144] Piro, L., et al. 2000, Science, 290, 955

[145] Porciani, C. & Madau, P. 2001, ApJ, 548, 522

[146] Preece, R.D., et al. 1998, ApJ, 496, 849

[147] Preece, R.D., et al. 2000, ApJSS, 126, 19

[148] Podsiadlowski, Ph., et al. 2004, ApJ, 607, L17

[149] Quilligan, F., et al. 2002, A&A, 385,377

[150] Ramirez-Ruiz, E. & Fenimore, E.E. 2000, ApJ, 539, 712

[151] Ramirez-Ruiz, E. & Merloni, A. MNRAS, 2001, 320, L25

[152] Rees, M.J. & Mészáros, P. 1994, ApJ, 430, L93

[153] Rees, M.J. & Mészáros, P. 2005, astro-ph/0412702

[154] Reichart, D., et al. 2001, ApJ, 552, 57

[155] Reichart, D. & Price, P.A. 2002, ApJ, 565, 174

[156] Rhoads, J.E., 1999, ApJ, 525, 737

[157] Rigon, L., et al. 2003, MNRAS, 340, 191

[158] Rubin, B.C., et al. 1996, AASS, 120, 687

[159] Rybicki, G.B. & Lightman, A.P., 1997, Radiative processes in astrophysics, New York Wiley

[160] Ryde, F. 2004, ApJ, 614, 827

[161] Ryde, F. 2005, ApJ, 625, L95

[162] Sahu, K.C., et al. 1997, Nature, 387, 476

[163] Sakamoto, T., et al. 2004, astro-ph/0409128

[164] Salmonson, J.D. 2000, ApJ, 544, L115

[165] Sari, R., et al. 1996, ApJ, 473, 204

[166] Sari, R., et al. 1998, ApJ, 497, L17

[167] Sari, R., et al. 1999, ApJ, 519, L17

[168] Sari, R. & Esin, A.A. 2001, ApJ, 548, 787

[169] Sazonov, S.Yu., et al. 2004, Nature, 430, 646

[170] Schaefer, B.E. & Walker,K.C. 1999, ApJ, 511, L89

[171] Schaefer, B.E. 2003, ApJ, 583, L71

[172] Schaefer, B.E. 2004, ApJ, 602, 306

[173] Schmidt, M. 1999, ApJ, 523, L117

[174] Schmidt, M. 2001, ApJ, 552, 36

[175] Shemi, A. & Piran, T. 1990, ApJ, 365, L55

[176] Sethi, S. & Bhargavi, S.G. 2001, 376, 10

[177] Soderberg A.M., et al. 2004, Nature, 430, 648

[178] Soderberg, A.M., et al. 2005, astro-ph/0502553

[179] Stanek, K.Z., et al. 2005, astro-ph/0502319

[180] Sokolov, V.V., et al. 2001, astro-ph/0104102

[181] Tavani M., 1996, ApJ, 466, 768

[182] Terlevich, R., et al. 1999, IAUC, 7269

[183] Valenti, S., et al. 2005, astro-ph/0505052

[184] Vanderspek, R., et al. 2004, astro-ph/0401311

[185] van Paradijs, J. et al., 1997, Nature, 386, 686

[186] van Paradijs, J. et al., 2000, Ann. Rev. A&A, 38, 379

[187] Vietri, M. & Stella, M. 1998, ApJ, 507, L45

[188] Wang, L. & Wheeler, J.C. 1998, ApJ, 504, L87

[189] Waxman, E. 2004, ApJ, 602, 886

[190] Wijers, R.A.M.J., et al. 1997, MNRAS, 288, L51

[191] Wijers, R.A.M.J., et al. 1999, ApJ, 523, L33

[192] Woosely, S.E. 1993, ApJ, 405, 273

[193] Yamazaki, R., et al. 2004, ApJ, 606, L33

[194] Yonetoku, D., et al. 2004, ApJ, 609, 935

[195] Zeh, A., et al. 2004, ApJ, 609, 952

[196] Zeh, A., et al. 2005, astro-ph/0503311

[197] Zhang, B. & Mèszàros, P. 2001, ApJ, 559, 110

[198] Zhang, B. & Mészáros, P. 2002, ApJ, 581, 1236

[199] Zhang, B. & Mészáros, P. 2004, Int.J.Mod.Phys, A19, 2385

[200] Zhang, W., et al. 2003, ApJ, 586, 356